Analysis of the *Dstac* Gene,

a Novel Regulator of Neuronal Function and Behavior in *Drosophila Melanogaster*

by

I-Uen Hsu

A dissertation submitted in partial fulfillment
of the requirements for the degree of
Doctor of Philosophy
(Molecular, Cellular and Developmental Biology)
in the University of Michigan
2020

Doctoral Committee:

Professor John Y. Kuwada
Professor Kenneth M. Cadigan
Associate Professor Catherine A. Collins
Professor Haoxing Xu
Associate Professor Bing Ye

I-Uen Hsu

iuenhsu@umich.edu

ORCID iD: 0000-0002-4089-6601

DEDICATION

To Mom and Dad.

Thank You for Always Being There for Me.

ACKNOWLEDGMENTS

This dissertation research is only possible because of the guidance, help and support from my advisor, committee, colleagues, friends and family.

I would like to thank my Ph.D. advisor Dr. John Kuwada. John is my science father. He demonstrated a role model that is a logical, critical, diligent, passionate and ethical scientist. He is always patient and gave me immediate, honest and helpful feedback on my presentations and scientific writing. His passion and curiosity toward science is contagious that often inspired and encouraged me to work harder, to be creative and critical. Particularly, I thank John for his trust in my development as a scientist and the progression of my research projects. I appreciate that we often made plans together in order to achieve goals such as submitting papers, producing antibodies, creating mutant *Drosophila* strains, applying for fellowships etc. Sometimes I doubted myself and felt that I couldn't achieve those goals, but with John's encouragement, trust and persistence, we eventually made it! When I felt stressed or frustrated with some failed experiments, John would cheer me up through discussing the data and searching for alternative solutions/experiments, or sometimes by chatting with me about delicious cuisine. Besides science, John has a passion for food, and I will always remember the food he cooked or brought for us!

I would like to thank Dr. Jeremy Linsley. Jeremy was my mentor who I worked alongside with when I started my rotation in John's lab. His knowledge and creativity on science influenced me tremendously. Through working with him, I became more flexible in being able to come up various approaches to tackle scientific questions. I appreciated the opportunities to collaborate on two of his papers. Jeremy set a primary, solid foundation of my dissertation projects that allowed

me to develop/expand the projects further. I thank Nadia Perez for being a considerate, kind and helpful lab mate who contributed friendly conversations and environments. I would like to thank the faithful technicians and undergraduate researchers who have worked and grown with me. Miranda Lum helped tremendously on characterizing the *Drosophila* mutant strain that I created. The screening and tests were abundant and sometimes tedious, but she managed to accomplish it well! Even after Miranda left the Kuwada lab for graduate school, she often checked in with me and encouraged me. Allison Orzel is a very organized hard worker. Ally established a systematic, reliable protocol for our *Drosophila* behavioral assay. Jade Varineau was an independent, hard-working and self-motivated undergraduate researcher that managed to identify a *Drosophila* mutant strain that turned out to be helpful in my dissertation research. Lilly Reid took great care of our important *Drosophila* stocks and helped performing/analyzing several live imaging experiments. Bethany Folk-Middlebrook and Ari Leflein were instrumental in many aspects of my science projects.

I would like to thank Dr. Catherine Collins and her lab. Cathy and her lab welcomed and "nourished" me when I was a newborn for *Drosophila* experiments in 2014. Cathy shared her fly genetics facility, *Drosophila* stocks and several reagents with me. Majority of the knowledges I have about flies came from Cathy and her lab members. Ryan Insolera, Laura Smithson, Jiaxing Li and Yan Hao taught me everything about *Drosophila* experiments. They created such a cheerful and open-minded environment that I feel that I have two home labs. Their generous and continuing supports moved my research using *Drosophila* forward smoothly.

I would like to thank Dr. Richard Hume. Rich gave me the opportunity to be a GSI with him in one of his neuroscience courses. Through teaching with him, I pursued to be a

responsible, reliable, sympathetic mentor/teacher who is able to effectively communicate with others. Rich also taught me electrophysiology experiments in *Drosophila* and set up the electrophysiology rig for me. He always gave me straightforward, practical advice that undoubtedly will benefit my whole life.

I would like to thank Dr. Kenneth Cadigan. Ken is the person I go to when I have questions about fly genetics and need advice on my scientific career. Ken always told me that hard work will pay off and reminded me that I should continue the hard work. I thank Ken's continuing supports and kind words that helped me move forward.

I often met Dr. Haoxing Xu on the ways to science seminars. Haoxing is always energetic, kind, stimulating, supportive and informative. He often had constructive criticisms about my work that helped shape my projects. I also thank Xu lab for being a very resourceful and generous neighbor. Whenever I urgently needed some reagents, 99.9% of the times they had what I needed and they offered!

I would like to thank Dr. Bing Ye for the kind words and constructive suggestions on my research projects and being on my dissertation committee. I would like to thank Dr. Swathi Yadlapalli, Dr. Josie Clowney, Dr. Bo Duan, and Dr. Mohammed Akaaboune for their helpful advice on my career path and research projects. I would like to thank Dr. Rafiqa Ameziane for giving me the chance to be her GSI and it's been my pleasure teaching with her under the COVID-19 crisis.

I thank the resourceful and collaborative *Drosophila* community at the University of Michigan and the inclusive and diverse MCDB community. Go Blue!

TABLE OF CONTENTS

LIST OF TABLES

LIST OF FIGURES

LIST OF APPENDICES

List of Abbreviations

AID: Alpha Interaction Domain

Ca_v channels: voltage-gated calcium channels

CaChs: Ca^{2+} channels

CDF: Ca^{2+} dependent facilitation

CDI: Ca^{2+} dependent inactivation

CICR: Ca^{2+} induced Ca^{2+} release

CRD: cysteine-rich domain

DCV: dense core vesicles

DHPR: dihydropyridine receptor

EC coupling: excitation-contraction coupling

ER: endoplasmic reticulum, the intracellular Ca^{2+} store

ERES: ER exit sites

FRAP: flourescence recovery after photobleaching

hpf: hours post fertilization

HVA: high voltage activated

l-LN_V: large lateral ventral neurons

s-LN_V: small lateral ventral neurons

LVA: low voltage activated

MIDAS: metal ion-dependent adhesion site

NAM: Native American Myopathy

NMJ: neuromuscular junction

NPY-pHluorin: pHluorin tagged neuropeptide Y

PDF: pigment dispersing factor

RBP: RIM-Binding Protein

RIM: Rab3-interacting molecule

RyR: ryanodine receptor

SERCA: the sarco/endoplasmic reticulum Ca^{2+}-ATPase

SH3: Src Homology 3

SM proteins: Sec1/Munc18-like proteins

SNARE proteins: soluble NSF attachment receptor proteins

SR: sarcoplasmic reticulum

SSV: small synaptic vesicles

T tubules: transverse tubules

U motif: unknown motif

VWA: von Willebrand actor A domain

wt: wild type

ABSTRACT

The *stac* genes encode a family of proteins with conserved CRD (cysteine-rich domain) and SH3 (Src Holomogy 3) domains found throughout the animal kingdom. *stac1* and *stac2* are expressed by subsets of neurons, and *stac3* by skeletal muscles in vertebrates. One process regulated by a Stac protein is excitation-contraction (EC) in vertebrate skeletal muscles. EC coupling is the process that transduces changes in muscle membrane potential to increases in cytosolic Ca^{2+} that initiate muscle contraction. EC coupling is mediated by the physical interaction between the L-type voltage gated calcium channel (Ca_v channel), DHPR, in the transverse tubules (T tubules) that serves as a voltage sensor and the ryanodine receptors (RyR) in the sarcoplasmic reticulum (SR) that is the Ca^{2+} release channel in vertebrate skeletal muscles. Studies from the Kuwada lab demonstrated that Stac3 regulates EC coupling by regulating the stability, organization and voltage dependency of L-type Ca_v channel in vertebrate skeletal muscles.

The goal of this dissertation is to understand the function of *stac* genes expressed by neurons, which was completely unknown. Towards this goal, we identified the *stac* gene in *Drosophila melanogaster* (*Dstac*) in order to take advantage of its unparalleled genetic/molecular toolbox and found that *Dstac* is expressed both by muscles and by specific classes of neurons. We first investigated the muscle function of Dstac. During EC coupling of invertebrate muscles, Ca^{2+} influx via L-type Ca_v channels activates RyR to release Ca^{2+} from the SR, a process called Ca^{2+} induced Ca^{2+} release (CICR). Dmca1D is the sole *Drosophila* L-type Ca_v

channel and we found that Dmca1D and Dstac were expressed in stripes within muscles. Knocking down *Dmca1D or Dstac* selectively in larval *Drosophila* body-wall muscles reduced Ca^{2+} transients that resulted from the influx of Ca^{2+} through Dmca1D channels and CICR during locomotion. Furthermore, immunolabeling showed decreased Dmca1D levels in *Dstac* mutant muscles, showing that Dstac regulates L-type Ca_v channels as does Stac3 in vertebrate skeletal muscles. These results suggest that muscle Dstac regulates Dmca1D, which induces CICR for proper EC coupling in *Drosophila* body-wall muscles.

In the *Drosophila* adult brain, we found that a set of clock neurons that releases the neuropeptide, pigment dispersing factor (PDF), to regulate circadian rhythm expresses *Dstac* as well as *Dmca1D*. Interestingly, selective knockdown of *Dstac* in PDF neurons disrupted circadian activity. This was the first neural function identified for a Stac protein. The results suggested the hypothesis that Dstac might regulate the Dmca1D L-type Ca_v channel and this in turn regulates the release of PDF for normal circadian rhythm.

We found that Dstac is also expressed by a subset of neurons including motor neurons in the larval CNS. We examined whether Dstac might regulate Dmca1D and neuropeptide release at the larval neuromuscular junction to take advantage of the accessibility of motor boutons for cellular and physiological analysis. We found that Dstac, Dmca1D and the proctolin neuropeptide are expressed by motor boutons. Previously it was shown that proctolin enhances muscle contractions in various insects including *Drosophila*. By a combination of immunolabeling, Ca^{2+} imaging, electrophysiology, live imaging of neuropeptide release and behavioral analysis in genetically manipulated larvae we found that Dstac regulates the voltage response of Dmca1D channels and the release of neuropeptides from motor boutons to

regulate locomotion by larvae. Since *Dstac* is expressed by other neuropeptide containing neurons, including the PDF+ clock neurons, in the CNS our results may be applicable to other neurons in the *Drosophila* CNS. Furthermore the expression of Stac1 and Stac2 in neurons in the vertebrate nervous system opens the intriguing possibility that these Stac proteins may also regulate the release of neuropeptides in at least some vertebrate neurons.

CHAPTER 1. Introduction

1.1 Overview of voltage-gated calcium channels

Voltage-gated calcium channels (Ca_v channels) are gated by membrane depolarization that leads to intracellular Ca^{2+} increase. The elevation of cytosolic Ca^{2+} initiates multiple physiological events including gene transcription, peptide/hormone secretion, synaptic transmission and muscle contraction (Nanou and Catterall, 2018). There are 3 families of Ca_v channels: Ca_v1 (L-type), Ca_v2 (P/Q-, N- and R-type) and Ca_v3 (T-type) (Nowycky et al., 1985). The different types of Ca_v channels vary according to their activation curves: the T-type is low voltage activated (LVA) channels and the other two family are high voltage activated (HVA) channels. Many electrically excitable cells contain both LVA and HVA Ca_v channels and in *Drosophila* these include muscles and motor neurons (Gielow et al., 1995; Kostyuk et al., 1988; Ryglewski et al., 2012; Tsien et al., 1988).

The 3 families of Ca_v channels can be distinguished by electrophysiological properties that vary in voltage dependent activation, inactivation, and kinetics of currents (Fox et al., 1987). They can also be distinguished by pharmacology. For example, Bay K8644 is an agonist for the dihydropyridine receptor, a skeletal muscle L-type calcium channel (DHPR), that shifts the voltage-dependency of the channel to more negative potentials, whereas nifedipine, can block these channels (Cauvin et al., 1983; Schramm et al., 1983). In mouse neuroblastoma,

chick DRG and *Drosophila* larval muscles, the T-type currents were blocked by amiloride, a potassium sparing diuretic (Gielow et al., 1995; Tang et al., 1988). The L- and P/Q-, N- and R-type Ca_v channels are blocked by cadmium, whereas the T-type currents are sensitive to nickel. The P/Q-type Ca_v channel are sensitive to ω-agatoxin IVA (a spider venom peptide). The N-type Ca_v channel can be blocked by ω-conotoxin GVIA and MVIIA (toxins from fish). The R-type channel can be blocked by SNX-482 (G P Miljanich and Ramachandran, 1995). Although the specificity and effects of the channel blockers might vary across a variety of species and cell types, these compounds greatly facilitate understanding the roles of Ca_v channels in the cells.

In vertebrates, the L-type Ca_v channel is encoded by the Ca_v1 gene family consisting of 4 members, *$Ca_v1.1$, $Ca_v1.2$, $Ca_v1.3$* and *$Ca_v1.4$*. $Ca_v1.1$ (DHPR) is specifically expressed in skeletal muscles, is sensitive to dihydropyridines and is a key component of excitation-contraction coupling (see section 1.2). $Ca_v1.2$ is expressed in the cardiac cells, smooth muscles and subsets of neurons (Fabiato, 1992) (see section 1.2). $Ca_v1.3$ plays a role in cardiac pacemaker activity and neurotransmission in auditory hair cells (Brandt et al., 2003; Mangoni et al., 2003). $Ca_v1.4$ has a predominate role in neurotransmission in the retina (Strom et al., 1998) . In *Drosophila melanogaster,* the L-type Ca_v channel is encoded by a single gene, *Dmca1D* (Eberl et al., 1998; Zheng et al., 1995). Genetic cloning of *Dmca1D* showed high sequence homology with vertebrate Ca_v1. Consistent with vertebrate Ca_v1 channels, *Dmca1D* is expressed by muscles and CNS, and *Dmca1D* null mutations are lethal (Eberl et al., 1998). Voltage-clamp recording of *Dmca1D* currents in *Dmca1D* mutant larval muscles demonstrated that the *Dmca1D* currents were sensitive to dihydropyridines (Ren et al., 1998). Voltage-clamp analysis showed that

Dmca1D is the predominant calcium channels in a subset of larval motor neurons (Worrell and Levine, 2008). However, unlike *Dmca1D* currents in larval muscles, motor neuron *Dmca1D* currents were not sensitive to dihydropyridines. This difference might be due to the fact that *Dmca1D* is alternatively spliced and that muscles and the CNS might express different isoforms of *Dmca1D*.

In vertebrates $Ca_v2.1$ encodes the P/Q-type channel, $Ca_v2.2$ the N-type channel and $Ca_v2.3$ the R-type channel. The Ca_v2 family is found primarily in neurons. In *Drosophila melanogaster*, the Ca_v2 family is encoded by one single gene, *Dmca1A*/*cacophony*. Inhibiting *Drosophila Dmca1A* genetically or pharmacologically inhibited evoked synaptic potentials at the larval neuromuscular junction (NMJ) (Kawasaki et al., 2000; Kawasaki et al., 2004; Ryglewski et al., 2012). Similarly, blocking $Ca_v2.1$ and $Ca_v2.2$ with toxins in the vertebrate nervous system demonstrated that Ca^{2+} influx through these subtypes of Ca_v2 channels was responsible for fast release of classical neurotransmitters (see section 1.3) (Dooley et al., 1987; Dunlap et al., 1995; Dutar et al., 1989; Horne and Kemp, 1991; Kamiya et al., 1988; Olivera et al., 1994; Wheeler et al., 1994).

In vertebrates $Ca_v3.1$, $Ca_v3.2$ and $Ca_v3.3$ all encode T-type Ca_v channels. The T-type channels are prominent in pace maker cells such as sinoatrial node and Purkinje cells of cardiac myocytes (Argibay et al., 1988), intestine/vascular/stomach smooth muscles (Smirnov et al., 1992), thalamic neurons (Lee et al., 2004) and secretory cells including pituitary cells, adrenal cells and pancreatic cells (Armstrong and Matteson, 1985; Cohen et al., 1988). In *Drosophila melanogaster*, the T-type Ca_v channel is encoded by one single gene, *Dmca1G*, and is present in

larval muscles and in embryonic and adult motor neurons (Baines and Bate, 1998; Ryglewski et al., 2012). Both in mammals and flies, the T-type currents were found to promote wakefulness while not having a noticeable impact on circadian rhythm (Jeong et al., 2015; Lee et al., 2004). Co-existence of *Dmca1A* and *Dmca1G* was found in *Drosophila* adult motor neurons; electrophysiology experiments and genetic manipulations demonstrated that *Dmca1A* currents are positively modulated by *Dmca1G*, suggesting a high level of complexity of Ca_v channel regulation (Ryglewski et al., 2012).

Consistent with their wide expression and diversity, dysregulation of Ca_v channels results in a variety of neurological, cardiovascular, muscular and psychiatric disorders. To name just a few, mutations in $Ca_v1.1$ were found to be causative for malignant hyperthermia (Monnier et al., 1997); mutations in $Ca_v1.2$ result in the Timothy Syndrome that features cardiac arrythmias (Splawski et al., 2005); mutations in Ca_v2 and Ca_v3 have been found to be associated with epilepsy (Heron et al., 2007; Jouvenceau et al., 2001). Clear understanding of Ca_v channels and their regulators should be useful for developing treatments for diseases caused by abnormalities of Ca_v channels.

The structure of skeletal muscle $Ca_v1.1$ has been resolved (Wu et al., 2016; Wu et al., 2015). Ca_v channels consist of multiple subunits, the pore forming α1 subunit, and the auxiliary subunits, β, γ and α2δ (see section 1.5.1). The α1 subunit forms the central pore that has four homologous repeats I-IV that each repeat consists of six transmembrane segments, S1-S6. The S5 and S6 segments and the intervening pore loop from the 4 repeats form the central pore that conducts calcium ions. Segment S6 of repeat IV is kinked and thus results in an asymmetric

activation gate. The pore loop contains conserved negatively charged amino acids, glutamate or aspartate, that are highly selective for passing Ca^{2+} and Ba^{2+} and therefore constitute the "selectivity filter gate" (Wu et al., 2015; Yang et al., 1993). Recent studies using amino acid substitution approach showed that the asymmetric selectivity filter gate is essential for calcium dependent inactivation (Abderemane-Ali et al., 2019). The S1-S4 segments in each repeat form the peripheral voltage sensing domains with the S4 segment containing many positively charged residues. The positively charged amino acid residues of the S4 segment in response to depolarization of membrane potential result in an intramembranous charge movement that produces a current preceding Ca^{2+} influx (Tao et al., 2010). The cytoplasmic parts of the α1 subunit, including the N-/C-terminus region and the intracellular loops between transmembrane segments, are targets for intracellular signaling process and integrations with other proteins for modulating channel properties. The crystal structure of $Ca_v1.1$ that was at a potentially inactivated state revealed a globular domain formed by the intracellular loop III-IV and the C-terminal region. Interestingly, the loop III-IV of $Ca_v1.1$ shared a similarity in structure with the isolated inactivation gate, in complex with calmodulin, of a rat voltage-gated sodium channel (Wu et al., 2016). This suggests possible conformational mechanisms regulated by calmodulin during calcium-dependent inactivation of Ca_v channels.

1.2 Ca^{2+} regulation of excitation-contraction coupling of muscles

Excitation-contraction coupling (EC coupling) is the process between electrical stimulation and contraction of muscles. During EC coupling, muscle membrane depolarization

causes Ca^{2+} release from the sarcoplasmic reticulum (SR), an intracellular Ca^{2+} store, to increase cytosolic Ca^{2+} concentrations. In vertebrate skeletal muscles, EC coupling occurs at the junction between transverse tubules (T tubules), which are tubular indentations of the plasma membrane into the interior of skeletal muscle, and SR called triads (Franzini-Armstrong, 1970). Two Ca^{2+} channels, $Ca_V1.1$ (also called the dihydropyridine receptor, DHPR) located in the T tubule membrane and the ryanodine receptor (RyR) in the SR membrane interact at triads to mediate EC coupling. $Ca_V1.1$ serves as the voltage detector for EC coupling (Rios and Brum, 1987). Depolarization of dysgenic myotubes, which are $Ca_v1.1$ null muscles, does not result in the release of Ca^{2+} from the SR. Expressing $Ca_v1.1$ cDNA in dysgenic myotubes restored the normal charge movement and EC coupling of dysgenic myotubes (Tanabe et al., 1988; Tanabe et al., 1987), confirming the essential role of $Ca_v1.1$ as the voltage sensor of skeletal muscle. The RyRs are the Ca^{2+} release channel at triads (Lai et al., 1988). Dyspedic myotubes, which are RyR null muscles, lacked EC coupling (Takeshima et al., 1994) and expressing RyR cDNA in dyspedic muscles restored the normal EC coupling of dyspedic muscles (Nakai et al., 1996). This confirms that RyR is the Ca^{2+} release channel during EC coupling.

Vertebrate skeletal muscles do not require extracellular Ca^{2+} for EC coupling and contractions. Vertebrate skeletal muscles continued to twitch when bathed in Ca^{2+} deficient media (Armstrong et al., 1972). Zebrafish DHPRs don't conduct Ca^{2+} and serve only as voltage sensors with gating currents resulted from depolarization-induced displacements of charges in the Ca_v channel's voltage sensing residues (Schredelseker et al., 2010). Non-Ca^{2+}-conducting DHPR knock-in mice displayed comparable EC coupling and muscle contraction to wild type

mice (Dayal et al., 2017). Although DHPRs are voltage-dependent Ca^{2+} channels, Ca^{2+} influx through DHPRs is not necessary for activation of RyRs and they act primarily as voltage detectors for EC coupling in vertebrates. Freeze-fracture EM studies showed ordered arrays of four $Ca_v1.1$ called tetrads located on the T tubules of skeletal muscles. Every other tetrad is aligned with the cytosolic portions of a RyR called RyR feet which appeared to be in contact with tetrads (Block et al., 1988; Franzini-Armstrong et al., 1998). Recent structural analysis of RyRs revealed that there are 4 domains of the RyR that were arranged so that each domain could bind one DHPR in a tetrad (Efremov et al., 2015; Yan et al., 2015; Zalk et al., 2015). This morphological data along with the independence of EC coupling in skeletal muscles of Ca^{2+} influx suggested that DHPRs directly activate RyRs at triads. Such mechanical coupling between $Ca_v1.1$ and RyR leads to the opening of RyR and thus Ca^{2+} release from SR in response to depolarization of skeletal muscle membrane followed by activation of $Ca_v1.1$ (Adams et al., 1990; Bannister and Beam, 2009; Block et al., 1988; Dayal et al., 2017; Rios and Brum, 1987; Takekura et al., 1994).

In contrast to skeletal muscles, cardiac muscle contraction depends on extracellular Ca^{2+} (Fabiato, 1983). Cardiac muscles express $Ca_V1.2$ but lack arrays of $Ca_v1.2$ tetrads suggesting that Ca_V 1.2 does not directly interact with RyR in cardiac myocytes (Franzini-Armstrong et al., 1998). In cardiac cells, Ca^{2+} influx through $Ca_v1.2$ activates RyR to release Ca^{2+} from SR via a process called Ca^{2+} induced Ca^{2+} release (CICR). In CICR, the Ca^{2+} influx through $Ca_V1.2$ channels binds to and activates RyRs and/or IP_3Rs (Roderick et al., 2003). The specificity of $Ca_v1.1$ function in

skeletal muscle and $Ca_v1.2$ function in cardiac muscle was demonstrated by failure in rescuing EC coupling of Cav1.1 null skeletal myotubes by expressing $Ca_v1.2$ (Tanabe et al., 1990).

In *Drosophila* larvae, voltage-dependent Ca^{2+} currents rather than voltage-dependent Na^+ currents are responsible for the rising phase of the action potential of body wall muscles (Gielow et al., 1995; Singh and Wu, 1990). Similar dependence on Ca^{2+} currents for muscle excitability is also observed in many other invertebrates such as honeybees (Collet, 2009). In fact, removing extracellular Ca^{2+} from invertebrate muscles completely abolished contraction (Györke and Palade, 1992). Invertebrate muscles appear not to contain tetrad arrays of Ca_V channels suggesting that EC coupling may not involve direct interactions between Ca_V channels and RyRs (Takekura and Franzini-Armstrong, 2002). In fact CICR is the mode of Ca^{2+} elevation during crayfish skeletal muscle contractions. Simultaneous voltage-clamp recoding of inward Ca^{2+} currents and Ca^{2+} imaging of crayfish skeletal muscles showed reduced cytosol Ca^{2+} elevation but unchanged inward Ca^{2+} current amplitude when inhibiting SR Ca^{2+} release (Györke and Palade, 1992). Thus CICR may be important for muscle contractions in invertebrate muscles including those of *Drosophila*.

1.3 Ca^{2+} regulation of synaptic transmission

Classical neurotransmitters are stored in clear, small synaptic vesicles (SSVs) that are exocytosed rapidly with exocytosis highly coupled with Ca^{2+} influx. At some synapses, the time between spike invasion of presynaptic terminals to postsynaptic response can be less than 1 millisecond (Sabatini and Regehr, 1999). The fast release of neurotransmitters is due to the fact

that Ca_v channels are located at the presynaptic release sites of SSVs, the active zones, where readily releasable SSVs are docked. This arrangement insures fast and large increases of Ca^{2+} at the active zones and the Ca_v channels are found to physically interact with the presynaptic active zone proteins to promptly regulate SSV exocytosis (Rettig et al., 1997).

Neuropeptides are also released by neurons and are packaged in larger dense core vesicles (DCVs) (Morris and Cannata, 1973). Numerous neuropeptides are thought to modulate complex behaviors including social behaviors and circadian rhythms (Nassel and Zandawala, 2019). In some neurons every bouton contains DCVs along with SSVs suggesting that SSV and DCV coexist in one synapse (Decavel and Van den Pol, 1990; Ohnuma et al., 2001). However, in contrast to SSVs that dock at active zones and are ready for exocytosis in response to activity, DCVs are widely spread at cell bodies, dendrites, axons as well as in boutons and stochastically move along the nerve without docking in any designated regions (Seward et al., 1995; Wong et al., 2012; Xia et al., 2009). Both SSVs and DCVs require Ca^{2+} to trigger exocytosis, however, a localized increase of Ca^{2+} at the presynaptic site is more effective at evoking exocytosis of SSVs, whereas a spatially uniform and longer duration of Ca^{2+} elevation effectively evokes exocytosis of DCVs (Burgoyne, 1991; Seward et al., 1995; Verhage et al., 1991). Despite the distinct requirement of Ca^{2+} kinetics for exocytosis of SSVs and DCVs, classical neurotransmitters and neuropeptides share some exocytotic proteins.

Fusion of SSVs is controlled by the SNARE proteins (soluble NSF attachment receptor proteins) and SM proteins (Sec1/Munc18-like proteins). The SNARE proteins, synaptobrevin, syntaxin-1 and SNAP-25 as well the SM protein, Munc18, perform an assembly/disassembly

cycle to complete fusion of SSVs to presynaptic plasma membrane and thus release of neurotransmitters (Hata et al., 1993; McMahon and Südhof, 1995; Okamoto and Südhof, 1997). This fusion pore opening process is driven by Ca^{2+} influx with the C2 domains of synaptogagmin-1 binding Ca^{2+} to induce interactions with SNAREs and phospholipids (Fernandez et al., 2001; Li et al., 1995; Sutton et al., 1995). There are 16 synaptotagmins found in the mammalian brain that exhibit different kinetics corresponding to the types of synapses they are expressed in. For example, synaptotagmin-2 has fast kinetics and is expressed in the neurons mediating sound localization to mediate fast SSV exocytosis (Sun et al., 2007), whereas synaptotagmin-9 has slower kinetics and is expressed in neurons of the limbic system that coordinate slower emotional responses (Xu et al., 2007).

Some synaptotagmins such as synaptotagmin 1 regulate both SSVs and DCVs. In neurons, a point mutation, R233Q, in murine synaptotagmin-1 reduced Ca^{2+} affinity while keeping normal structure of synaptotagmin-1 and resulted in decreased SSV exocytosis, confirming the crucial role of Ca^{2+} and synaptotagmin-1 in triggering synaptic transmission (Fernández-Chacón et al., 2001; Pang et al., 2006). In adrenal chromaffin cells that contain a large number of DCVs that contain catecholamines, the same R233Q mutation of synaptotagmin-1 led to delayed release of DCVs when stimulated by controlled amounts of Ca^{2+}, showing that Ca^{2+} binding to synaptotagmin-1 regulates exocytosis of DCVs (Sørensen et al., 2003) as well as SSVs in neurons.

DCV exocytosis can be detected by patch-clamp measurements of cell membrane capacitance in combination with amperometry and simultaneous Ca^{2+} recording (Alvarez de

Toledo et al., 1993). Using this method, adrenal chromaffin cells were found to have heterogeneous DCV components that showed different release rates, the “readily releasable” pool that is released immediately upon increase in cytosolic Ca^{2+} and “slowly releasable” pool that is released more slowly (Neher and Marty, 1982). Further analysis showed that synaptotagmin-1 regulates the exocytosis of the readily releasable pool of DCVs (Voets et al., 2001) and synaptotagmin-7 the exocytosis of the slowly releasable pool to control DCV secretion in chromaffin cells (Schonn et al., 2008). Such evidence suggests that different synaptotagmins can be co-expressed by the same cell and cooperate to regulate DCV exocytosis.

The *Drosophila* genome contains seven synaptotagmin genes with synaptotagmin-1 and synaptotagmin-7 showing highest homology with the corresponding vertebrate synaptotagmins (Adolfsen et al., 2004). Immunolabeling of *Drosophila* NMJ showed that only synaptotagmin-1 is present in the motor neuron boutons. Furthermore, *Drosophila* synaptotagmin-1 null larvae exhibit reduced locomotion and diminished SSV exocytosis. This mutant phenotype was not rescued by expression of synaptotagmin-4 or synaptotagmin-7 that are also present in *Drosophila* CNS (Adolfsen et al., 2004), suggesting the specific role of synaptotagmin-1 in SSV exocytosis at boutons.

The molecular machinery at presynaptic specializations that enable synaptic vesicles to dock and fuse with the plasma membrane is critical for neurotransmission. Three of the major components in the machinery are RIM (Rab3-interacting molecule), RIM-Binding Protein (RBP), and Rab3. The elimination of RBP in motor neurons at the *Drosophila* NMJ decreased the

probability of SSV exocytosis and dramatically diminished the evoked synaptic potential (Liu et al., 2011). Furthermore, the expression level of *Drosophila* Ca_v2 channel, *Dmca1A*, was decreased at the *Drosophila* NMJ lacking RBP, suggesting interaction and regulation of *Dmca1A* by RBP (Liu et al., 2011). In fact, RBP was found to bind $Ca_v1.3$ in retinal neurons and $Ca_v2.2$ in a heterologous system (Hibino et al., 2002). RIM was found to tether the Ca_v2 channel at the active zone by directly binding to Ca_v2 channels. RIM lacking the binding motif for RBP failed to tether the Ca_v2 channel properly and voltage-dependent influx of Ca^{2+} was significantly decreased in RIM knockout neurons (Han et al., 2011; Kaeser et al., 2011). Therefore, it appears that RIM binds to RBP and RIM/RBP bind to presynaptic Ca_v2 channels to ensure proper Ca^{2+} influx through Ca_v2 channels and thus exocytosis. Rab3 is critical for docking of SSVs at active zones. Rab3 directly binds SSVs (Fischer von Mollard et al., 1990; Schlüter et al., 2002) and RIM (Gracheva et al., 2008). Thus the RIM/RBP/Rab3 complex regulates both Ca_v channels at active zones as well as docking and exocytosis of SSVs. Recently, deletion of RIM or Rab3 was found to severely block fusion of DCVs and that binding between RIM and Rab3 is crucial for regulating DCV fusion events (Persoon et al., 2019). Thus the RIM/RBP/Rab3 complex may regulate exocytosis of both SSVs and DCVs.

1.4 Neuropeptide release

Compared with SSV release, very little is known about release of neuropeptides. Unlike classic neurotransmitters that are released from designated presynaptic sites and diffuse within the synaptic cleft to bind postsynaptic receptors, neuropeptides can be released from cell

bodies, dendrites and axons and act on cells that are micrometers away (Cowley et al., 2001; Jan and Jan, 1982; Xia et al., 2009). By studying cholinergic motor neurons of Aplysia that contain both acetylcholine and the small cardioactive peptides, it was demonstrated that peptide secretion requires higher stimulation frequencies than that required for small neurotransmitter release (Whim and Lloyd, 1989). Neuropeptides are released in the mode of "kiss-and-run" that is triggered and modulated by Ca^{2+} (Alés et al., 1999; Alvarez de Toledo et al., 1993; Elhamdani et al., 2006; Engisch and Nowycky, 1996; Xia et al., 2009). Electrophysiology and pharmacology studies of cultured neurons and non-neural cells demonstrated that L-type currents are necessary for peptide secretion. In adrenal chromaffin cells, DCV exocytosis was found to selectively require the L-type Ca_v channels (Akiyama et al., 2004). Research in cultured hippocampal neurons using eGFP tagged neuropeptide to visualize DCV exocytosis showed that neuropeptide release was dramatically reduced by blocking L-type Ca_v channels with Verapamil, a L-type channel blocker, but was unaffected by antagonists of other subtypes of Ca_v channels, suggesting at least in some neurons, neuropeptide secretion is selectively regulated by L-type Ca_v channels (Xia et al., 2009). Studies in mouse pancreatic B cells using single channel recording and pharmacology showed that L-type Ca_v channels are in close proximity to subcellular areas showing high DCV density and suggested that local increase of Ca^{2+} initiated by L-type Ca_v channels regulates insulin secretion (Bokvist et al., 1995).

One caveat in the study of neuropeptide release is that much of the research was performed in cultured cell systems rather than *in vivo*. One *in vivo* system that allows for the analysis of neuropeptide release is the *Drosophila* NMJ. Shakiryanova et al., 2005 using a post-

tetanus stimulation protocol that matched the native rhythmic bursting of *Drosophila* larval NMJ (Klose et al., 2005) showed that DCV mobilization is a priming step for DCV exocytosis and that the DCV movements are random and depend on Ca^{2+} influx through Ca_v channels (Shakiryanova et al., 2005). Furthermore, pharmacologically blocking the intracellular Ca^{2+} store (ER) by inhibiting RyR and SERCA, the Ca^{2+}-ATPase, diminished DCV mobilization and release of neuropeptide in *Drosophila* motor neuron boutons. This evidence showed that Ca^{2+} influx through Ca_v channels cannot induce normal DCV mobilization and subsequent normal release on its own but requires release of Ca^{2+} from the ER perhaps involving calcium induced calcium release (CICR) (Shakiryanova et al., 2007; Shakiryanova et al., 2005). Thus neuropeptide release at the *Drosophila* NMJ may require Ca^{2+} influx through Ca_V and subsequent CICR.

1.5 Regulation of Ca_v channels

This Dissertation describes a novel regulator of Ca_V channels in neurons. Here we summarize some known aspects of Ca_V channel regulation.

1.5.1 Regulation by auxiliary subunits

The Ca_v channels are structured by the channel-forming subunit, α_1, and other auxiliary subunits β, γ, and $\alpha_2\delta$. In mammals, four genes encode the β subunits, 10 genes for the γ subunits, and four genes for the $\alpha_2\delta$ subunits. *Drosophila melanogaster* have one gene for the β subunit, three genes for $\alpha_2\delta$ subunits and possibly one gene for the γ subunit (Littleton and Ganetzky, 2000). The L-type Ca_v channel was the first to be purified from T tubules of skeletal muscles due to its high affinity binding with dihydropyridines. Protein electrophoresis of the

purified Ca_v channels from T tubules showed five distinct bands: α_1 (~175 kDa), β (~54 kDa), γ (~32 kDa), α_2 (~150 kDa), δ (17-25 kDa). The α_1 subunit was confirmed to be a pore-forming subunit because of its specific affinity to dihydropyridines and the blockage of channel function by dihydropyridines (Curtis and Catterall, 1984; Tanabe et al., 1987).

The mammalian β subunits, β1-4, are expressed differentially to regulate their corresponding α_1 subunits. β1 is only present in skeletal muscles and essential for EC coupling (Ruth et al., 1989). β2 is found in cardiac muscles (Hullin et al., 1992). β3 and β4 are expressed in the CNS (Castellano et al., 1993). Voltage-clamp recording of Xenopus oocytes co-expressing $Ca_v1.2$ and a β subunit showed larger $Ca_v1.2$ Ca^{2+} currents compared with oocytes expressing $Ca_v1.2$ alone (Shistik et al., 1995) and that the β subunit shifted the voltage-dependency of $Ca_v1.2$ to more hyperpolarized potentials, and increased the activation rate of $Ca_v1.2$ (Wei et al., 1991). Crystal structures of the β subunits showed a SH3 (Src Homology 3) domain and a guanylase kinase domain (Cheng et al., 2005; Opatowsky et al., 2004; Van Petegem et al., 2004). A screen of Ca_v1 epitope library and crystallography showed that the Alpha Interaction Domain (AID) within the intracellular loop I-II of Ca_v1 binds with a conserved hydrophobic sequence in the guanylase kinase domain of the β subunits (Chen et al., 2004; Opatowsky et al., 2004; Pragnell et al., 1994; Van Petegem et al., 2004) and via this interaction β subunits accelerate voltage-dependent activation and inactivation of the Ca_v channels (He et al., 2007; Varadi et al., 1991). AID is conserved in both Ca_v1 and Ca_v2 and binds to all four β subunits (De Waard et al., 1995). Crystal structures suggest that the SH3 domain of β subunits likely interacts with guanylase kinase domain for intramolecular binding (Chen et al., 2004). Furthermore, it was

found that the SH3 domain of β1 might bind intramolecularly with a motif within its own C terminus and this interaction is necessary for proper EC coupling of skeletal muscles (Dayal et al., 2013).

In mammals, the $\alpha_2\delta$ subunits are encoded by 4 genes, $\alpha_2\delta$-1, $\alpha_2\delta$-2, $\alpha_2\delta$-3, and $\alpha_2\delta$-4. The α_2 subunit was found to bind the δ subunit through disulfide bonds and it was demonstrated later that the two subunits are expressed from the same gene (De Jongh et al., 1990). The $\alpha_2\delta$-1 was found to express at the T tubules of skeletal muscles where $\alpha_2\delta$-1 interacts with $Ca_v1.1$, and in cardiac muscles and smooth muscles where $\alpha_2\delta$-1 interacts $Ca_v1.2$ (Chang and Hosey, 1988; Ellis et al., 1988). The $\alpha_2\delta$-1, $\alpha_2\delta$-2, $\alpha_2\delta$-3 subunits are widely expressed in the CNS and $\alpha_2\delta$-1 is expressed in DRG neurons and many other neuron types and in the excitatory presynapses (Cole et al., 2005). $\alpha_2\delta$-2 expression correlates partially with GABAergic neurons such as Purkinje cells (Brodbeck et al., 2002). $\alpha_2\delta$-3 is expressed throughout the brain including hippocampus, cerebral cortex, and caudate putamen (Cole et al., 2005). Different from the other 3 members, $\alpha_2\delta$-4 was expressed in endocrine cells and at low levels in the brain (Qin et al., 2002).

The *Drosophila* $\alpha_2\delta$-3 homolog, *Straitjacket*, was shown to interact with *Dmca1A*, the *Drosophila* homolog of Ca_v2 channels that regulates transmitter release. The null mutation of *Straitjacket* is embryonic lethal and the lethality can be rescued by expressing wild type *Straitjacket* in the CNS, suggesting a neuronal function for $\alpha_2\delta$-3. A *Straitjacket* hypomorph mutation led to a large reduction in evoked synaptic potential at the NMJ, suggesting that $\alpha_2\delta$-3 is necessary for transmitter release (Dickman et al., 2008) . Moreover, the level of *Dmca1A* at

the active zone was reduced in *Straitjacket* hypomorph mutants, but neuronal overexpression of *Dmca1A* in *Straitjacket* null failed to rescue the evoked synaptic potential, suggesting that the mutant phenotype is not due to a decrease in Dmca1A.

Electron-microscopy and crystallography evidence showed that the $\alpha_2\delta$ subunits have the von Willebrand actor A domain (VWA domain) that generally is involved in protein-protein interaction and it's very likely that the $\alpha_2\delta$ subunits interact with proteins upon divalent cation-dependent complex formation (Cantí et al., 2005; Wu et al., 2016; Wu et al., 2015). Specifically, the extracellular metal ion-dependent adhesion site (MIDAS) motif within this domain is found to be important in protein interaction and SSV exocytosis. Overexpression of $\alpha_2\delta$-1, $\alpha_2\delta$-2 and $\alpha_2\delta$-3 individually in hippocampal neurons all led to an increase in vesicle exocytosis probability in response to a single action potential. Consistent with the *Drosophila* study, endogenous level of Ca_v2 was increased in hippocampal neurons that were overexpressed with the $\alpha_2\delta$ subunits (Hoppa et al., 2012). These studies demonstrated the critical role of $\alpha_2\delta$ subunits for normal function of Ca_v2 and thus SSV exocytosis.

1.5.2 Regulation by calmodulin and phosphoinositides

The Ca_v channels are controlled by Ca^{2+} dependent facilitation (CDF) and Ca^{2+} dependent inactivation (CDI). Such positive and negative feedback mechanism keeps ionic homeostasis and controls cell excitability. CDF amplifies Ca^{2+} influx following depolarization followed by CDI to block Ca^{2+} influx. Calmodulin is the key regulator for both CDF and CDI by interacting with the IQ domain of Ca_v channels (Van Petegem et al., 2005; Zühlke et al., 1999). The proposed model is

that N- and C-termini of calmodulin allosterically binds with the C terminus of Ca_v channels to biphasically control CDF and CDI (Lee et al., 2003). Ca^{2+} binding to calmodulin induced clustering of $Ca_v1.2$ and increased Ca^{2+} influx in cardiac myocytes (Dixon et al., 2015). The Ca^{2+}-calmodulin induced clustering of Ca_v channels and CDF was also observed in the short isoform of neuronal $Ca_v1.3$ in hippocampal neurons (Moreno et al., 2016).

$PI(4,5)P_2$ is the most abundant phosphoinositide in the membrane and regulates many plasma membrane associated proteins and activities. Chromaffin cells that were treated with phospholipase C and thus had reduced amounts of $PI(4,5)P_2$ showed inhibited Ca^{2+} dependent catecholamine secretion (Eberhard et al., 1990), the first evidence showing that $PI(4,5)P_2$ regulates exocytosis of DCV. $PI(4,5)P_2$ localizes at the plasma membrane as patches that partially colocalize with DCVs (James et al., 2008) and is involved in the priming steps for DCV exocytosis (Grishanin et al., 2004). Depleting $PI(4,5)P_2$ in cells that heterologously expressed $Ca_v1.3$ or $Ca_v2.2$ depressed voltage-gated Ca^{2+} currents (Suh et al., 2010). Optogenetically depleting $PI(4,5)P_2$ in pancreatic B cells also showed an inhibition of L-type Ca_v currents and subsequent release of insulin (Xie et al., 2016). These studies suggest that $PI(4,5)P_2$ regulates Ca_v1 channels and Ca^{2+} dependent exocytosis.

1.6 Regulation of Ca_v1 by Stac proteins

The *stac* gene family consist of three members, *stac1*, *stac2* and *stac3*. *stac1* was discovered by systematic scanning the methylation status of the proteins from the mouse brain in high resolutions two dimensional gels and found to contain a cysteine-rich domain (CRD) and

a Src homology 3 (SH3) domain (Suzuki et al., 1996), which are the defining features of stac proteins. *In situ* hybridization showed that *stac1* mRNA was selectively expressed in a subset of neurons such as the CA1 and dentate gyrus neurons in hippocampus, Purkinje cells in cerebellum, and inferior olive neurons in the medulla oblongata. Subsequent research showed that *stac1* and *stac2* were expressed by subsets of DRG neurons in a mutually exclusive fashion. *stac1* was expressed in nociceptive peptidergic neurons while *stac2* in a subset of non-peptidergic Ret+ neurons, in all TrkB+ neurons and in a subset of TrkC+ neurons (Legha et al., 2010). The entire expression patterns of *stac1* and *stac2* in subsets of neurons can be seen in the Allen Brain Library project (Lein et al., 2007). *stac3* was identified from a mutagenesis screen in zebrafish to be expressed specifically by skeletal muscles that is required for muscle contractions (Horstick et al., 2013). *stac3* is also selectively expressed by skeletal muscles and required for contractions in the mouse (Nelson et al., 2013). The importance of *stac3* in skeletal muscle contraction is underscored by the discovery that a point mutation in the first SH3 domain of human *STAC3* gene where a tryptophan is transferred to a serine is the basis of a debilitating congenital muscle disease, Native American Myopathy (NAM) (Horstick et al., 2013; Stamm et al., 2008a; Stamm et al., 2008b). Subsequent research reported that compound heterogeneous mutations of *STAC3* leading to truncated or missense Stac3 proteins were found in individuals with non-Amerindian decent (Grzybowski et al., 2017; Telegrafi et al., 2017).

stac3 regulation of muscle contraction has been demonstrated in several systems including the powerful zebrafish model using behavioral, biochemical, electrophysiological, imaging and genetic approaches. The homozygous *stac3* null zebrafish embryos display very

little movement and can't swim forward in response to touch and eventually died around 7 days post fertilization due to a defect in EC coupling (Horstick et al., 2013). Furthermore, *stac3* null zebrafish expressing the NAM allele of *stac3* also exhibited defects in swimming. This is not surprising since NAM patients display muscle weakness and 36% mortality by age 18 (Stamm et al., 2008a). Research using the *stac3* null zebrafish and NAM zebrafish model demonstrated that Stac3 is crucial in regulating EC coupling. Co-immunolabeling of Stac3, $Ca_v1.1$ and RyR with antibodies showed that Stac3 colocalized with $Ca_v1.1$ and RyR at triads, the sites within skeletal muscles where the T tubules are in contact with the SR, which are the sites of EC coupling (Horstick et al., 2013). In *stac3* null and NAM mutants, depolarizing voltage steps initiated very little increases in cytosolic Ca^{2+} due to defective regulation of $Ca_V1.1$ (Linsley et al., 2017). First, quantification of antibody labeled $Ca_V1.1$ at triads in skeletal muscles found a decrease in $Ca_V1.1$ in mutants. Second, freeze-fracture EM showed that Stac3 was required for normal levels of $Ca_V1.1$ particles in T tubules as well as formation of $Ca_V1.1$ into tetrads. Third, quantitative fluorescence imaging of skeletal muscles in zebrafish expressing a fusion of the photoconvertible mEOS protein with Stac3 in skeletal muscles found that Stac3 was required for the stability of $Ca_v1.1$. However, FRAP analysis demonstrated that *stac3* mutations did not interfere with the trafficking of $Ca_v1.1$. within skeletal muscles. Finally, electrophysiological recordings showed that Stac3 was required for the normal voltage response of $Ca_V1.1$. There was a significant decrease in the gating current of $Ca_v1.1$ in both null and NAM *stac3* muscles compared with controls. Thus Stac3 regulates the stability, tetrad formation and voltage response of $Ca_V1.1$ (Linsley et al., 2017).

Co-crystallization showed that the first SH3 domain of Stac2 binds with the II-III intracellular loop of $Ca_v1.2$ (Wong King Yuen et al., 2017). Binding between the second SH3 domain and the II-III intracellular loop was not observed, but it aids the binding affinity between the first SH3 and $Ca_v1.2$. The main chain of the $Ca_V1.1$ II-III loop sits in a "pocket" lined by the tryptophan residue of the first SH3 domain that was previously found to be disrupted in NAM (Wong King Yuen et al., 2017). The structural analysis and *stac3* NAM studies in the zebrafish model conclude that the interaction of Stac3 SH3 and $Ca_v1.1$ loop II-III regulates EC coupling (Linsley et al., 2017; Wong King Yuen et al., 2017).

From heterologous expression experiments, it was found that Stac proteins inhibit CDI by interacting with an upstream region of IQ domain in the C terminus of Ca_v1, while CDI of Ca_v2 was unaffected by Stac (Niu et al., 2018). Two-hybrid FRET assays showed that Stac proteins don't compete with calmodulin to bind with the Ca_v1 channels, suggesting that Stac and calmodulin modify CDI via distinct sites on C terminus of Ca_v1 channels. A new unknown motif (U motif) in the linker between the CRD and SH3 domain was proposed to be crucial in suppressing CDI since pipette dialysis of U motif peptide to adult guinea pig ventricular myocytes that endogenously express Stac2 reduced CDI of endogenous $Ca_v1.2$ (Niu et al., 2018). Since $Ca_v1.2$ in cardiac muscles conducts Ca^{2+} that triggers intracellular Ca^{2+} release from the SR, this cardiac $Ca_v1.2$ regulation by Stac2 implies that Stac proteins can modulate Ca^{2+} induced Ca^{2+} release.

Despite the relatively well understood role of Stac3 in vertebrate skeletal muscles, the role of neuronal Stac proteins was completely unknown. By analogy with Stac3 in vertebrate

skeletal muscles, it is reasonable to predict that neuronal Stac proteins regulate L-type Ca_v channels in the CNS. Given the importance of neuronal L-type Ca_v channels in regulating many cellular events including DCV exocytosis, the hypothesized neuronal Stac regulation of neuronal L-type Ca_v channels predicts that Stac proteins might regulate DCV exocytosis via regulation of L-type Ca_v channels. The goal of this dissertation research is to clarify the function of Stac proteins in neurons by identifying and examining the function of a Stac protein in *Drosophila*, which will allow for utilization of the powerful toolbox of methods of *Drosophila melanogaster*.

1.7 References

Abderemane-Ali, F., Findeisen, F., Rossen, N.D., and Minor, D.L. (2019). A Selectivity Filter Gate Controls Voltage-Gated Calcium Channel Calcium-Dependent Inactivation. Neuron 101, 1134-1149.e1133.

Adams, B.A., Tanabe, T., Mikami, A., Numa, S., and Beam, K.G. (1990). Intramembrane charge movement restored in dysgenic skeletal muscle by injection of dihydropyridine receptor cDNAs. Nature 346, 569-572.

Adolfsen, B., Saraswati, S., Yoshihara, M., and Littleton, J.T. (2004). Synaptotagmins are trafficked to distinct subcellular domains including the postsynaptic compartment. The Journal of cell biology 166, 249-260.

Akiyama, T., Yamazaki, T., Mori, H., and Sunagawa, K. (2004). Effects of Ca2+ channel antagonists on acetylcholine and catecholamine releases in the in vivo rat adrenal medulla. Am J Physiol Regul Integr Comp Physiol 287, R161-166.

Alés, E., Tabares, L., Poyato, J.M., Valero, V., Lindau, M., and Alvarez de Toledo, G. (1999). High calcium concentrations shift the mode of exocytosis to the kiss-and-run mechanism. Nat Cell Biol 1, 40-44.

Alvarez de Toledo, G., Fernández-Chacón, R., and Fernández, J.M. (1993). Release of secretory products during transient vesicle fusion. Nature 363, 554-558.

Argibay, J.A., Fischmeister, R., and Hartzell, H.C. (1988). Inactivation, reactivation and pacing dependence of calcium current in frog cardiocytes: correlation with current density. J Physiol 401, 201-226.

Armstrong, C.M., Bezanilla, F.M., and Horowicz, P. (1972). Twitches in the presence of ethylene glycol bis(β -aminoethyl ether)-N,N ´ -tetraacetic acid. Biochimica et Biophysica Acta (BBA) - Bioenergetics 267, 605-608.

Armstrong, C.M., and Matteson, D.R. (1985). Two distinct populations of calcium channels in a clonal line of pituitary cells. Science 227, 65-67.

Baines, R.A., and Bate, M. (1998). Electrophysiological development of central neurons in the Drosophila embryo. The Journal of neuroscience : the official journal of the Society for Neuroscience 18, 4673-4683.

Bannister, R.A., and Beam, K.G. (2009). Ryanodine modification of RyR1 retrogradely affects L-type Ca2+ channel gating in skeletal muscle. Journal of Muscle Research and Cell Motility 30, 217-223.

Block, B.A., Imagawa, T., Campbell, K.P., and Franzini-Armstrong, C. (1988). Structural evidence for direct interaction between the molecular components of the transverse tubule/sarcoplasmic reticulum junction in skeletal muscle. The Journal of cell biology 107, 2587-2600.

Bokvist, K., Eliasson, L., Ammälä, C., Renström, E., and Rorsman, P. (1995). Co-localization of L-type Ca2+ channels and insulin-containing secretory granules and its significance for the initiation of exocytosis in mouse pancreatic B-cells. The EMBO Journal 14, 50-57.

Brandt, A., Striessnig, J., and Moser, T. (2003). CaV1.3 channels are essential for development and presynaptic activity of cochlear inner hair cells. The Journal of neuroscience : the official journal of the Society for Neuroscience 23, 10832-10840.

Brodbeck, J., Davies, A., Courtney, J.-M., Meir, A., Balaguero, N., Canti, C., Moss, F.J., Page, K.M., Pratt, W.S., Hunt, S.P*., et al.* (2002). The Ducky Mutation in Cacna2d2 Results in Altered Purkinje Cell Morphology and Is Associated with the Expression of a Truncated α2δ-2 Protein with Abnormal Function. Journal of Biological Chemistry 277, 7684-7693.

Burgoyne, R.D. (1991). Control of exocytosis in adrenal chromaffin cells. Biochimica et Biophysica Acta (BBA) - Reviews on Biomembranes 1071, 174-202.

Cantí, C., Nieto-Rostro, M., Foucault, I., Heblich, F., Wratten, J., Richards, M.W., Hendrich, J., Douglas, L., Page, K.M., Davies, A., and Dolphin, A.C. (2005). The metal-ion-dependent adhesion site in the Von Willebrand factor-A domain of alpha2delta subunits is key to trafficking voltage-gated Ca2+ channels. Proc Natl Acad Sci U S A 102, 11230-11235.

Castellano, A., Wei, X., Birnbaumer, L., and Perez-Reyes, E. (1993). Cloning and expression of a neuronal calcium channel beta subunit. The Journal of biological chemistry 268, 12359-12366.

Cauvin, C., Loutzenhiser, R., and Van Breemen, C. (1983). Mechanisms of calcium antagonist-induced vasodilation. Annual review of pharmacology and toxicology 23, 373-396.

Chang, F.C., and Hosey, M.M. (1988). Dihydropyridine and phenylalkylamine receptors associated with cardiac and skeletal muscle calcium channels are structurally different. The Journal of biological chemistry 263, 18929-18937.

Chen, Y.H., Li, M.H., Zhang, Y., He, L.L., Yamada, Y., Fitzmaurice, A., Shen, Y., Zhang, H., Tong, L., and Yang, J. (2004). Structural basis of the alpha1-beta subunit interaction of voltage-gated Ca2+ channels. Nature 429, 675-680.

Cheng, W., Altafaj, X., Ronjat, M., and Coronado, R. (2005). Interaction between the dihydropyridine receptor Ca2+ channel beta-subunit and ryanodine receptor type 1 strengthens excitation-contraction coupling. Proc Natl Acad Sci U S A 102, 19225-19230.

Cohen, C.J., McCarthy, R.T., Barrett, P.Q., and Rasmussen, H. (1988). Ca channels in adrenal glomerulosa cells: K+ and angiotensin II increase T-type Ca channel current. Proc Natl Acad Sci U S A 85, 2412-2416.

Cole, R.L., Lechner, S.M., Williams, M.E., Prodanovich, P., Bleicher, L., Varney, M.A., and Gu, G. (2005). Differential distribution of voltage-gated calcium channel alpha-2 delta (alpha2delta) subunit mRNA-containing cells in the rat central nervous system and the dorsal root ganglia. J Comp Neurol 491, 246-269.

Collet, C. (2009). Excitation-contraction coupling in skeletal muscle fibers from adult domestic honeybee. Pflugers Arch 458, 601-612.

Cowley, M.A., Smart, J.L., Rubinstein, M., Cerdan, M.G., Diano, S., Horvath, T.L., Cone, R.D., and Low, M.J. (2001). Leptin activates anorexigenic POMC neurons through a neural network in the arcuate nucleus. Nature 411, 480-484.

Curtis, B.M., and Catterall, W.A. (1984). Purification of the calcium antagonist receptor of the voltage-sensitive calcium channel from skeletal muscle transverse tubules. Biochemistry 23, 2113-2118.

Dayal, A., Bhat, V., Franzini-Armstrong, C., and Grabner, M. (2013). Domain cooperativity in the β1a subunit is essential for dihydropyridine receptor voltage sensing in skeletal muscle. Proc Natl Acad Sci U S A 110, 7488-7493.

Dayal, A., Schrötter, K., Pan, Y., Föhr, K., Melzer, W., and Grabner, M. (2017). The Ca2+ influx through the mammalian skeletal muscle dihydropyridine receptor is irrelevant for muscle performance. Nature Communications 8, 475.

De Jongh, K.S., Warner, C., and Catterall, W.A. (1990). Subunits of purified calcium channels. Alpha 2 and delta are encoded by the same gene. The Journal of biological chemistry 265, 14738-14741.

De Waard, M., Witcher, D.R., Pragnell, M., Liu, H., and Campbell, K.P. (1995). Properties of the alpha 1-beta anchoring site in voltage-dependent Ca2+ channels. The Journal of biological chemistry 270, 12056-12064.

Decavel, C., and Van den Pol, A.N. (1990). GABA: a dominant neurotransmitter in the hypothalamus. J Comp Neurol 302, 1019-1037.

Dickman, D.K., Kurshan, P.T., and Schwarz, T.L. (2008). Mutations in a Drosophila alpha2delta voltage-gated calcium channel subunit reveal a crucial synaptic function. The Journal of neuroscience : the official journal of the Society for Neuroscience 28, 31-38.

Dixon, R.E., Moreno, C.M., Yuan, C., Opitz-Araya, X., Binder, M.D., Navedo, M.F., and Santana, L.F. (2015). Graded Ca2+/calmodulin-dependent coupling of voltage-gated CaV1.2 channels. eLife 4, e05608.

Dooley, D.J., Lupp, A., and Hertting, G. (1987). Inhibition of central neurotransmitter release by ω-conotoxin GVIA, a peptide modulator of the N-type voltage-sensitive calcium channel. Naunyn-Schmiedeberg's Archives of Pharmacology 336, 467-470.

Dunlap, K., Luebke, J.I., and Turner, T.J. (1995). Exocytotic Ca2+ channels in mammalian central neurons. Trends in Neurosciences 18, 89-98.

Dutar, P., Rascol, O., and Lamour, Y. (1989). ω-Conotoxin GVIA blocks synaptic transmission in the CA1 field of the hippocampus. European Journal of Pharmacology 174, 261-266.

Eberhard, D.A., Cooper, C.L., Low, M.G., and Holz, R.W. (1990). Evidence that the inositol phospholipids are necessary for exocytosis. Loss of inositol phospholipids and inhibition of secretion in permeabilized cells caused by a bacterial phospholipase C and removal of ATP. Biochem J 268, 15-25.

Eberl, D.F., Ren, D., Feng, G., Lorenz, L.J., Van Vactor, D., and Hall, L.M. (1998). Genetic and developmental characterization of Dmca1D, a calcium channel α1 subunit gene in Drosophila melanogaster. Genetics 148, 1159-1169.

Efremov, R.G., Leitner, A., Aebersold, R., and Raunser, S. (2015). Architecture and conformational switch mechanism of the ryanodine receptor. Nature 517, 39-43.

Elhamdani, A., Azizi, F., and Artalejo, C.R. (2006). Double Patch Clamp Reveals That Transient Fusion (Kiss-and-Run) Is a Major Mechanism of Secretion in Calf Adrenal Chromaffin Cells: High Calcium Shifts the Mechanism from Kiss-and-Run to Complete Fusion. The Journal of Neuroscience 26, 3030-3036.

Ellis, S.B., Williams, M.E., Ways, N.R., Brenner, R., Sharp, A.H., Leung, A.T., Campbell, K.P., McKenna, E., Koch, W.J., Hui, A., and et al. (1988). Sequence and expression of mRNAs encoding the alpha 1 and alpha 2 subunits of a DHP-sensitive calcium channel. Science 241, 1661-1664.

Engisch, K., and Nowycky, M. (1996). Calcium dependence of large dense-cored vesicle exocytosis evoked by calcium influx in bovine adrenal chromaffin cells. The Journal of Neuroscience 16, 1359-1369.

Fabiato, A. (1983). Calcium-induced release of calcium from the cardiac sarcoplasmic reticulum. The American journal of physiology 245, C1-14.

Fabiato, A. (1992). Calcium-induced release of calcium from the cardiac sarcoplasmic reticulum. Journal of Molecular and Cellular Cardiology 24, 28.

Fernandez, I., Araç, D., Ubach, J., Gerber, S.H., Shin, O.H., Gao, Y., Anderson, R.G.W., Südhof, T.C., and Rizo, J. (2001). Three-dimensional structure of the synaptotagmin 1 C2B-domain: Synaptotagmin 1 as a phospholipid binding machine. Neuron 32, 1057-1069.

Fernández-Chacón, R., Königstorfer, A., Gerber, S.H., García, J., Matos, M.F., Stevens, C.F., Brose, N., Rizo, J., Rosenmund, C., and Südhof, T.C. (2001). Synaptotagmin I functions as a calcium regulator of release probability. Nature 410, 41-49.

Fischer von Mollard, G., Mignery, G.A., Baumert, M., Perin, M.S., Hanson, T.J., Burger, P.M., Jahn, R., and Südhof, T.C. (1990). rab3 is a small GTP-binding protein exclusively localized to synaptic vesicles. Proc Natl Acad Sci U S A 87, 1988-1992.

Fox, A.P., Nowycky, M.C., and Tsien, R.W. (1987). Kinetic and pharmacological properties distinguishing three types of calcium currents in chick sensory neurones. The Journal of Physiology 394, 149-172.

Franzini-Armstrong, C. (1970). STUDIES OF THE TRIAD : I. Structure of the Junction in Frog Twitch Fibers. The Journal of cell biology 47, 488-499.

Franzini-Armstrong, C., Protasi, F., and Ramesh, V. (1998). Comparative ultrastructure of Ca2+ release units in skeletal and cardiac muscle. Ann N Y Acad Sci 853, 20-30.

G P Miljanich, a., and Ramachandran, J. (1995). Antagonists of Neuronal Calcium Channels: Structure, Function, and Therapeutic Implications. Annual review of pharmacology and toxicology 35, 707-734.

Gielow, M., Gu, G., and Singh, S. (1995). Resolution and pharmacological analysis of the voltage-dependent calcium channels of Drosophila larval muscles. The Journal of Neuroscience 15, 6085-6093.

Gracheva, E.O., Hadwiger, G., Nonet, M.L., and Richmond, J.E. (2008). Direct interactions between C. elegans RAB-3 and Rim provide a mechanism to target vesicles to the presynaptic density. Neuroscience letters 444, 137-142.

Grishanin, R.N., Kowalchyk, J.A., Klenchin, V.A., Ann, K., Earles, C.A., Chapman, E.R., Gerona, R.R.L., and Martin, T.F.J. (2004). CAPS acts at a prefusion step in dense-core vesicle exocytosis as a PIP<inf>2</inf> binding protein. Neuron 43, 551-562.

Grzybowski, M., Schanzer, A., Pepler, A., Heller, C., Neubauer, B.A., and Hahn, A. (2017). Novel STAC3 Mutations in the First Non-Amerindian Patient with Native American Myopathy. Neuropediatrics 48, 451-455.

Györke, S., and Palade, P. (1992). Calcium-induced calcium release in crayfish skeletal muscle. J Physiol 457, 195-210.

Han, Y., Kaeser, P.S., Südhof, T.C., and Schneggenburger, R. (2011). RIM determines Ca^{2}+ channel density and vesicle docking at the presynaptic active zone. Neuron 69, 304-316.

Hata, Y., Slaughter, C.A., and Südhof, T.C. (1993). Synaptic vesicle fusion complex contains unc-18 homologue bound to syntaxin. Nature 366, 347-351.

He, L.L., Zhang, Y., Chen, Y.H., Yamada, Y., and Yang, J. (2007). Functional modularity of the beta-subunit of voltage-gated Ca2+ channels. Biophys J 93, 834-845.

Heron, S.E., Khosravani, H., Varela, D., Bladen, C., Williams, T.C., Newman, M.R., Scheffer, I.E., Berkovic, S.F., Mulley, J.C., and Zamponi, G.W. (2007). Extended spectrum of idiopathic generalized epilepsies associated with CACNA1H functional variants. Ann Neurol 62, 560-568.

Hibino, H., Pironkova, R., Onwumere, O., Vologodskaia, M., Hudspeth, A.J., and Lesage, F. (2002). RIM Binding Proteins (RBPs) Couple Rab3-Interacting Molecules (RIMs) to Voltage-Gated Ca2+ Channels. Neuron 34, 411-423.

Hoppa, M.B., Lana, B., Margas, W., Dolphin, A.C., and Ryan, T.A. (2012). α2δ expression sets presynaptic calcium channel abundance and release probability. Nature 486, 122-125.

Horne, A.L., and Kemp, J.A. (1991). The effect of ω-conotoxin GVIA on synaptic transmission within the nucleus accumbens and hippocampus of the rat in vitro. British Journal of Pharmacology 103, 1733-1739.

Horstick, E.J., Linsley, J.W., Dowling, J.J., Hauser, M.A., McDonald, K.K., Ashley-Koch, A., Saint-Amant, L., Satish, A., Cui, W.W., Zhou, W.*, et al.* (2013). Stac3 is a component of the excitation-contraction coupling machinery and mutated in Native American myopathy. Nature communications 4, 1952-1952.

Hullin, R., Singer-Lahat, D., Freichel, M., Biel, M., Dascal, N., Hofmann, F., and Flockerzi, V. (1992). Calcium channel beta subunit heterogeneity: functional expression of cloned cDNA from heart, aorta and brain. Embo j 11, 885-890.

James, D.J., Khodthong, C., Kowalchyk, J.A., and Martin, T.F. (2008). Phosphatidylinositol 4,5-bisphosphate regulates SNARE-dependent membrane fusion. The Journal of cell biology 182, 355-366.

Jan, L.Y., and Jan, Y.N. (1982). Peptidergic transmission in sympathetic ganglia of the frog. J Physiol 327, 219-246.

Jeong, K., Lee, S., Seo, H., Oh, Y., Jang, D., Choe, J., Kim, D., Lee, J.-H., and Jones, W.D. (2015). Ca-α1T, a fly T-type Ca2+ channel, negatively modulates sleep. Scientific Reports 5, 17893.

Jouvenceau, A., Eunson, L.H., Spauschus, A., Ramesh, V., Zuberi, S.M., Kullmann, D.M., and Hanna, M.G. (2001). Human epilepsy associated with dysfunction of the brain P/Q-type calcium channel. The Lancet 358, 801-807.

Kaeser, P.S., Deng, L., Wang, Y., Dulubova, I., Liu, X., Rizo, J., and Südhof, T.C. (2011). RIM proteins tether Ca2+ channels to presynaptic active zones via a direct PDZ-domain interaction. Cell 144, 282-295.

Kamiya, H., Sawada, S., and Yamamoto, C. (1988). Synthetic ω-conotoxin blocks synaptic transmission in the hippocampus in vitro. Neuroscience Letters 91, 84-88.

Kawasaki, F., Felling, R., and Ordway, R.W. (2000). A Temperature-Sensitive Paralytic Mutant Defines a Primary Synaptic Calcium Channel in Drosophila. The Journal of Neuroscience 20, 4885-4889.

Kawasaki, F., Zou, B., Xu, X., and Ordway, R.W. (2004). Active zone localization of presynaptic calcium channels encoded by the cacophony locus of Drosophila. The Journal of neuroscience : the official journal of the Society for Neuroscience 24, 282-285.

Klose, M.K., Chu, D., Xiao, C., Seroude, L., and Robertson, R.M. (2005). Heat Shock–Mediated Thermoprotection of Larval Locomotion Compromised by Ubiquitous Overexpression of Hsp70 in Drosophila melanogaster. Journal of Neurophysiology 94, 3563-3572.

Kostyuk, P.G., Shuba, Y.M., and Savchenko, A.N. (1988). Three types of calcium channels in the membrane of mouse sensory neurons. Pflügers Archiv European Journal of Physiology 411, 661-669.

Lai, F.A., Erickson, H.P., Rousseau, E., Liu, Q.Y., and Meissner, G. (1988). Purification and reconstitution of the calcium release channel from skeletal muscle. Nature 331, 315-319.

Lee, A., Zhou, H., Scheuer, T., and Catterall, W.A. (2003). Molecular determinants of Ca(2+)/calmodulin-dependent regulation of Ca(v)2.1 channels. Proc Natl Acad Sci U S A 100, 16059-16064.

Lee, J., Kim, D., and Shin, H.S. (2004). Lack of delta waves and sleep disturbances during non-rapid eye movement sleep in mice lacking alpha1G-subunit of T-type calcium channels. Proc Natl Acad Sci U S A 101, 18195-18199.

Legha, W., Gaillard, S., Gascon, E., Malapert, P., Hocine, M., Alonso, S., and Moqrich, A. (2010). Stac1 and stac2 genes define discrete and distinct subsets of dorsal root ganglia neurons. Gene Expression Patterns 10, 368-375.

Lein, E.S., Hawrylycz, M.J., Ao, N., Ayres, M., Bensinger, A., Bernard, A., Boe, A.F., Boguski, M.S., Brockway, K.S., Byrnes, E.J*., et al.* (2007). Genome-wide atlas of gene expression in the adult mouse brain. Nature 445, 168-176.

Li, C., Ullrich, B., Zhang, J.Z., Anderson, R.G.W., Brose, N., and Südhof, T.C. (1995). Ca2+-dependent and -independent activities of neural and non-neural synaptotagmins. Nature 375, 594-599.

Linsley, J.W., Hsu, I.U., Groom, L., Yarotskyy, V., Lavorato, M., Horstick, E.J., Linsley, D., Wang, W., Franzini-Armstrong, C., Dirksen, R.T., and Kuwada, J.Y. (2017). Congenital myopathy results from misregulation of a muscle Ca2+ channel by mutant Stac3. Proc Natl Acad Sci U S A 114, E228-E236.

Littleton, J.T., and Ganetzky, B. (2000). Ion channels and synaptic organization: analysis of the Drosophila genome. Neuron 26, 35-43.

Liu, K.S., Siebert, M., Mertel, S., Knoche, E., Wegener, S., Wichmann, C., Matkovic, T., Muhammad, K., Depner, H., Mettke, C*., et al.* (2011). RIM-binding protein, a central part of the active zone, is essential for neurotransmitter release. Science 334, 1565-1569.

Mangoni, M.E., Couette, B., Bourinet, E., Platzer, J., Reimer, D., Striessnig, J., and Nargeot, J. (2003). Functional role of L-type Cav1.3 Ca2+ channels in cardiac pacemaker activity. Proc Natl Acad Sci U S A 100, 5543-5548.

McMahon, H.T., and Südhof, T.C. (1995). Synaptic core complex of synaptobrevin, syntaxin, and SNAP25 forms high affinity alpha-SNAP binding site. The Journal of biological chemistry 270, 2213-2217.

Monnier, N., Procaccio, V., Stieglitz, P., and Lunardi, J. (1997). Malignant-hyperthermia susceptibility is associated with a mutation of the alpha 1-subunit of the human dihydropyridine-sensitive L-type voltage-dependent calcium-channel receptor in skeletal muscle. American journal of human genetics 60, 1316-1325.

Moreno, C.M., Dixon, R.E., Tajada, S., Yuan, C., Opitz-Araya, X., Binder, M.D., and Santana, L.F. (2016). Ca2+ entry into neurons is facilitated by cooperative gating of clustered CaV1.3 channels. eLife 5, e15744.

Morris, J.F., and Cannata, M.A. (1973). Ultrastructural preservation of the dense core of posterior pituitary neurosecretory granules and its implications for hormone release. J Endocrinol 57, 517-529.

Nakai, J., Dirksen, R.T., Nguyen, H.T., Pessah, I.N., Beam, K.G., and Allen, P.D. (1996). Enhanced dihydropyridine receptor channel activity in the presence of ryanodine receptor. Nature 380, 72-75.

Nanou, E., and Catterall, W.A. (2018). Calcium Channels, Synaptic Plasticity, and Neuropsychiatric Disease. Neuron 98, 466-481.

Nassel, D.R., and Zandawala, M. (2019). Recent advances in neuropeptide signaling in Drosophila, from genes to physiology and behavior. Prog Neurobiol 179, 101607.

Neher, E., and Marty, A. (1982). Discrete changes of cell membrane capacitance observed under conditions of enhanced secretion in bovine adrenal chromaffin cells. Proceedings of the National Academy of Sciences 79, 6712-6716.

Nelson, B.R., Wu, F., Liu, Y., Anderson, D.M., McAnally, J., Lin, W., Cannon, S.C., Bassel-Duby, R., and Olson, E.N. (2013). Skeletal muscle-specific T-tubule protein STAC3 mediates voltage-induced Ca2+ release and contractility. Proceedings of the National Academy of Sciences of the United States of America 110, 11881-11886.

Niu, J., Dick, I.E., Yang, W., Bamgboye, M.A., Yue, D.T., Tomaselli, G., Inoue, T., and Ben-Johny, M. (2018). Allosteric regulators selectively prevent Ca(2+)-feedback of CaV and NaV channels. Elife 7.

Nowycky, M.C., Fox, A.P., and Tsien, R.W. (1985). Three types of neuronal calcium channel with different calcium agonist sensitivity. Nature 316, 440-443.

Ohnuma, K., Whim, M.D., Fetter, R.D., Kaczmarek, L.K., and Zucker, R.S. (2001). Presynaptic target of Ca2+ action on neuropeptide and acetylcholine release in Aplysia californica. J Physiol 535, 647-662.

Okamoto, M., and Südhof, T.C. (1997). Mints, Munc18-interacting proteins in synaptic vesicle exocytosis. The Journal of biological chemistry 272, 31459-31464.

Olivera, B.M., Miljanich, G.P., Ramachandran, J., and Adams, M.E. (1994). CALCIUM CHANNEL DIVERSITY AND NEUROTRANSMITTER RELEASE: The ω-Conotoxins and ω-Agatoxins. Annual Review of Biochemistry 63, 823-867.

Opatowsky, Y., Chen, C.C., Campbell, K.P., and Hirsch, J.A. (2004). Structural analysis of the voltage-dependent calcium channel beta subunit functional core and its complex with the alpha 1 interaction domain. Neuron 42, 387-399.

Pang, Z.P., Shin, O.-H., Meyer, A.C., Rosenmund, C., and Südhof, T.C. (2006). A Gain-of-Function Mutation in Synaptotagmin-1 Reveals a Critical Role of Ca²⁺-Dependent Soluble N-Ethylmaleimide-Sensitive Factor Attachment Protein Receptor Complex Binding in Synaptic Exocytosis. The Journal of Neuroscience 26, 12556-12565.

Persoon, C.M., Hoogstraaten, R.I., Nassal, J.P., van Weering, J.R.T., Kaeser, P.S., Toonen, R.F., and Verhage, M. (2019). The RAB3-RIM Pathway Is Essential for the Release of Neuromodulators. Neuron 104, 1065-1080.e1012.

Pragnell, M., De Waard, M., Mori, Y., Tanabe, T., Snutch, T.P., and Campbell, K.P. (1994). Calcium channel beta-subunit binds to a conserved motif in the I-II cytoplasmic linker of the alpha 1-subunit. Nature 368, 67-70.

Qin, N., Yagel, S., Momplaisir, M.L., Codd, E.E., and D'Andrea, M.R. (2002). Molecular cloning and characterization of the human voltage-gated calcium channel alpha(2)delta-4 subunit. Mol Pharmacol 62, 485-496.

Ren, D., Xu, H., Eberl, D.F., Chopra, M., and Hall, L.M. (1998). A mutation affecting dihydropyridine-sensitive current levels and activation kinetics in Drosophila muscle and mammalian heart calcium channels. Journal of Neuroscience 18, 2335-2341.

Rettig, J., Heinemann, C., Ashery, U., Sheng, Z.H., Yokoyama, C.T., Catterall, W.A., and Neher, E. (1997). Alteration of Ca2+ dependence of neurotransmitter release by disruption of Ca2+ channel/syntaxin interaction. Journal of Neuroscience 17, 6647-6656.

Rios, E., and Brum, G. (1987). Involvement of dihydropyridine receptors in excitation–contraction coupling in skeletal muscle. Nature 325, 717-720.

Roderick, H.L., Berridge, M.J., and Bootman, M.D. (2003). Calcium-induced calcium release. Current Biology 13, R425.

Ruth, P., Röhrkasten, A., Biel, M., Bosse, E., Regulla, S., Meyer, H.E., Flockerzi, V., and Hofmann, F. (1989). Primary structure of the beta subunit of the DHP-sensitive calcium channel from skeletal muscle. Science 245, 1115-1118.

Ryglewski, S., Lance, K., Levine, R.B., and Duch, C. (2012). Ca(v)2 channels mediate low and high voltage-activated calcium currents in Drosophila motoneurons. The Journal of physiology 590, 809-825.

Sabatini, B.L., and Regehr, W.G. (1999). Timing of synaptic transmission. Annu Rev Physiol 61, 521-542.

Schlüter, O.M., Khvotchev, M., Jahn, R., and Südhof, T.C. (2002). Localization versus function of Rab3 proteins: Evidence for a common regulatory role in controlling fusion. Journal of Biological Chemistry 277, 40919-40929.

Schonn, J.-S., Maximov, A., Lao, Y., Südhof, T.C., and Sørensen, J.B. (2008). Synaptotagmin-1 and -7 are functionally overlapping Ca²⁺ sensors for exocytosis in adrenal chromaffin cells. Proceedings of the National Academy of Sciences 105, 3998-4003.

Schramm, M., Thomas, G., Towart, R., and Franckowiak, G. (1983). Novel dihydropyridines with positive inotropic action through activation of Ca2+ channels. Nature 303, 535-537.

Schredelseker, J., Shrivastav, M., Dayal, A., and Grabner, M. (2010). Non–Ca²⁺-conducting Ca²⁺ channels in fish skeletal muscle excitation-contraction coupling. Proceedings of the National Academy of Sciences 107, 5658-5663.

Seward, E., Chernevskaya, N., and Nowycky, M. (1995). Exocytosis in peptidergic nerve terminals exhibits two calcium- sensitive phases during pulsatile calcium entry. The Journal of Neuroscience 15, 3390-3399.

Shakiryanova, D., Klose, M.K., Zhou, Y., Gu, T., Deitcher, D.L., Atwood, H.L., Hewes, R.S., and Levitan, E.S. (2007). Presynaptic ryanodine receptor-activated calmodulin kinase II increases vesicle mobility and potentiates neuropeptide release. Journal of Neuroscience 27, 7799-7806.

Shakiryanova, D., Tully, A., Hewes, R.S., Deitcher, D.L., and Levitan, E.S. (2005). Activity-dependent liberation of synaptic neuropeptide vesicles. Nature Neuroscience 8, 173-178.

Shistik, E., Ivanina, T., Puri, T., Hosey, M., and Dascal, N. (1995). Ca2+ current enhancement by alpha 2/delta and beta subunits in Xenopus oocytes: contribution of changes in channel gating and alpha 1 protein level. J Physiol 489 (Pt 1), 55-62.

Singh, S., and Wu, C.F. (1990). Properties of potassium currents and their role in membrane excitability in Drosophila larval muscle fibers. The Journal of experimental biology 152, 59-76.

Smirnov, S.V., Zholos, A.V., and Shuba, M.F. (1992). Potential-dependent inward currents in single isolated smooth muscle cells of the rat ileum. J Physiol 454, 549-571.

Sørensen, J.B., Fernández-Chacón, R., Südhof, T.C., and Neher, E. (2003). Examining synaptotagmin 1 function in dense core vesicle exocytosis under direct control of Ca2+. J Gen Physiol 122, 265-276.

Splawski, I., Timothy, K.W., Decher, N., Kumar, P., Sachse, F.B., Beggs, A.H., Sanguinetti, M.C., and Keating, M.T. (2005). Severe Arrhythmia Disorder Caused by Cardiac L-Type Calcium Channel Mutations. Proceedings of the National Academy of Sciences of the United States of America 102, 8089-8096.

Stamm, D.S., Aylsworth, A.S., Stajich, J.M., Kahler, S.G., Thorne, L.B., Speer, M.C., and Powell, C.M. (2008a). Native American myopathy: congenital myopathy with cleft palate, skeletal anomalies, and susceptibility to malignant hyperthermia. Am J Med Genet A 146a, 1832-1841.

Stamm, D.S., Powell, C.M., Stajich, J.M., Zismann, V.L., Stephan, D.A., Chesnut, B., Aylsworth, A.S., Kahler, S.G., Deak, K.L., Gilbert, J.R., and Speer, M.C. (2008b). Novel congenital myopathy locus identified in Native American Indians at 12q13.13-14.1. Neurology 71, 1764-1769.

Strom, T.M., Nyakatura, G., Apfelstedt-Sylla, E., Hellebrand, H., Lorenz, B., Weber, B.H.F., Wutz, K., Gutwillinger, N., Rüther, K., Drescher, B.*, et al.* (1998). An L-type calcium-channel gene mutated in incomplete X-linked congenital stationary night blindness. Nature Genetics 19, 260-263.

Suh, B.-C., Leal, K., and Hille, B. (2010). Modulation of High-Voltage Activated Ca2+ Channels by Membrane Phosphatidylinositol 4,5-Bisphosphate. Neuron 67, 224-238.

Sun, J., Pang, Z.P., Qin, D., Fahim, A.T., Adachi, R., and Südhof, T.C. (2007). A dual-Ca2+-sensor model for neurotransmitter release in a central synapse. Nature 450, 676-682.

Sutton, R.B., Davletov, B.A., Berghuis, A.M., Sudhof, T.C., and Sprang, S.R. (1995). Structure of the first C2 domain of synaptotagmin I: A novel Ca2+/phospholipid-binding fold. Cell 80, 929-938.

Suzuki, H., Kawai, J., Taga, C., Yaoi, T., Hara, A., Hirose, K., Hayashizaki, Y., and Watanabe, S. (1996). Stac, a novel neuron-specific protein with cysteine-rich and SH3 domains. Biochem Biophys Res Commun 229, 902-909.

Takekura, H., Bennett, L., Tanabe, T., Beam, K.G., and Franzini-Armstrong, C. (1994). Restoration of junctional tetrads in dysgenic myotubes by dihydropyridine receptor cDNA. Biophys J 67, 793-803.

Takekura, H., and Franzini-Armstrong, C. (2002). The structure of Ca(2+) release units in arthropod body muscle indicates an indirect mechanism for excitation-contraction coupling. Biophys J 83, 2742-2753.

Takeshima, H., lino, M., Takekura, H., Nishi, M., Kuno, J., Minowa, O., Takano, H., and Noda, T. (1994). Excitation-contraction uncoupling and muscular degeneration in mice lacking functional skeletal muscle ryanodine-receptor gene. Nature 369, 556-559.

Tanabe, T., Beam, K.G., Adams, B.A., Niidome, T., and Numa, S. (1990). Regions of the skeletal muscle dihydropyridine receptor critical for excitation-contraction coupling. Nature 346, 567-569.

Tanabe, T., Beam, K.G., Powell, J.A., and Numa, S. (1988). Restoration of excitation—contraction coupling and slow calcium current in dysgenic muscle by dihydropyridine receptor complementary DNA. Nature 336, 134-139.

Tanabe, T., Takeshima, H., Mikami, A., Flockerzi, V., Takahashi, H., Kangawa, K., Kojima, M., Matsuo, H., Hirose, T., and Numa, S. (1987). Primary structure of the receptor for calcium channel blockers from skeletal muscle. Nature 328, 313-318.

Tang, C.M., Presser, F., and Morad, M. (1988). Amiloride selectively blocks the low threshold (T) calcium channel. Science 240, 213-215.

Tao, X., Lee, A., Limapichat, W., Dougherty, D.A., and MacKinnon, R. (2010). A Gating Charge Transfer Center in Voltage Sensors. Science 328, 67-73.

Telegrafi, A., Webb, B.D., Robbins, S.M., Speck-Martins, C.E., FitzPatrick, D., Fleming, L., Redett, R., Dufke, A., Houge, G., van Harssel, J.J.T*., et al.* (2017). Identification of STAC3 variants in non-Native American families with overlapping features of Carey-Fineman-Ziter syndrome and Moebius syndrome. Am J Med Genet A 173, 2763-2771.

Tsien, R.W., Lipscombe, D., Madison, D.V., Bley, K.R., and Fox, A.P. (1988). Multiple types of neuronal calcium channels and their selective modulation. Trends Neurosci 11, 431-438.

Van Petegem, F., Chatelain, F.C., and Minor, D.L., Jr. (2005). Insights into voltage-gated calcium channel regulation from the structure of the CaV1.2 IQ domain-Ca2+/calmodulin complex. Nat Struct Mol Biol 12, 1108-1115.

Van Petegem, F., Clark, K.A., Chatelain, F.C., and Minor, D.L., Jr. (2004). Structure of a complex between a voltage-gated calcium channel beta-subunit and an alpha-subunit domain. Nature 429, 671-675.

Varadi, G., Lory, P., Schultz, D., Varadi, M., and Schwartz, A. (1991). Acceleration of activation and inactivation by the beta subunit of the skeletal muscle calcium channel. Nature 352, 159-162.

Verhage, M., McMahon, H.T., Ghijsen, W.E., Boomsma, F., Scholten, G., Wiegant, V.M., and Nicholls, D.G. (1991). Differential release of amino acids, neuropeptides, and catecholamines from isolated nerve terminals. Neuron 6, 517-524.

Voets, T., Moser, T., Lund, P.-E., Chow, R.H., Geppert, M., Südhof, T.C., and Neher, E. (2001). Intracellular calcium dependence of large dense-core vesicle exocytosis in the absence of synaptotagmin I. Proceedings of the National Academy of Sciences 98, 11680-11685.

Wei, X.Y., Perez-Reyes, E., Lacerda, A.E., Schuster, G., Brown, A.M., and Birnbaumer, L. (1991). Heterologous regulation of the cardiac Ca2+ channel alpha 1 subunit by skeletal muscle beta and gamma subunits. Implications for the structure of cardiac L-type Ca2+ channels. The Journal of biological chemistry 266, 21943-21947.

Wheeler, D.B., Randall, A., and Tsien, R.W. (1994). Roles of N-type and Q-type Ca2+ channels in supporting hippocampal synaptic transmission. Science 264, 107-111.

Whim, M.D., and Lloyd, P.E. (1989). Frequency-dependent release of peptide cotransmitters from identified cholinergic motor neurons in Aplysia. Proceedings of the National Academy of Sciences 86, 9034-9038.

Wong King Yuen, S.M., Campiglio, M., Tung, C.-C., Flucher, B.E., and Van Petegem, F. (2017). Structural insights into binding of STAC proteins to voltage-gated calcium channels. Proceedings of the National Academy of Sciences 114, E9520-E9528.

Wong, M.Y., Zhou, C., Shakiryanova, D., Lloyd, T.E., Deitcher, D.L., and Levitan, E.S. (2012). Neuropeptide delivery to synapses by long-range vesicle circulation and sporadic capture. Cell 148, 1029-1038.

Worrell, J.W., and Levine, R.B. (2008). Characterization of voltage-dependent Ca2+ currents in identified drosophila motoneurons in situ. Journal of Neurophysiology 100, 868-878.

Wu, J., Yan, Z., Li, Z., Qian, X., Lu, S., Dong, M., Zhou, Q., and Yan, N. (2016). Structure of the voltage-gated calcium channel Cav1.1 at 3.6 Å resolution. Nature 537, 191-196.

Wu, J., Yan, Z., Li, Z., Yan, C., Lu, S., Dong, M., and Yan, N. (2015). Structure of the voltage-gated calcium channel Cav1.1 complex. Science 350, aad2395.

Xia, X., Lessmann, V., and Martin, T.F.J. (2009). Imaging of evoked dense-core-vesicle exocytosis in hippocampal neurons reveals long latencies and kiss-and-run fusion events. Journal of Cell Science 122, 75-82.

Xie, B., Nguyen, P.M., Guček, A., Thonig, A., Barg, S., and Idevall-Hagren, O. (2016). Plasma Membrane Phosphatidylinositol 4,5-Bisphosphate Regulates Ca2+-Influx and Insulin Secretion from Pancreatic β Cells. Cell Chemical Biology 23, 816-826.

Xu, J., Mashimo, T., and Südhof, T.C. (2007). Synaptotagmin-1, -2, and -9: Ca2+ Sensors for Fast Release that Specify Distinct Presynaptic Properties in Subsets of Neurons. Neuron 54, 567-581.

Yan, Z., Bai, X., Yan, C., Wu, J., Li, Z., Xie, T., Peng, W., Yin, C., Li, X., Scheres, S.H.W.*, et al.* (2015). Structure of the rabbit ryanodine receptor RyR1 at near-atomic resolution. Nature 517, 50-55.

Yang, J., Ellinor, P.T., Sather, W.A., Zhang, J.F., and Tsien, R.W. (1993). Molecular determinants of Ca2+ selectivity and ion permeation in L-type Ca2+ channels. Nature 366, 158-161.

Zalk, R., Clarke, O.B., des Georges, A., Grassucci, R.A., Reiken, S., Mancia, F., Hendrickson, W.A., Frank, J., and Marks, A.R. (2015). Structure of a mammalian ryanodine receptor. Nature 517, 44-49.

Zheng, W., Feng, G., Ren, D., Eberl, D.F., Hannan, F., Dubald, M., and Hall, L.M. (1995). Cloning and characterization of a calcium channel alpha 1 subunit from Drosophila melanogaster with similarity to the rat brain type D isoform. The Journal of neuroscience : the official journal of the Society for Neuroscience 15, 1132-1143.

Zühlke, R.D., Pitt, G.S., Deisseroth, K., Tsien, R.W., and Reuter, H. (1999). Calmodulin supports both inactivation and facilitation of L-type calcium channels. Nature 399, 159-162.

CHAPTER 2. Dstac Regulates L-type Calcium Channels and Excitation-Contraction Coupling in *Drosophila* Body Wall Muscles

I-Uen Hsu, Jeremy W. Linsley, Lilly E. Reid, Richard I. Hume, Ari Leflein and John Y. Kuwada

[Manuscript in preparation]

2.1 Abstract

Stac3 regulates excitation-contraction coupling (EC coupling) in vertebrate skeletal muscles by regulating the L-type voltage-gated calcium channel (Ca_v channel). Recently a *stac*-like gene, *Dstac*, was identified in *Drosophila* and found to be expressed by both a subset of neurons and muscles. Here, we showed that *Dstac* is co-expressed with *Drosophila* L-type Ca_v channel, *Dmca1D*, by larval body-wall muscles and regulates EC coupling. Furthermore, Dstac is required for normal expression level of Dmca1D in body-wall muscles. These results suggest that Dstac regulates Dmca1D during EC coupling and thus muscle contraction.

2.2 Introduction

Muscle contractions are initiated by depolarizations of muscle membrane potential due to the release of neurotransmitter at the neuromuscular junction. EC coupling is the process that transduces changes in membrane voltage to increases in cytosolic Ca^{2+} due to the release of Ca^{2+} from the sarcoplasmic reticulum (SR) and subsequently contraction. In vertebrate skeletal muscles EC coupling is thought to be mediated by a direct interaction between the L-

type Ca_v channel, dihydropyridine receptor (DHPR), which is in the transverse tubule (T tubule) membrane and is the voltage sensor for EC coupling, and the ryanodine receptor (RyR), which is the Ca^{2+} release channel in the SR membrane (Adams et al., 1990; Block et al., 1988; Paolini et al., 2004; Rios and Brum, 1987; Schneider and Chandler, 1973; Takeshima et al., 1989; Tanabe et al., 1987).

Stac3 was identified as a novel adaptor protein that is required for EC coupling in zebrafish skeletal muscle and a missense mutation in *STAC3* is causal for the congenital Native American myopathy (Horstick et al., 2013). Stac3 also regulates EC coupling in murine skeletal muscles (Nelson et al., 2013) and murine muscle development (Cong et al., 2016; Ge et al., 2014). In zebrafish Stac3 colocalizes with DHPR and RyR and regulates DHPR levels, stability and functionality, including the voltage dependency of DHPRs but not trafficking of DHPRs (Linsley et al., 2017a; Linsley et al., 2017b). Stac3 appears not to be required for normal levels or functionality of RyRs, however.

Recently, a *stac*-like gene, *Dstac*, was identified in *Drosophila* (Hsu et al., 2018). There is a single *stac* gene in *Drosophila* and it is expressed both by muscles and a subset of neurons including in the lateral ventral neurons (LN_V) that express the neuropeptide, pigment dispersing factor (PDF), in the brain. Genetic manipulation of PDF demonstrated the necessity of PDF for circadian rhythm *in Drosophila* (Shafer and Taghert, 2009). Interestingly, knocking down *Dstac* specifically in PDF neurons disrupted circadian rhythm demonstrating the requirement of Dstac in PDF neurons for normal circadian rhythm (Hsu et al., 2018).

Dstac expression by muscles in *Drosophila* (Hsu et al., 2018) suggests that Dstac might regulate EC coupling in *Drosophila* muscles as does Stac3 in vertebrate skeletal muscles

(Horstick et al., 2013; Nelson et al., 2013). As previously mentioned, EC coupling in vertebrate skeletal muscles involves the direct interaction of the L-type Ca_v channel, DHPR, in the T tubules with RyR in the SR. In mammalian skeletal muscles DHPR conducts Ca^{2+} from the external solution to the cytosol but this is not required for EC coupling (Dayal et al., 2017). Interestingly in teleost skeletal muscles EC coupling is similarly independent of Ca^{2+} influx from the exterior and DHPR appears to have evolved so that it no longer conducts Ca^{2+} (Schredelseker et al., 2010).

EC coupling in vertebrate cardiac and smooth muscles, however, does require an influx of Ca^{2+} through Ca_v channels which initiates Ca^{2+} induced Ca^{2+} release (CICR) from internal Ca^{2+} stores (Bolton et al., 1999). Similarly, invertebrate muscle EC coupling appears to involve CICR (Collet, 2009; Györke and Palade, 1992; Maryon et al., 1998; Takekura and Franzini-Armstrong, 2002). CICR may also be necessary for EC coupling in *Drosophila* muscles. In *Drosophila* larvae RyR is expressed widely including the body wall muscles and systemic application of ryanodine and a partial loss-of-function *RyR* mutation both decreased locomotion by larvae (Sullivan et al., 2000), which is consistent with the involvement of CICR in body wall muscles for contractions. Furthermore, SERCA, the Ca^{2+}-ATPase in the ER/SR that pumps Ca^{2+} from the cytosol into the ER/SR, is expressed by muscles and a dominant heat inducible mutation of *SERCA* paralyzes larvae (Sanyal et al., 2005). Finally, *Dmca1D*, the *Drosophila* L-type Ca_v channel is widely expressed (Zheng et al., 1995). *Dmca1D* null embryos exhibit little movement and are larval lethal. Pupae of *AR66* partial loss-of-function allele of *Dmca1D* do not eclose (Eberl et al., 1998). Dmca1D in larval muscle conducts voltage-dependent Ca^{2+} currents that are sensitive to dihydropyridines (Ren et al., 1998). These findings suggest that in *Drosophila* larval muscle Ca^{2+}

influx via Dmca1D channels might initiate CICR. Here, locomotion analysis, *in vivo* Ca^{2+} imaging, and immunolabeling showed that Dstac is required for normal levels of Dmca1D in the T tubules and that both Dstac and Dmca1D regulate Ca^{2+} transients during larval locomotion. Our finding suggests that Dstac regulates Dmca1D and possibly CICR mediated EC coupling during muscle contraction.

2.3 Methods

2.3.1 *Drosophila melanogaster* strains

All crosses and larvae were kept at 25 ˚C and supplied with food that uses molasses as sugar source (Food R purchased from LabExpress). The number of flies used in crosses were controlled so the vials were not overcrowded with larvae. All experiments used age and size matched larvae. *Dmca1D* knockdown experiments and *in vivo* Ca^{2+} imaging used 2nd instar larvae of both genders; all the other experiments used both female and male 3rd instar larvae. All experiments were conducted at room temperature (21˚C – 23.5°C). *UAS:Dcr-2* was present in all knockdown experiments using RNAi strains except for the TRiP RNAi lines that don't require Dcr-2. The fly stocks used in this study were: *Mef2:GAL4* (RRID:BDSC_27390), *UAS:Dcr2* (RRID:BDSC_24651), *UAS:GCaMP6f* (RRID:BDSC_52869), *UAS:mCD8tdtomato* (From Bing Ye), *UAS:Dstac-RNAi* (VDRC 105848), *UAS:Dmca1D-RNAi* (RRID:BDSC_33413), *UAS:Luciferase-RNAi* (RRID:BDSC_31603), w^{1118} (RRID:BDSC_3605), $Dstac^{\Delta SH3}/CyO$ (Hsu et al., submitted).

2.3.2 Immunostaining

3rd instar larvae were filleted in HL3 solution and fixed in 4% paraformaldehyde in PBS. Immunolabeling followed the procedure described in Hsu et al., 2018. The primary antibodies used were: chicken anti-Dmca1D (1:20 - 1:100) (Hsu et al., submitted), rabbit anti-Dstac (1:100 - 1:150) (Hsu et al., 2018), mouse anti-discs large (DSHB Cat# 4F3, RRID:AB_528203). Secondary antibodies used were (1:1000): Donkey anti-chicken Alexa Fluor 488 (Jackson ImmunoResearch Labs Cat# 703-545-155, RRID:AB_2340375), Goat Anti-Chicken Alexa Fluor 647 (Abcam Cat# ab150175, RRID:AB_2732800), Donkey anti-chicken Alexa Fluor 633 (Sigma-Aldrich, SAB4600127), Goat anti-rabbit Alexa Fluor 647 (Thermo Fisher Scientific, Cat # A-21245, RRID AB_2535813), Goat anti-rabbit Alexa Fluor 488 (Thermo Fisher Scientific, Cat # A-11034, RRID: AB_2576217), Goat anti-Mouse Alexa Fluor 568 (Thermo Fisher Scientific, Cat# A-11004, RRID AB_2534072), Goat anti-Mouse Alexa Fluor Plus 647 (Thermo Fisher Scientific, Cat# A32728, RRID AB_2633277), Goat anti-Mouse Alexa Fluor 488 (Thermo Fisher Scientific, Cat# A-11001, RRID AB_2534069). Images were acquired with a Leica SP5 and SP8 confocal microscopes using a 100x or 63x oil objective.

2.3.3 Analysis of Eclosion

3rd instar larvae were collected 5 days after the crosses were set. Between 7 and 10 days after the collection of larvae, the number of pupae and adult flies that eclosed were counted. All vials were kept at 25 ˚C.

2.3.4 Motility assay

Freely moving 3rd instar larvae were acclimated on a 10 cm 2% agar plate for 1 minute and then recorded with a digital camera for 10 seconds at a frame rate of 7.5 Hz. Each larva was recorded 3 times with each time constituting a single trial. Larvae that hit the petri dish wall during the 10-second recording were excluded from the analysis. The assay was performed at 23.5 ˚C. Larval movements were tracked by the "multitracker" plugin of imageJ that produced the (x,y) location of each larva in each frame. The distance between frames were calculated from the (x,y) locations and were summed to get the total distance traveled during the 10 seconds. The controls and experimental groups were coded to blind the genotypes. After completing the assay and analysis, the genotypes were unveiled.

2.3.5 *In vivo* Ca^{2+} imaging

Live intact 2nd instar larvae of both genders selectively expressing GCaMP6f in body-wall muscles (*Mef2:GAL4>UAS:GCaMP6f*) were placed into a microfluidics chip (Ghannad-Rezaie et al., 2012; Mishra et al., 2014) and GCaMP fluorescence was observed on a spinning disc confocal imaging system composed of an Olympus IX81 inverted microscope, a CSU-X1 scanner (Yokogawa), an iXon electron multiplying charge-coupled device camera (Andor), and MetaMorph Advanced Imaging acquisition software v.7.7.8.0 (Molecular Devices). Imaging was acquired with a 10X Olympus objective. The *Mef2:GAL4* line also expressed *UAS:mCD8tdTomato* to allow visualization of body-wall muscles. The larvae were mounted on its side in the chip in order to image muscle 4, 5, 8, 12, 21 that have some parts that don't overlap with other muscles. Images were captured every 0.5 sec for 5 min. The *mCD8tdTomato*

expressed by *Mef2*:*GAL4* was used to locate the muscles. The larvae that moved a lot were not used. Region of interests (ROI) were drawn over parts of muscles that don't layer with other muscles and the position of the ROI was re-adjusted manually according to the movements of the samples. Time series analyzer v3 plugin of imageJ was used to measure fluorescence intensity of the ROI. Five frames of GCaMP6f fluorescence before and after the peaks were averaged and used as basal GCaMP6f level (F_{basal}) to calculate the fold change of GCaMP6f fluorescence intensity [$\Delta F/F=(F-F_{basal})/F_{basal}$]. Prism GraphPad was used to find the peak values. Basal GCaMP6f levels or Ca^{2+} peaks per muscles were averaged as one experiment sample. Both the experiments and analysis were done blind.

2.3.6 Quantification of Dmca1D immunostaining at T tubule striations of body-wall muscles

Images of muscle 4 from segments A3 to A5 were acquired at 1024 x 1024 pixels as z stacks (5 planes, 0.5 µm/focal plane) with a Leica SP8 confocal microscope with a 100x objective. Confocal settings were kept constant between controls and experimental groups. Five focal plane images were stacked to a single image using imageJ. ROIs were drawn to encompass the striations labeled with anti-Dmca1D and the fluorescence intensities of the ROIs were measured using imageJ.

2.3.7 Statistical analysis

Statistical analyses were performed using Prism GraphPad software. The normality of data distribution was tested by D'Agostino and Pearson test. If the data fit a normal distribution, unpaired t test was used. If the data were not normally distributed, the Mann-

Whitney test was used. For experiment in which the change in results can be predicted by our hypothesis, one-tailed tests were performed; otherwise two-tailed tests were performed. In all figures, ns, *, **, ***, **** represent $P>0.05$, $P<0.05$, $P<0.01$, $P<0.001$, and $P<0.0001$. Error bars are standard errors of the mean.

2.4 Results

2.4.1 Dstac and Dmca1D appear to be expressed by the T tubule network of larval body-wall muscles.

In zebrafish skeletal muscles, the L-type calcium channel, DHPR, and Stac3 colocalize at the junctions of the T tubules and SR (Horstick et al., 2013; Linsley et al., 2017a). To examine the expression pattern of Dstac and Dmca1D within larval body wall muscles by application of anti-Dstac (Hsu et al., 2018) and anti-Dmca1D (Hsu et al., submitted). Anti-Dstac labeled bands orthogonal to the longitudinal axis of the muscles with some longitudinal linear structures within the bands that were co-labeled by anti-DLG (Razzaq et al., 2001), which recognizes the Discs Large protein that localizes to the T tubules (Figure 2.1A). Notable were relatively large puncta labeled with anti-DLG that were also labeled by anti-Dstac (arrowheads) within the orthogonal stripes. Similarly, anti-Dmca1D also labeled orthogonal bands with some longitudinal linear structures that were co-labeled with anti-DLG (Figure 2.1B). Merged images of Dstac/DLG and Dmca1D/DLG co-labeling showed that within the orthogonal bands there was some co-localization of between the Dstac and DLG and between Dmca1D and DLG (arrowheads). Furthermore, co-labeling with anti-Dstac and anti-Dmca1D found that the orthogonal bands were labeled for Dstac and Dmca1D with some punctate co-labeling

(arrowheads) (Figure 2.1C). In fact the orthogonal bands labeled by anti-Dstac and anti-Dmca1D are similar to those seen when T tubules were visualized by expression of mCD8:GFP that labels the plasma membrane including the T tubules (Fujita et al., 2017), suggesting that the orthogonal bands labeled by ant-Dstac and anti-Dmca1D are regions of muscles containing T tubules. Thus, it appears that Dstac and Dmca1D localize to the region containing T tubules with perhaps some co-localization of Dstac and Dmca1D in *Drosophila* larval muscles, but the co-localization was not nearly as robust as that seen between DHPR and Stac3 in zebrafish skeletal muscles.

2.4.2 Larvae with *Dstac* knocked down in body wall muscles exhibited decreased locomotion and failed to eclose.

Knocking down *Dstac* selectively in body wall muscles using a RNAi line that was previously shown to knockdown *Dstac* (Hsu et al., 2018) led to decreased locomotion compared with control larvae (Figure 2.2A). In $Dstac^{RNAi}$ larvae, anti-DLG labeling of body-wall muscles showed that the T tubules were comparable with that in control larvae (Figure 2.2B). This result suggests that knockdown of Dstac does not have a deleterious effect on T tubules of body-wall muscles and thus the decreased locomotion is likely not due to any morphological defect in the T tubules. Larvae with Dstac knocked down selectively in body-wall muscles were able to develop to pupae that appeared similarly to control pupae, but failed to eclose presumably due to decreased muscle function. The pharate adults released manually from the cocoon by dissection exhibited apparent normal morphology (Figure 2.2C). Thus Dstac in body wall

muscles is required for normal locomotion and appears not to be necessary for normal morphological development.

2.4.3 Larvae with *Dmca1D* knocked down in body wall muscles exhibited decreased locomotion and muscle Ca^{2+} transients.

Previously we showed that the ubiquitous *AR66* partial loss-of-function allele of *Dmca1D* exhibited decrease larval locomotion (Hsu et al., submitted). To see if a deficiency in *Dmca1D* specifically in muscle could lead to decreased locomotion, we selectively knocked down *Dmca1D* in body wall muscles (*Mef2:GAL4>UAS:Dmca1D*^{RNAi}). *Dmca1D*^{RNAi} larvae developed to the size of 2nd instar larvae and died around 10 days after hatching. Anti-Dmca1D labeling in body wall muscles was decreased in 2nd instar *Dmca1D*^{RNAi} larvae compared with 2nd instar control larvae (Figure 2.3A), confirming that Dmca1D was indeed knocked down in muscles. Furthermore, *Dmca1D*^{RNAi} larvae showed reduced locomotion compared with size and age matched 2nd instar control larvae (Figure 2.3B). These results indicate that normal levels of Dmca1D in body-wall muscles is required for normal locomotion.

To see if the decreased locomotion of larvae with a muscle deficiency in Dmca1D was due to a defect in EC coupling, we examined transient increases in cytosolic Ca^{2+} in body wall muscles during locomotion in larvae expressing GCaMP6f selectively in muscles. Ca^{2+} imaging of body-wall muscles was performed in live, intact larvae placed in a microfluidics chamber designed to physically restrain larvae (Mishra et al., 2014). Under these conditions, Ca^{2+} transient increases that presumably were associated with restrained contractions of the muscles were observed within body-wall muscles of control larvae (*Mef2:GAL4>UAS:GCaMP6f;UAS:mCD8tdTomato;UAS:Luciferase*^{RNAi}) as well as larvae that were

Dmca1D selectively knocked down by body-wall muscles (*Mef2:GAL4>UAS:GCaMP6f;UAS:mCD8tdTomato;UAS:Dmca1D^{RNAi}*) (Figure 2.3C). The GCaMP6f fluorescence levels when larvae were quiescent were similar in *Dmca1D^{RNAi}* larvae and control larvae (Figure 2.3D). Thus, expression of GCaMP was unaffected by the knockdown of Dmca1D in body wall muscles. However, the peak of Ca^{2+} transients recorded from *Dmca1D^{RNAi}* larvae was decreased compared with controls (Figure 2.3E), but the frequency of transients was comparable (Figure 2.3F). These results showed that the output of the central pattern generator was not dependent on normal Dmca1D in muscles, but more importantly that the normal, physiological activation of muscles requires Ca^{2+} transients that are regulated by Dmca1D. Thus, EC coupling requires Dmca1D.

2.4.4 *Dstac* deficiency reduced *Dmca1D* expression at T tubules striations and Ca^{2+} transients during locomotion.

Since both Dmca1D and Dstac regulate larval locomotion and Dmca1D regulates Ca^{2+} transients during EC coupling, we asked if Dstac regulates Dmca1D. Immunolabeling the body wall muscles of wt and *Dstac$^{\Delta SH3}$* mutant larvae (Hsu et al., submitted) with anti-Dmca1D showed that Dmca1D expression was reduced in *Dstac$^{\Delta SH3}$* compared with wt larvae (Figure 2.4A). The finding that the T tubule morphology/organization appears unperturbed when Dstac is knocked down (Figure 2.2B) argues against the possibility that the decreased Dmca1D in *Dstac* mutants might be a by-product of a defect in the morphology/organization of T tubules. This finding is consistent with the earlier finding that DHPR levels of skeletal muscles were reduced in *stac3* null zebrafish (Linsley et al., 2017a).

The decreased Dmca1D in body wall muscles predicts that Ca^{2+} transients should also be reduced when Dstac is knocked down in body-wall muscles (*Mef2:GAL4>UAS:GCaMP6f,UAS-Dstac^{RNAi}*). As before Ca^{2+} transients were assayed in larvae selectively expressing GCaMP6f in body wall muscles (Figure 2.4B). The basal GCamP6f level when muscles were quiescent was higher in *Dstac^{RNAi}* larvae compared with control larvae (Figure 2.4C), but peak Ca^{2+} transients were decreased (Figure 2.4D) but not their frequency (Figure 2.4E). Thus, Dstac appears to regulate Dmca1D to mediate normal Ca^{2+} transients during EC coupling.

Figure 2.1

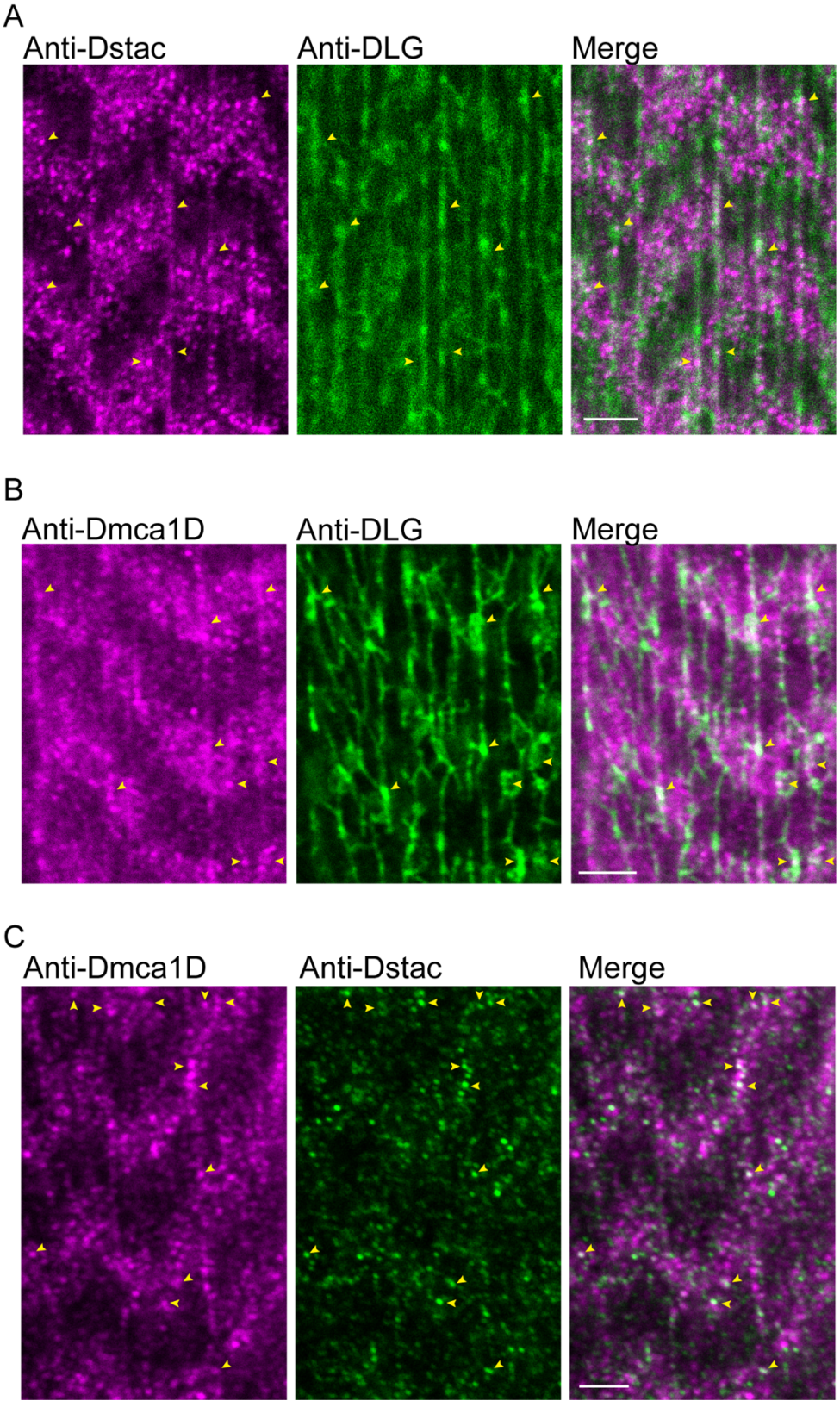
A
Anti-Dstac
Anti-DLG
Merge
B
Anti-Dmca1D
Anti-DLG
Merge
C
Anti-Dmca1D
Anti-Dstac
Merge

Figure 2.1 Dstac and Dmca1D are expressed in regions of 3rd instar larval body-wall muscles containing T tubules.
(A) Anti-Dstac labeling of 3rd instar body-wall muscles showed expression of Dstac in stripes orthogonal to the longitudinal axis of the muscles (left). In these stripes anti-DLG labeled longitudinally arrayed T tubules (middle and right). Puncta that are co-labeled by anti-Dstac and anti-DLG are indicated by arrowheads. The images are a single focal plane. Scale bar, 3 µm. (B) Anti-Dmca1D labeling of 3rd instar body-wall muscles showed expression of Dmca1D in stripes similar to that of anti-Dstac labeling (left). In these stripes anti-DLG labeled longitudinally arrayed T tubules (middle and right). Puncta that are co-labeled by anti-Dmca1D and anti-DLG are indicated by arrowheads. The images are a single focal plane. Scale bar, 3 µm. (C) Co-immunostaining of 3rd instar larval body wall muscles with anti-Dstac and anti-Dmca1D showed co-expression of Dstac and Dmca1D in the same stripes. Arrowheads indicate some puncta that co-labeled with anti-Dstac and anti-Dmca1D. The images are a single focal plane. Scale bar, 3 µm.

Figure 2.2

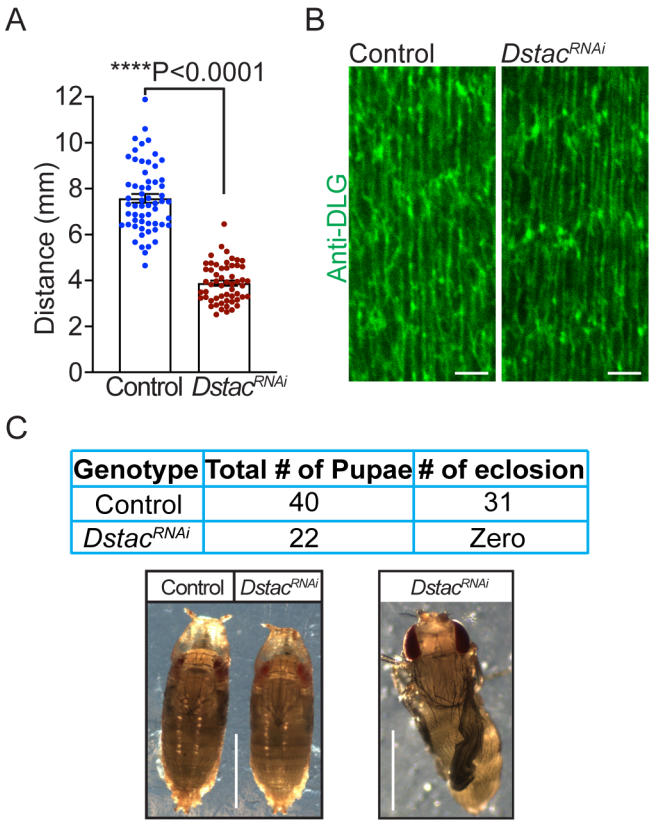

Figure 2.2 Knockdown of *Dstac* in body wall muscles reduced larval locomotion.
(A) *Dstac*^{RNAi} larvae in which *Dstac* was knocked down in body wall muscles (*Mef2:GAL4>UAS-Dstac*^{RNAi}) showed decreased locomotion compared with control *Luciferase*^{RNAi} larvae (*Mef2:GAL4>UAS-Luciferase*^{RNAi}). Control n=59, *Dstac*^{RNAi} n=56. One-tailed, unpaired t test. (B) Labeling T tubules of body-wall muscles with anti-DLG showed that T tubules of *Dstac*^{RNAi} larvae (*Mef2:GAL4>UAS-Dstac*^{RNAi}) are similar in morphology and structure to control *Luciferase*^{RNAi} larvae (*Mef2:GAL4>UAS-Luciferase*^{RNAi}). The images are a single focal plane. Scale bar, 3 µm. (C) *Dstac*^{RNAi} larvae in which *Dstac* was knocked down in body wall muscles (*Mef2:GAL4>UAS-Dstac*^{RNAi}) could develop to mature pharate adults in the pupae but couldn't eclose. The left lower image shows a control *Luciferase*^{RNAi} pupa and a *Dstac*^{RNAi} pupa that are similar in morphology. The right lower image shows a pharate adult of *Dstac*^{RNAi} that was dissected out from its cocoon in which the wings were not inflated and did not survive. Scale bar, 1 mm.

Figure 2.3

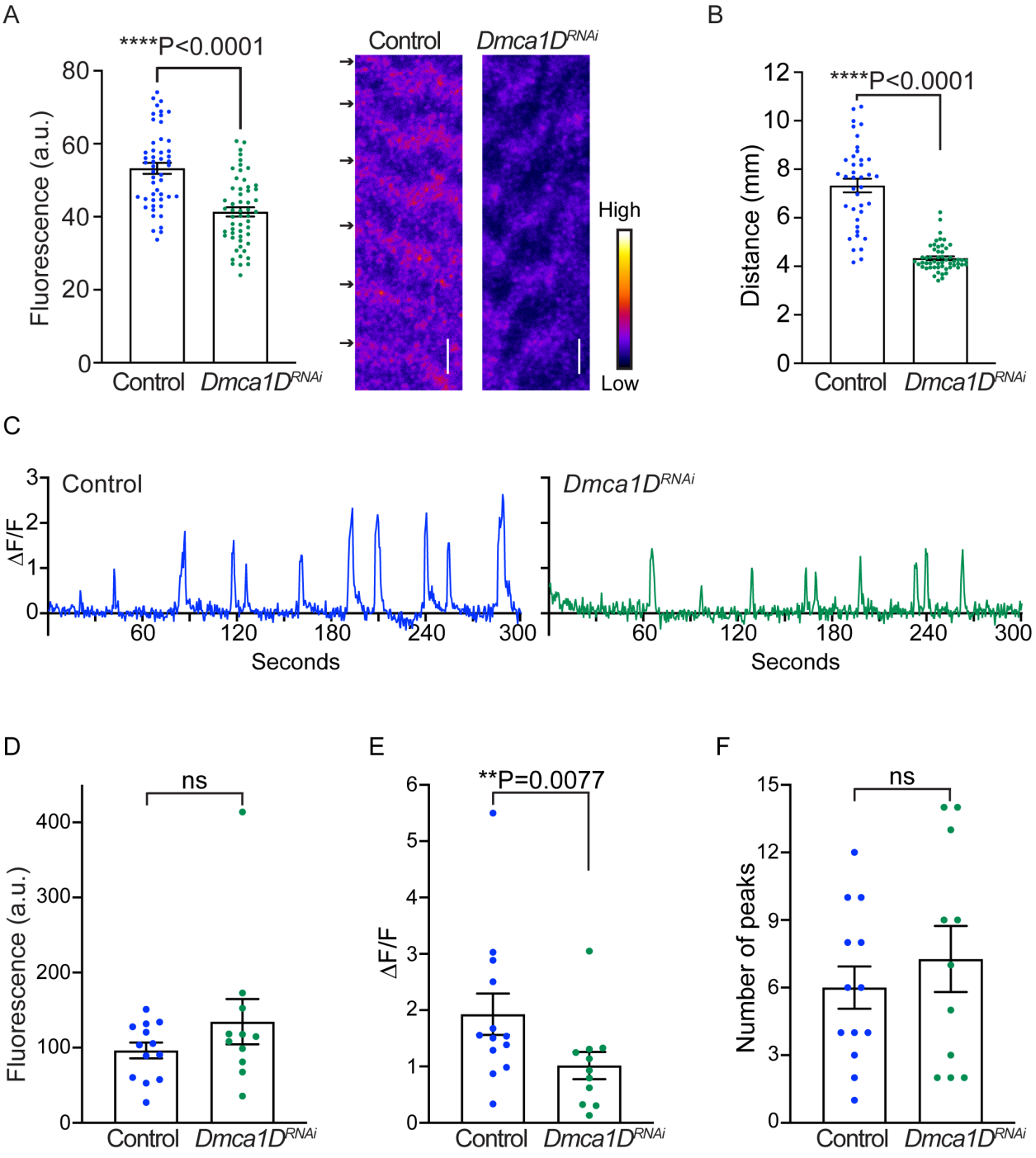
A
****P<0.0001
Fluorescence (a.u.)
80
60
40
20
0
Control
Dmca1D^RNAi
Control
Dmca1D^RNAi
High
Low
B
****P<0.0001
Distance (mm)
12
10
8
6
4
2
0
Control
Dmca1D^RNAi
C
Control
Dmca1D^RNAi
ΔF/F
3
2
1
0
60
120
180
240
300
Seconds
60
120
180
240
300
Seconds
D
ns
Fluorescence (a.u.)
400
300
200
100
0
Control
Dmca1D^RNAi
E
**P=0.0077
ΔF/F
6
5
4
3
2
1
0
Control
Dmca1D^RNAi
F
ns
Number of peaks
15
12
9
6
3
0
Control
Dmca1D^RNAi

Figure 2.3 Knockdown of *Dmca1D* selectively in muscles reduced larval locomotion and muscle Ca^{2+} transients.
(A) Anti-Dmca1D labeling of muscles of larvae with Dmca1D knocked down selectively in body-wall muscles (*Mef2:GAL4>UAS:Dmca1D^{RNAi}*) (n=55 dyads from 11 muscles) confirmed that Dmca1D was knocked down compared with control muscles (*Mef2:GAL4>UAS:Luciferase^{RNAi}*) (n=50 dyads from 10 muscles). One-tailed, unpaired t test. Right images are a single focal plane of muscle 4 of a control and a *Dmca1D^{RNAi}* larvae. Arrows denote the striations of Dmca1D clusters. Scale bar, 3 µm. (B) *Dmca1D^{RNAi}* larvae in which Dmca1D was knocked down in body-wall muscles (*Mef2:GAL4>UAS:Dmca1D^{RNAi}*) showed decreased locomotion compared with control *Luciferase^{RNAi}* larvae (*Mef2:GAL4>UAS:Luciferase^{RNAi}*). Control n=39, Dmca1D^{RNAi} n=54. One-tailed Mann-Whitney test. (C) Example of Ca^{2+} transients from a muscle in a control larva (*Mef2:GAL4>UAS:GCaMP6f;UAS:mCD8tdTomato;UAS:Luciferase^{RNAi}*) and a *Dmca1D^{RNAi}* larva (*Mef2:GAL4>UAS:GCaMP6f;UAS:mCD8tdTomato;UAS:Dmca1D^{RNAi}*). (D) Expression of GCaMP6f by muscles of *Dmca1D^{RNAi}* larvae was comparable to that of control. Mann-Whitney test. (E) The peaks of Ca^{2+} transients in the muscles of *Dmca1D^{RNAi}* larvae were smaller compared with controls. One-tailed, Mann-Whitney test. (F) The number of Ca^{2+} transients over 5 min in *Dmca1D^{RNAi}* and control muscles were comparable. Unpaired t test. Data in D-F were from 13 muscles of 7 control larvae (*Mef2:GAL4>UAS:GCaMP6f;UAS:mCD8tdTomato;UAS:Luciferase^{RNAi}*) and from 11 muscles of 6 *Dmca1D^{RNAi}* larvae (*Mef2:GAL4>UAS:GCaMP6f;UAS:mCD8tdTomato;UAS:Dmca1D^{RNAi}*).

Figure 2.4

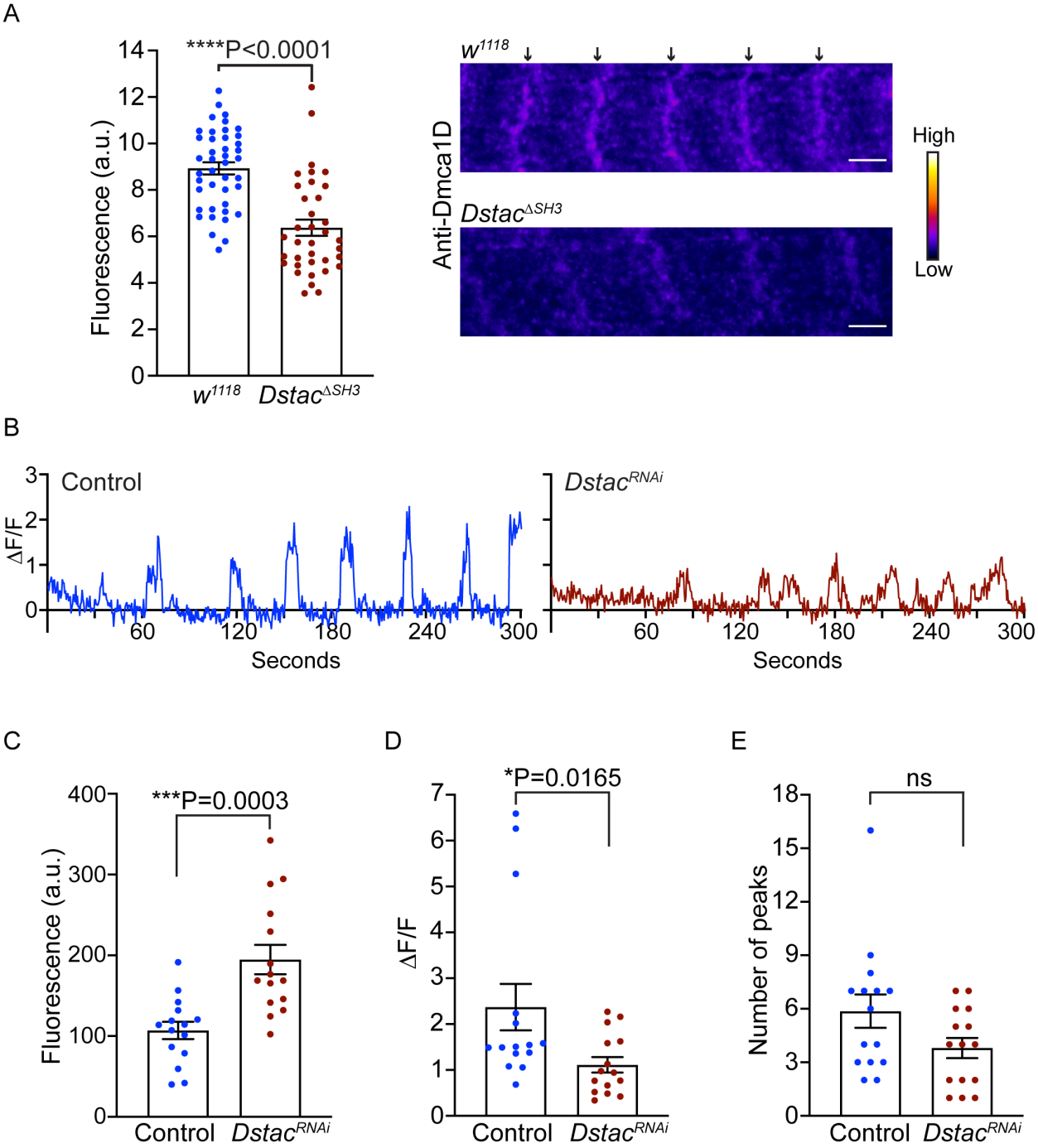
A
****P<0.0001
Fluorescence (a.u.)
14
12
10
8
6
4
2
0
w1118
DstacΔSH3
w1118
Anti-Dmca1D
DstacΔSH3
High
Low
B
Control
DstacRNAi
ΔF/F
3
2
1
0
60
120
180
240
300
Seconds
C
***P=0.0003
Fluorescence (a.u.)
400
300
200
100
0
Control
DstacRNAi
D
*P=0.0165
ΔF/F
7
6
5
4
3
2
1
0
Control
DstacRNAi
E
ns
Number of peaks
18
15
12
9
6
3
0
Control
DstacRNAi

Figure 2.4 Knockdown of *Dstac* in body-wall muscles reduced Dmca1D expression level and muscle Ca^{2+} transients.
(A) Anti-Dmca1D labeling of *Dstac*$^{\Delta SH3}$ larval muscles (n=36 dyads from 12 muscles) showed decreased level of Dmca1D at T tubules compared with wt (n=42 dyads from 14 muscles). One-tailed Mann Whitney test. Right images are a single focal plane of muscle 4 of a wt and a *Dstac*$^{\Delta SH3}$ larvae. Arrows denote striations of Dmca1D clusters. Scale bar, 3 μm. (B) Example of Ca^{2+} transients from a muscle in a control larva (*Mef2:GAL4>UAS:GCaMP6f;UAS:mCD8tdTomato;UAS:Luciferase*^{RNAi}) and a *Dstac*^{RNAi} larva (*Mef2:GAL4>UAS:GCaMP6f;UAS:mCD8tdTomato;UAS:Dstac*^{RNAi}). (C) Expression of GCaMP6f by muscles of *Dstac*^{RNAi} larvae was higher than that of control. Unpaired t test. (D) The peaks of Ca^{2+} transients in the muscles of *Dstac*^{RNAi} larvae were smaller compared with controls. One-tailed Mann-Whitney test. (E) The number of Ca^{2+} transients over 5 min in *Dstac*^{RNAi} and control muscles were comparable. Mann-Whitney test. Data in B-D were from 15 muscles of 5 control larvae (*Mef2:GAL4>UAS:GCaMP6f;UAS:mCD8tdTomato;UAS:Luciferase*^{RNAi}) and from 15 muscles of 5 *Dstac*^{RNAi} larvae (*Mef2:GAL4>UAS:GCaMP6f;UAS:mCD8tdTomato;UAS:Dstac*^{RNAi}).

2.5 Discussion

In invertebrates, CICR appears to be important for muscle contraction (Collet, 2009; Györke and Palade, 1992), much like vertebrate cardiac and smooth muscles (Fabiato, 1983), and inhibiting CICR by blocking SERCA led to paralysis of larvae (Sanyal et al., 2005). Thus, our results suggested that Ca^{2+} influx via Dmca1D might initiate CICR that leads to Ca^{2+} transients during EC coupling and thus muscle contraction.

Vertebrate skeletal muscles EC coupling, however, is independent of an influx of Ca^{2+} from Ca_v channels but rather involves direct interaction of the voltage dependent L-type calcium channel in the T tubules and the RyR Ca^{2+} release channel in the SR (Dayal et al., 2017; Paolini et al., 2004). Stac3 is a key regulator of EC coupling in vertebrate skeletal muscles that regulates the stability and voltage-dependency of DHPR in T tubules (Linsley et al., 2017a). The results in this study showed that Dstac plays a conserved role as vertebrate Stac3 in regulating EC coupling. First, Dstac and Dmca1D localize at T tubule striations of body-wall muscles. Second, knockdown of Dstac or Dmca1D in body-wall muscles reduced larval locomotion. Third, knockdown of Dstac or Dmca1D decreased Ca^{2+} transients in body wall muscles during locomotion. Finally, Dmca1D expression was reduced in *Dstac*$^{\Delta SH3}$ mutant body-wall muscles. Thus, Dstac is required for normal levels of Dmca1D at T tubules and normal EC coupling.

Stac3 regulates the stability and thus the level of DHPRs in zebrafish skeletal muscles (Linsley et al., 2017a). The finding that the levels of Dmca1D were decreased in *Dstac* mutants is consistent with the regulation of the stability of Dmca1D by Dstac. Live imaging of a fusion of Dmca1D with a photoconvertible protein will be needed to assay whether the stability of Dmca1D is regulated by Dstac. Stac3 also regulates the voltage response of DHPRs in zebrafish

skeletal muscles (Linsley et al., 2017a). Whether Dstac also regulates the voltage response of Dmca1D await to be examined by voltage clamp experiments.

Besides the Src Homology 3 (SH3) and cysteine-rich domain (CRD) that define the Stac proteins, Dstac has a putative BAR domain as do the other invertebrate Stac proteins but not the vertebrate Stac proteins (Hsu et al., 2018). The function of the putative BAR domain of Dstac is unknown. Amphiphysin, a protein containing a SH3 and a BAR domains, was found to regulate the development and organization of T tubules and thereby EC coupling (Razzaq et al., 2001). This result is consistent with a role for BAR domains for mediating membrane curvature (Salzer et al., 2017). Our results suggested that Dstac is dispensable for the morphology and organization of the T tubules, since muscle of $Dstac^{RNAi}$ larvae appear to contain normal T tubules (Figure 2.2B). This finding appears to consistent with no role of the Dstac BAR domain for the formation of T tubules. However, Dstac is alternatively spliced and $Dstac^{RNAi}$ targeted the linker sequence between the CRD and SH3 domains that is downstream of the BAR domain (Hsu et al., 2018). In fact there are 13 transcripts containing a BAR domain and only 3 of these would have been targeted by the RNAi. Thus, it is premature to draw any conclusions regarding the role of Dstac for the formation of T tubules.

Our results showed that $Dstac^{RNAi}$ larvae exhibited higher basal Ca^{2+} levels during the quiescent stage of locomotion. Control and $Dstac^{RNAi}$ larvae carried same numbers of *GAL4* and *UAS* elements so this difference was not likely due to the expression level of GCaMP6f. Cytosolic Ca^{2+} in muscles at resting states is strictly regulated by extracellular Ca^{2+} influx through L-type Ca_v channels, SR luminal Ca^{2+} release through RyR, removal of cytosolic Ca^{2+} by SERCA and store-operated channels on plasma membrane. Increased cytosolic Ca^{2+} levels in

Dstac^{RNAi} muscles could be explained by decreased ability to sequester Ca^{2+} and store Ca^{2+} within the SR or through an increase in steady-state SR Ca^{2+} leak. However, in *Dmca1D*^{RNAi} larvae, the elevated GCaMP6f level during quiescent stage was not observed as it was in *Dstac*^{RNAi} larvae. These results imply that Dstac might regulate some Dmca1D-independent mechanisms to maintain cytosolic Ca^{2+} levels.

Electrophysiology showed that *Drosophila* larval body-wall muscles express not only the L-type channel, *Dmca1D*, but also the T-type channel, *Dmca1G* (Gielow et al., 1995). While vertebrate skeletal muscles only express DHPR, the co-existence of L- and T-type Ca_v channels in *Drosophila* body-wall muscles is perplexing. Interestingly, vertebrate neuronal Stac1 was found to form a complex with a mammalian T-type Ca_v channel, $Ca_v3.2$, and is required for $Ca_v3.2$ expression at plasma membrane. It would be interesting to examine if Dstac also regulates Dmca1G, if Dmca1D and Dmca1G interact, and if Dstac is involved in such interaction.

2.6 AUTHOR CONTRIBUTIONS

Conceptualization, I.H., J.W.L. and J.Y.K.; Methodology, I.H. and J.Y.K.; Formal Analysis, I.H.; Investigation, I.H., J.W.L., L.E.R., and A.L.; Resources, R.I.H., and J.Y.K.; Writing-Original Draft, I.H. and J.Y.K.; Supervision, J.Y.K.; Funding Acquisition, J.Y.K.

2.7 ACKNOWLEDGEMENTS

We thank Miranda Lum, Allison Orzel, Bethany Folk-Middlebrook for technical assistance, Catherine Collins and Collins lab for advice and use of facilities for the genetics.

2.8 References

Adams, B.A., Tanabe, T., Mikami, A., Numa, S., and Beam, K.G. (1990). Intramembrane charge movement restored in dysgenic skeletal muscle by injection of dihydropyridine receptor cDNAs. Nature 346, 569-572.

Block, B.A., Imagawa, T., Campbell, K.P., and Franzini-Armstrong, C. (1988). Structural evidence for direct interaction between the molecular components of the transverse tubule/sarcoplasmic reticulum junction in skeletal muscle. The Journal of cell biology 107, 2587-2600.

Bolton, T.B., Prestwich, S.A., Zholos, A.V., and Gordienko, D.V. (1999). Excitation-contraction coupling in gastrointestinal and other smooth muscles. Annu Rev Physiol 61, 85-115.

Collet, C. (2009). Excitation-contraction coupling in skeletal muscle fibers from adult domestic honeybee. Pflugers Arch 458, 601-612.

Cong, X., Doering, J., Mazala, D.A.G., Chin, E.R., Grange, R.W., and Jiang, H. (2016). The SH3 and cysteine-rich domain 3 (Stac3) gene is important to growth, fiber composition, and calcium release from the sarcoplasmic reticulum in postnatal skeletal muscle. Skeletal muscle 6, 17-17.

Dayal, A., Schrötter, K., Pan, Y., Föhr, K., Melzer, W., and Grabner, M. (2017). The Ca2+ influx through the mammalian skeletal muscle dihydropyridine receptor is irrelevant for muscle performance. Nature Communications 8, 475.

Eberl, D.F., Ren, D., Feng, G., Lorenz, L.J., Van Vactor, D., and Hall, L.M. (1998). Genetic and developmental characterization of Dmca1D, a calcium channel α1 subunit gene in Drosophila melanogaster. Genetics 148, 1159-1169.

Fabiato, A. (1983). Calcium-induced release of calcium from the cardiac sarcoplasmic reticulum. The American journal of physiology 245, C1-14.

Fujita, N., Huang, W., Lin, T.-h., Groulx, J.-F., Jean, S., Nguyen, J., Kuchitsu, Y., Koyama-Honda, I., Mizushima, N., Fukuda, M., and Kiger, A.A. (2017). Genetic screen in Drosophila muscle identifies autophagy-mediated T-tubule remodeling and a Rab2 role in autophagy. eLife 6, e23367.

Ge, X., Zhang, Y., Park, S., Cong, X., Gerrard, D.E., and Jiang, H. (2014). Stac3 inhibits myoblast differentiation into myotubes. PLoS ONE 9.

Ghannad-Rezaie, M., Wang, X., Mishra, B., Collins, C., and Chronis, N. (2012). Microfluidic chips for in vivo imaging of cellular responses to neural injury in Drosophila larvae. PLoS One 7, e29869.

Gielow, M., Gu, G., and Singh, S. (1995). Resolution and pharmacological analysis of the voltage-dependent calcium channels of Drosophila larval muscles. The Journal of Neuroscience 15, 6085-6093.

Györke, S., and Palade, P. (1992). Calcium-induced calcium release in crayfish skeletal muscle. J Physiol 457, 195-210.

Horstick, E.J., Linsley, J.W., Dowling, J.J., Hauser, M.A., McDonald, K.K., Ashley-Koch, A., Saint-Amant, L., Satish, A., Cui, W.W., Zhou, W.*, et al.* (2013). Stac3 is a component of the excitation-contraction coupling machinery and mutated in Native American myopathy. Nature communications 4, 1952-1952.

Hsu, I.U., Linsley, J.W., Varineau, J.E., Shafer, O.T., and Kuwada, J.Y. (2018). Dstac is required for normal circadian activity rhythms in Drosophila. Chronobiol Int, 1-11.

Hsu, I.U., Linsley, J.W., Zhang, X., Varineau, J.E., Berkhoudt, D.A., Reid, L.E., Lum, M.C., Orzel, A.M., Leflein, A., Xu, H.*, et al.* (submitted). Stac Protein Regulates Release of Neuropeptides.

Linsley, J.W., Hsu, I.U., Groom, L., Yarotskyy, V., Lavorato, M., Horstick, E.J., Linsley, D., Wang, W., Franzini-Armstrong, C., Dirksen, R.T., and Kuwada, J.Y. (2017a). Congenital myopathy results from misregulation of a muscle Ca2+ channel by mutant Stac3. Proc Natl Acad Sci U S A 114, E228-E236.

Linsley, J.W., Hsu, I.U., Wang, W., and Kuwada, J.Y. (2017b). Transport of the alpha subunit of the voltage gated L-type calcium channel through the sarcoplasmic reticulum occurs prior to localization to triads and requires the beta subunit but not Stac3 in skeletal muscles. Traffic (Copenhagen, Denmark) 18, 622-632.

Maryon, E.B., Saari, B., and Anderson, P. (1998). Muscle-specific functions of ryanodine receptor channels in Caenorhabditis elegans. J Cell Sci 111 (Pt 19), 2885-2895.

Mishra, B., Ghannad-Rezaie, M., Li, J., Wang , X., Hao, Y., Ye, B., Chronis, N., and Collins, C.A. (2014). Using Microfluidics Chips for Live Imaging and Study of Injury Responses in Drosophila Larvae. JoVE, e50998.

Nelson, B.R., Wu, F., Liu, Y., Anderson, D.M., McAnally, J., Lin, W., Cannon, S.C., Bassel-Duby, R., and Olson, E.N. (2013). Skeletal muscle-specific T-tubule protein STAC3 mediates voltage-induced Ca2+ release and contractility. Proceedings of the National Academy of Sciences of the United States of America 110, 11881-11886.

Paolini, C., Fessenden, J.D., Pessah, I.N., and Franzini-Armstrong, C. (2004). Evidence for conformational coupling between two calcium channels. Proceedings of the National Academy of Sciences of the United States of America 101, 12748-12752.

Razzaq, A., Robinson, I.M., McMahon, H.T., Skepper, J.N., Su, Y., Zelhof, A.C., Jackson, A.P., Gay, N.J., and O'Kane, C.J. (2001). Amphiphysin is necessary for organization of the excitation-contraction coupling machinery of muscles, but not for synaptic vesicle endocytosis in Drosophila. Genes Dev 15, 2967-2979.

Ren, D., Xu, H., Eberl, D.F., Chopra, M., and Hall, L.M. (1998). A mutation affecting dihydropyridine-sensitive current levels and activation kinetics in Drosophila muscle and mammalian heart calcium channels. Journal of Neuroscience 18, 2335-2341.

Rios, E., and Brum, G. (1987). Involvement of dihydropyridine receptors in excitation–contraction coupling in skeletal muscle. Nature 325, 717-720.

Salzer, U., Kostan, J., and Djinović-Carugo, K. (2017). Deciphering the BAR code of membrane modulators. Cell Mol Life Sci 74, 2413-2438.

Sanyal, S., Consoulas, C., Kuromi, H., Basole, A., Mukai, L., Kidokoro, Y., Krishnan, K.S., and Ramaswami, M. (2005). Analysis of Conditional Paralytic Mutants in Drosophila Sarco-Endoplasmic Reticulum Calcium ATPase Reveals Novel Mechanisms for Regulating Membrane Excitability. Genetics 169, 737-750.

Schneider, M.F., and Chandler, W.K. (1973). Voltage Dependent Charge Movement in Skeletal Muscle: a Possible Step in Excitation–Contraction Coupling. Nature 242, 244-246.

Schredelseker, J., Shrivastav, M., Dayal, A., and Grabner, M. (2010). Non-Ca2+-conducting Ca2+ channels in fish skeletal muscle excitation-contraction coupling. Proc Natl Acad Sci U S A 107, 5658-5663.

Shafer, O.T., and Taghert, P.H. (2009). RNA-interference knockdown of Drosophila pigment dispersing factor in neuronal subsets: the anatomical basis of a neuropeptide's circadian functions. PLoS One 4, e8298.

Sullivan, K.M., Scott, K., Zuker, C.S., and Rubin, G.M. (2000). The ryanodine receptor is essential for larval development in Drosophila melanogaster. Proceedings of the National Academy of Sciences of the United States of America 97, 5942-5947.

Takekura, H., and Franzini-Armstrong, C. (2002). The structure of Ca(2+) release units in arthropod body muscle indicates an indirect mechanism for excitation-contraction coupling. Biophys J 83, 2742-2753.

Takeshima, H., Nishimura, S., Matsumoto, T., Ishida, H., Kangawa, K., Minamino, N., Matsuo, H., Ueda, M., Hanaoka, M., Hirose, T., and Numa, S. (1989). Primary structure and expression from complementary DNA of skeletal muscle ryanodine receptor. Nature 339, 439-445.

Tanabe, T., Takeshima, H., Mikami, A., Flockerzi, V., Takahashi, H., Kangawa, K., Kojima, M., Matsuo, H., Hirose, T., and Numa, S. (1987). Primary structure of the receptor for calcium channel blockers from skeletal muscle. Nature 328, 313-318.

Zheng, W., Feng, G., Ren, D., Eberl, D.F., Hannan, F., Dubald, M., and Hall, L.M. (1995). Cloning and characterization of a calcium channel alpha 1 subunit from Drosophila melanogaster with similarity to the rat brain type D isoform. The Journal of neuroscience : the official journal of the Society for Neuroscience 15, 1132-1143.

CHAPTER 3. *Dstac* is required for normal circadian activity rhythms in *Drosophila*

I-Uen Hsu, Jeremy W. Linsley, Jade E. Varineau, Orie T. Shafer and John Y. Kuwada

[Published in 2018]

Chronobiology International, 35:7, 1016-1026. DOI: 10.1080/07420528.2018.1454937

3.1 Abstract

The genetic, molecular and neuronal mechanism underlying circadian activity rhythms is well characterized in the brain of *Drosophila*. The small ventrolateral neurons (s-LN$_V$s) and pigment dispersing factor (PDF) expressed by them are especially important for regulating circadian locomotion. Here we describe a novel gene, *Dstac*, which is similar to the *stac* genes found in vertebrates that encode adaptor proteins, which bind and regulate L-type voltage-gated Ca^{2+} channels (CaChs). We show that Dstac is coexpressed with PDF by the s-LN$_V$s and regulates circadian activity. Furthermore, the L-type CaCh, Dmca1D, appears to be expressed by the s-LN$_V$s. Since vertebrate Stac3 regulates an L-type CaCh we hypothesize that Dstac regulates Dmca1D in s-LN$_V$s and circadian activity.

3.2 Introduction

The *Drosophila* brain contains a network of neurons that express clock genes and regulate circadian locomotion (Nitabach and Taghert 2008). A subset of neurons that expresses the pigment dispersing factor (PDF) neuropeptide is critical for rhythmicity of locomotor

behavior. These are the large and small ventrolateral neurons (l-LN$_V$s and s-LN$_V$s) (Helfrich-Forster 1997; Renn et al., 1999). Genetic ablation of PDF$^+$ neurons, genetic silencing of PDF$^+$ neurons and null mutations in *pdf* all disrupt circadian rhythms in locomotion (Renn et al., 1999; Nitabach et al., 2002; Sheeba et al., 2010). Specific knockdown of PDF in s-LN$_V$ neurons disrupts circadian locomotion; demonstrating the critical role of PDF in the s-LN$_V$ neurons for circadian rhythms (Shafer and Taghert 2009). Furthermore PDF, sNPF, which is another neuropeptide expressed by s-LNv neurons, and light act to set the phases of circadian neurons that are sequentially active via inhibition of Ca^{2+} activity in these neurons (Liang et al., 2017). This includes negative feedback onto the s-LN$_V$ neurons. Thus proper activity of PDF$^+$ neurons is key to proper circadian rhythm.

Vertebrate genomes contain a small family of *stac* (SH3 and cysteine-rich domain (CRD) containing protein) genes with *stac3* expressed selectively by skeletal muscles (Suzuki et al., 1996; Horstick et al., 2013; Nelson et al., 2013; Reinholt et al., 2013). Stac3 is a regulator of electrical/contraction (EC) coupling in skeletal muscles and is required for release of Ca^{2+} from the sarcoplasmic reticulum of skeletal muscles and normal muscle contraction in both zebrafish and mice (Horstick et al., 2013; Nelson et al., 2013). Stac3 regulates EC coupling by controlling the stability, organization and voltage-dependency of the dihydropyridine receptor, a L-type Ca^{2+} channel (CaCh) (Linsley et al., 2017), which is the voltage sensor for EC coupling in skeletal muscles. Stac3 binds to Ca$_V$1.1, the α subunit of the skeletal muscle dihydropyridine receptor (Campligio and Flucher 2017; Wong King Yuen et al., 2017), and a missense mutation in *STAC3* is causal for the congenital Native American myopathy (Horstick et al., 2013). The other *stac* genes are expressed by a subset of neurons in the vertebrate nervous system (Suzuki et al.,

1996; Lein et al., 2007; Legha et al., 2010) but their function is unknown. The finding that Stac3 regulates L-type CaChs, however, suggests that the other Stac proteins may also regulate CaChs in neurons. In fact Stac1 can form a molecular complex with $Ca_V3.2$ to regulate the surface expression of this T-type CaChs in mammalian cell lines (Rzhepetskyy et al., 2016), and the tandem SH3 domains of Stac2 each bind $Ca_v1.1$ and $Ca_v1.2$ (Wong King Yuen et al., 2017). Thus it is possible that neuronal Stac proteins may regulate CaChs for normal nervous system function.

To better understand how the s-LN_Vs regulate circadian locomotion in the *Drosophila* brain we identified a novel gene *Dstac* that is similar to the vertebrate *stac* genes. *Dstac* is expressed by a subset of neurons in the *Drosophila* brain including the PDF^+ s- and l-LN_Vs and regulates circadian locomotion in *Drosophila*. Furthermore, the L-type CaCh, Dmca1D, appears to be expressed by these same neurons. These findings define a functional role for a *stac* gene expressed by neurons and suggest the hypothesis that Dstac regulates the L-type CaCh, Dmca1D, in the s-LN_V neurons and that this is important for the regulation of circadian rhythm by PDF.

3.3 Methods

3.3.1 Fly strains

Fly strains used in this paper were: w^{1118}, *yw*, *Pdf (M)-GAL4* (Renn et al. 1999), *UAS-DCR2* (BL#24651), *UAS-Dstac-RNAi* (VDRC 103824 used in the behavioral analysis and VDRC 105848 used in western blot), *UAS-Luciferase-RNAi* (BL#31603), *Mef2-GAL4* (BL#27390), *Dmca1D-GAL4* (VDRC 202490), *Dstac-gfp trap* (BL#40742) and *UAS-mCD8-tdtomato* (a gift from

Dr Bing Ye, University of Michigan).

3.3.2 Anti-Dstac production

A *Dstac* cDNA that contained sequences for the CRD and SH3 domains were cloned and expressed with a His-SUMO fusion protein in BL21 (DE3) cells, and purified using Ni-NTA agarose (Invitrogen). The His-SUMO tag was cleaved by SUMO proteases to obtain the untagged Dstac proteins. The purified untagged Dstac proteins were further purified by NuPAGE 4-12% SDS-polyacrylamide gel electrophoresis (SDS-PAGE) using a Bis-Tris Gel (Invitrogen) followed by excision of the appropriate Coomassie-stained band. Rabbits were immunized by a commercial vendor (ProSci) with gel slices of purified Dstac proteins. Dstac antibodies in the antiserum were purified by using a NHS-activated agarose column that was conjugated with Dstac fusion proteins. The specificity of the anti-Dstac was confirmed by Western blot analysis.

3.3.3 Western blot analysis

Muscles from larvae with *Dstac* knockdowned specifically in body wall muscles (*UAS-Dstac-RNAi/+; UAS-DCR2/Mef2-GAL4*, n = 37) and control larvae (*UAS-DCR2/+;UAS-Luciferase-RNAi/Mef2-GAL4*, n = 37) were dissected and frozen immediately on dry ice. Muscles were homogenized in RIPA buffer (ThermoFisher) with protease inhibitors (ThermoFisher) and centrifuged to exclude debris. The muscle lysates were loaded (seven wells/genotype) and separated by SDS-PAGE. The antibodies used for immunoblotting were rabbit anti-Dstac (1:500), mouse anti-actin (1:10000, MP Biomedicals), anti-rabbit IgG HRP (1:2000, Santa Cruz

Biotechnology), and anti-mouse IgG HRP (1:10000, Santa Cruz Biotechnology). The protein bands were detected with Chemidoc MP imaging system (Bio-Rad). The intensities of protein bands were quantified by gel analyzer of imageJ. The sizes of the protein bands were estimated from the Western blots using a regression analysis.

3.3.4 Immunofluorescence labeling

Third instar larval brains of *Dstac-gfp* trap were dissected in ice-cold 1x phosphate buffered saline (PBS) and fixed immediately in 4% paraformaldehyde in 1xPBS for 30 minutes at room temperature (RT). We rinsed the tissues with 1xPBS with 0.1% Triton X-100 (1xPBSTX-100) five times, 5 minutes/time, and permeabilized with 0.25% TX-100 in 1XPBS for 15 min at RT. After five washes (5 minutes/wash) with 1xPBSTX-100, we blocked the brains with 1% normal goat serum (NGS), 0.2% bovine serum albumin (BSA), and 0.1% TX-100 in 1xPBS for an hour at RT. The brains were incubated with chicken anti-GFP (1:5000, Aves Laboratories, Tigard, OR) in the blocking solution at 4°C for 2 days. The brains were washed with 1xPBSTX- 100 for 5 times, 5 minutes/time, and then incubated with anti-chicken Alexa Fluor 488 (1:2000 Jackson ImmunoResearch). Following five washes (5 minutes/wash) with 1xPBSTX-100, we mounted the brains with FluoroGel with DABCO (Electron Microscopy Sciences).

Adult *Dstac-gfp* trap brains were dissected in ice-cold 1xPBS and fixed immediately in 4% paraformaldehyde in 1xPBS for 30 minutes at RT. The brains were rinsed with 1xPBSTX-100 for 5 times, 15 minutes/time. The brains were blocked with 10% NGS in 1xPBS with 2% TX-100 for 2 h at RT. The brains were incubated with mouse anti-PDF (Blau 2005) (1:500, PDF C7 (deposited by Blau, Justin (DSHB Hybridoma Product PDF C7)) in 1xPBS with 1% NGS and 0.25%

TX-100 (dilution buffer) overnight at RT. The brains were washed with 1xPBS with 3% NaCl and 1% TX-100 (wash buffer) for 3 times, 15 minutes/time. We incubated the brains with anti-mouse Alexa Fluor 647 (1:1000, Invitrogen) in dilution buffer overnight at RT. The brains were then washed with wash buffer and incubated with chicken anti-GFP (1:5000, Aves Laboratories) and anti-chicken Alexa Fluor 488 (1:2000 Jackson ImmunoResearch) following the same procedures described above. The brains were mounted with DABCO FluoroGel.

w^{1118} adult brains were dissected and immunolabeled following the same procedures described above except that the brains were fixed overnight with Bouin's fixative and treated with 0.05% collagenase (Worthington Biochemical) for 10 minutes. The antibodies used were mouse anti-PDF (1:500, Developmental Studies Hybridoma Bank at the University of Iowa), anti-mouse Alexa Fluor 647 (1:500; Invitrogen), rabbit anti-Dstac (1:50, this paper) and anti-rabbit 488 (1:1000; Invitrogen).

The antibodies used in the labeling of *UAS-mCD8-tdtomato/+;Dmca1D-GAL4/+* adult brains were mouse anti-PDF (1:500, Developmental Studies Hybridoma Bank at the University of Iowa), anti-mouse Alexa Fluor 488 (1:1000, Invitrogen), rabbit anti-RFP (1:1000, Rockland) and anti-rabbit 647 (1:1000. Invitrogen).

The *Dstac-gfp* trap larval/adult brains and larval muscles were imaged using an upright Leica SP5 confocal microscope with a 20x or 63x objective. The others were imaged using a Leica SP8 confocal microscope with a 63x or 100x objective and digital zoom.

3.3.5 In situ hybridization

A 0.28-kilobase pair fragment of the Dstac cDNA was cloned into a TA vector. The

sequence of the fragment was: cgcaatggagcctccagcacagcctccgagccgc tgcgtcccaatctggatggcagccaccatctgcaggagtacacctacaagaagataacggcctgcgacgtctgctcccagattctgagagggca cacacgccagggattacgctgccgcatctgcaagctgaacgcccatggagattgcgcccccaatctgccgcgctgccagccaaagcagaagctg ctccggcgacagaagagcacatcggagctggagaatcgtgttgatatcgaggaagaaa.

The *Dstac* RNA probe was synthesized using T7 and SP6 RNA polymerases (Promega) and digoxigenin-labeled dNTPs (Roche Diagnostics). In situ hybridization was performed on the third instar larval muscles of *Dstac-gfp* trap. The third instar larval muscles were dissected in 1xPBS and fixed with 4% PFA immediately after dissection. Samples were washed by 1xPBS with 0.1% tween20 (PBT) and dehydrated with 25%, 50%, 75% and 100% methanol and rehydrated with methanol. Samples were washed with 1xPBT and incubated with 5ug/mL Proteinase K in 1xPBT for 30 minutes at RT. The samples were washed with 1xPBT and fixed again with 4% PFA and 0.25% Glutaraldehyde in 1xPBT. The samples were washed by 1xPBT, one wash with the hybridization buffer (HB) (5xSSC containing 50% formamide, 0.1% tween-20, 0.29 mg/mL tRNA (Roche Diagnostics), 0.05 mg/ mL Heparin, and 9.2 mM citric acid), and incubated with HB for 2 h at 65°C. The samples were then incubated with 1.2 ng/uL Dstac RNA probes overnight at 65°C. Following hybridization, the samples were washed four times with mixture of HB and 2xSSC with 0.1% tween-20 (SSCT), twice with 2xSSCT, and twice with 0.2xSSCT at 65°C. Samples were washed with mixture of 0.2xSSCT and 1xPBT for six times at RT. Samples were blocked with 5% sheep serum and 0.2% BSA in 1xPBT for 2 h at RT. Samples were incubated with alkaline phosphatase-conjugated anti-digoxigenin Fab fragment (1:5000, Roche Diagnostics, Risch-Rotkreuz, Switzerland) at 4°C overnight. Samples were washed 15 times with 1xPBT and 3 times with NTMT (0.1M NaCl, 0.1 M Tris-HCl pH 9.5, 50 mM $MgCl_2$, 1% tween-20 and 0.24

mg/mL Levamisole). The *Dstac* RNA probe hybridization was visualized by incubating the samples with Fast-Red (Roche Diagnostics). The development was stopped by 2 washes of NTMT and 10 washes of 1xPBT. The samples were fixed again with 4% PFA and 0.25% Glutaraldehyde in 1xPBT. *Dstac-gfp* trap was labeled following the immunofluorescence labeling protocol with rabbit anti-GFP (1:1000, Torrey Pines Biolabs) and anti-rabbit Alexa Fluor 488 (1:1000, Invitrogen). Samples were washed with 50% and 70% of glycerol in 1xPBT and mounted. Samples were imaged using a Leica SP5 confocal microscope with a 20x objective.

3.3.6 Analysis of activity rhythms

All flies for the activity rhythm analysis were reared at 25°C under a 12 h:12 h light dark cycle (LD). Adult males aged between 1 and 5 days were placed individually in glass tubes and loaded onto the Trikinetics DAM2 monitors (Waltham, MA) for locomotor activity recordings. Flies were entrained for 6 days at 25°C under LD and then subjected to constant darkness (DD) for 14 days. The locomotor activity data were processed by the *Drosophila* Activity Monitoring system (Trikinetics, Waltham, MA) into 30 minutes bins for activity analysis under LD and 1 minute bin under DD. The activity rhythm analysis under LD was analyzed by a counting macro (Pfeiffenberger et al., 2010). The normalized morning startle response was determined as the ratio of the activity of the first bin in light/activity of the last bin in dark (Stoleru et al., 2004). Thus a ratio of 1 would signify the loss of the morning startle response. The morning and evening anticipation were calculated by the “anticipation phase score” method (ratio of the activity 3 h prior to lights on/off to the activity 6 h prior to lights on/off; Harrisingh et al., 2007). Clocklab (Actimetrics) was used for the circadian rhythm analysis. Dead flies were determined

by loss of activity according to the actograms and were excluded from the analysis. The rhythmicity and free-running periods of individual flies were determined by Chi-square analysis with a confidence level of 0.01 (Sokolove and Bushell 1978). “Power” is the peak activity in the Chi-square periodogram and “significance” is the minimum value in the periodogram where a fly is considered rhythmic. The rhythmic power was calculated by subtracting the “significance” values from the “power” values that are generated by the Chi-square periodogram analysis. A fly with a rhythmic power equal to or less than zero was considered arrhythmic. The free running periods were analyzed with the range between 14 and 36 h with 0.5 h interval. The analysis of free-running periods only included flies displaying significant periodicities under constant darkness and temperature.

3.3.7 Statistical analysis

The rhythmic ratio (number of rhythmic flies/number of total flies × 100%) of the experimental group (*Pdf-GAL4/y;UAS-Dstac-RNAi/+;UAS-DCR2/+*) and the other control groups was compared by Fischer’s Exact test. The free-running periods and morning and evening anticipation were analyzed by one-way ANOVA (Kruskal–Wallis test) among all the groups and Dunn’s multiple comparison tests were used to compare the control groups particularly with the experimental group. The normalized morning startle response was compared with the hypothetical value of 1 (defined as loss of morning startle response) by Wilcoxon Signed Rank Test. The protein band intensities between Dstac knock- down muscles and control muscles were compared by the Mann–Whitney U test. D’Agostino-Pearson omnibus normality test was used to decide the parametric tests or nonparametric tests to be used.

3.4 Results

3.4.1 *Dstac* is similar to the vertebrate *stac* genes

We identified a single *Drosophila* gene (CG43729) that was potentially related to the human *STAC1* (SH3 and CRD) gene with an Ensembl search (http://www.ensembl.org/Homo_sapiens/Gene/Compara_Tree?db=core;g=ENSG00000144681; r= 3:36380344-36548007; Aken et al., 2017). An EnsemblMetazoa search further found potential *stac* genes in numerous invertebrate lineages (http://metazoa.ensembl.org/Drosophila_melanogaster/Gene/Compara_Tree/pan_compara?db=core; g=FBgn0263980;r=2R:15401096-15471884;t=FBtr0330009;collapse=none). CG43729 appears to be alternatively spliced (Figure 3.1F) and encodes for a protein containing a SH3 domain and CRD that are the defining features unique to vertebrate *stac* genes (Suzuki et al., 1996). Furthermore as determined by EMBOSS (Rice et al., 2000), the amino acid sequences of the SH3 and CRD of CG43729 are well conserved with those of zebrafish Stac1 (67% and 59% similarity, respectively), human Stac1 (71% and 65%, respectively), zebrafish Stac3 (67% and 57% similarity, respectively) and human Stac3 (71% and 61%) (Figure 3.1A, 3.1B) suggesting that CG43729 encodes for a Stac protein and thus named this gene *Dstac*. The putative Dstac protein also appears to contain a BAR domain normally associated with membrane curvature (reviewed in Salzer et al., 2017) in the N terminal region of Dstac that is not found in vertebrate Stac proteins but is found in invertebrate Stac proteins.

3.4.2 *Dstac* appears to be expressed by PDF^{+} neurons in the brain

Examination of a MiMIC transposon mediated transgenic line (Venken et al., 2011) in

which *gfp* is inserted into the *Dstac* locus (*Dstac-gfp trap*) showed that *Dstac* appears to be expressed by both body wall muscles and a subset of neurons in the CNS of third instar larvae and adult brain (Figure 3.1C). Interestingly in the adult brain the l-LNvs and s-LNVs that are key regulators of circadian locomotor rhythms express *Dstac*. In *Dstac-gfp* flies anti-PDF labeled l-LNvs and s-LNVs also expressed GFP (Figure 3.1D). Furthermore, these neurons were colabeled with anti-PDF and anti-Dstac (Figure 3.1E). Western blots from larval muscles probed with anti-Dstac labeled four bands (40, 69, 94 and 108 kD) suggesting that there are at least four isoforms of Dstac in muscles (Figure 3.1F). The protein levels of all four isoforms were significantly reduced when Dstac was knocked down in muscles (Figure 3.1F), indicating that anti-Dstac specifically detected Dstac proteins and that *Dstac* RNAi is effective.

3.4.3 The L-type CaCh, *Dmca1d*, appears to be expressed by PDF$^+$ neurons in the brain

Since Stac3 regulates a L-type CaCh in vertebrate skeletal muscles (Linsley et al., 2017), we wondered whether Dstac might regulate a L-type CaCh in the PDF$^+$ s-LN$_V$s and l-LN$_V$s. To see if this was possible we examined whether a L-type CaCh is coexpressed with PDF in the s-LN$_V$s and l-LN$_V$s. The *Drosophila* genome appears to contain a single L-type CaCh, *Dmca1D* (Zheng et al., 1995; Eberl et al., 1998). Anti-PDF labeling of *Dmca1D:GAL4;UAS:mCD8tdTomato* flies showed that the s-LN$_V$s and l-LN$_V$s coexpress mCD8tdTomato and PDF (Figure 3.1G). Thus it is possible that Dstac and Dmca1D are coexpressed by PDF$^+$ s-LN$_V$s and l-LN$_V$s although the specificity of the *Dmca1D:GAL4;UAS:mCD8tdTomato* flies is as yet uncharacterized.

3.4.4 Knockdown of Dstac in PDF$^+$ neurons disrupts circadian locomotion

Since Dstac is expressed by the PDF$^+$ s-LN$_V$s and l-LN$_V$s, we tested whether knocking down Dstac specifically in PDF$^+$ neurons might affect circadian locomotion (Table 3.1). *Pdf:GAL4;UAS:DstacRNAi* flies but not control flies displayed altered circadian locomotor rhythms (Figure 3.2A); a significant increase in arrhythmic flies in constant dark (DD) conditions and a small but significant increase in the free-running period of flies displaying significant periodicities under DD. Furthermore, under LD conditions, the startle response to light onset was eliminated, but there was no change in the morning nor evening anticipation (Figure 3.2B, 3.2D). There were no obvious morphological defects in *Pdf:GAL4;UAS:DstacRNAi* flies (Figure 3.2C) and other than the loss of the morning startle response their activity under LD was comparable to wt con-trol flies suggesting that in these flies the altered circadian locomotor rhythm was not due to any obvious deleterious effect on locomotion in general.

Table 1. Knocking down *Dstac* in PDF neurons increases arrhythmicity and free-running periods in DD and decreases morning startle response in LD.

Genotype	DD 5-13				LD 3-6	
	Rhythmicity		Free-running periods		Morning startle response	
	n rhythmic (%)	p (Fischer's Exact test)	Hours Mean (±SEM)	p (Dunn's Multiple Comparison test)	Normalized Mean (±SEM)	p (Wilcoxon Signed Rank test)
yw,PDF-GAL4/y;+;+	32 (100)	0.0001	24.11 (±0.04)	< 0.0001	6.168 (±2.37)	<0.0001
yw/y;+;UAS-DCR2/+	29 (93)	0.0106	24.16 (±0.08)	0.0001	6.605 (±1.24)	<0.0001
yw/y;UAS-Dstac-RNAi/+;+	29 (93)	0.0106	24.24 (±0.16)	0.0139	14.590 (±6.18)	<0.0001
yw/y;UAS-Dstac-RNAi/+:UAS-DCR2/+	31 (96)	0.0012	24.42 (±0.37)	< 0.0001	7.601 (±2.85)	<0.0001
yw,PDF-GAL4/y;+;UAS-DCR2/+	27 (90)	0.0311	24.06 (±0.33)	0.0368	1.879 (±0.11)	<0.0001
yw,PDF-GAL4/y;UAS-Dstac-RNAi/+;+	28 (93)	0.0106	24.80 (±0.05)	> 0.9999	2.115 (±0.34)	0.0002
yw,PDF-GAL4/y;UAS-Dstac-RNAi/+;UAS-DCR2/+	20 (64)	------	24.80 (±0.11)[#]	------	1.156 (±0.10)	0.1870

n = number of flies tested

# denotes significantly different from all other genotypes except for *yw,PDF-GAL4/y;UAS-Dstac-RNAi/+;+*

Figure 3.1

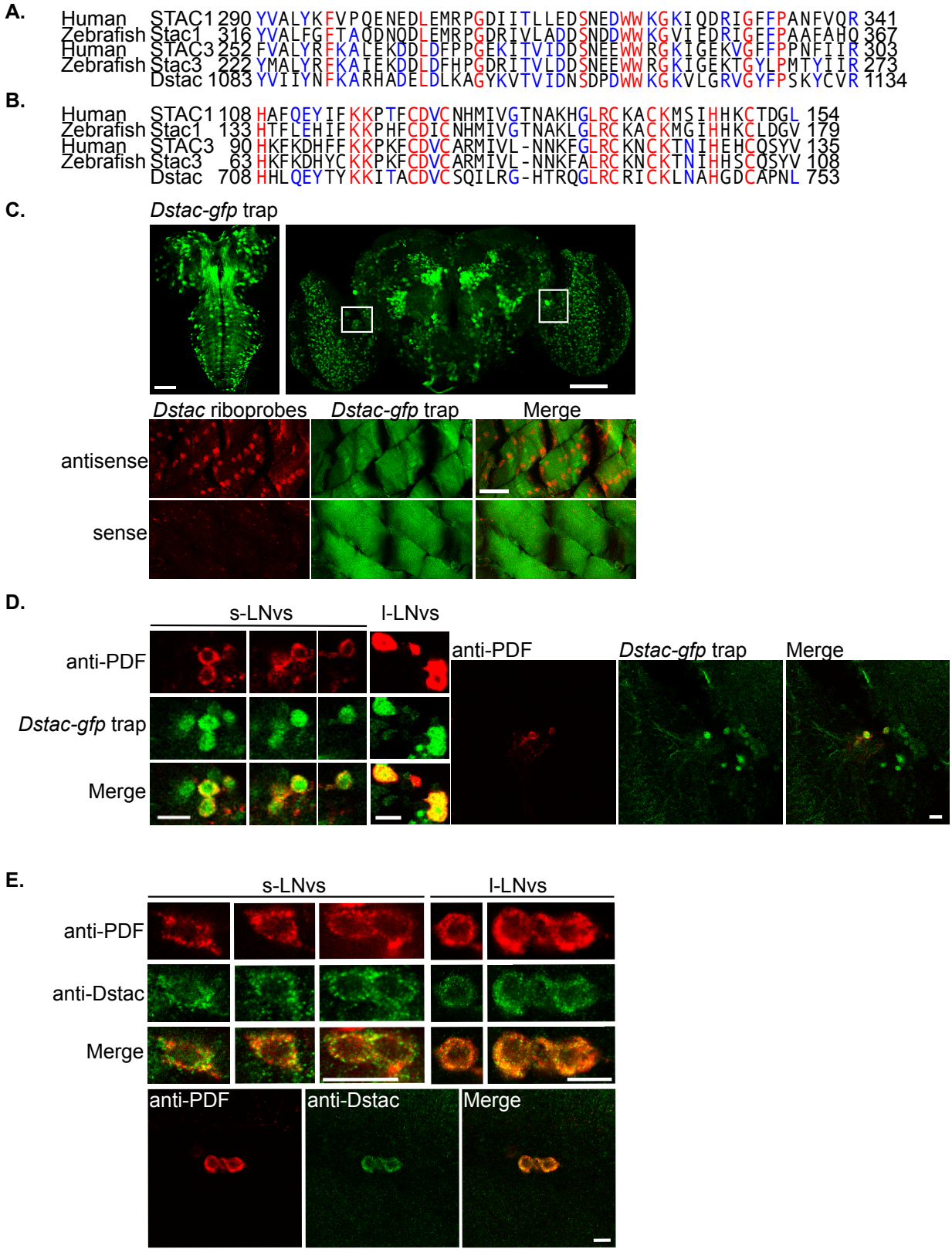
A.
Human STAC1 290 YVALYKFVPQENEDLEMRPGDIITLLEDSNEDWWKGKIQDRIGFFPANFVQR 341
Zebrafish Stac1 316 YVALFGFTAQDNQDLEMRPGDRIVLADDSNDDWWKGVIEDRIGFFPAAFAHQ 367
Human STAC3 252 FVALYRFKALEKDDLDFPPGEKITVIDDSNEEWWRGKIGEKVGFFPPNFIIR 303
Zebrafish Stac3 222 YMALYRFKAIEKDDLDFHPGDRITVLDDSNEEWWRGKIGEKTGYLPMTYIIR 273
Dstac 1083 YVIIYNFKARHADELDLKAGYKVTVIDNSDPDWWKGKVLGRVGYFPSKYCVR 1134
B.
Human STAC1 108 HAFQEYIFKKPTFCDVCNHMIVGTNAKHGLRCKACKMSIHHKCTDGL 154
Zebrafish Stac1 133 HTFLEHIFKKPHFCDICNHMIVGTNAKLGLRCKACKMGIHHKCLDGV 179
Human STAC3 90 HKFKDHFFKKPKFCDVCARMIVL-NNKFGLRCKNCKTNIHEHCQSYV 135
Zebrafish Stac3 63 HKFKDHYCKKPKFCDVCARMIVL-NNKFALRCKNCKTNIHHSCQSYV 108
Dstac 708 HHLQEYTYKKITACDVCSQILRG-HTRQGLRCRICKLNAHGDCAPNL 753
C.
Dstac-gfp trap
Dstac riboprobes
Dstac-gfp trap
Merge
antisense
sense
D.
s-LNvs
l-LNvs
anti-PDF
Dstac-gfp trap
Merge
anti-PDF
Dstac-gfp trap
Merge
E.
s-LNvs
l-LNvs
anti-PDF
anti-Dstac
Merge
anti-PDF
anti-Dstac
Merge

Figure 3.1 (continued)

F.

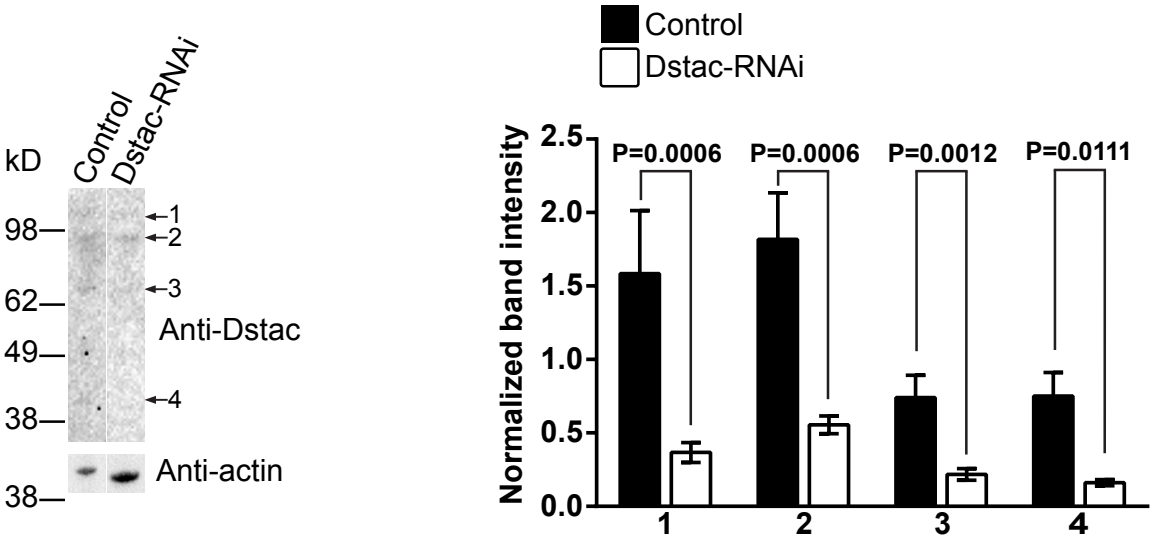

G.

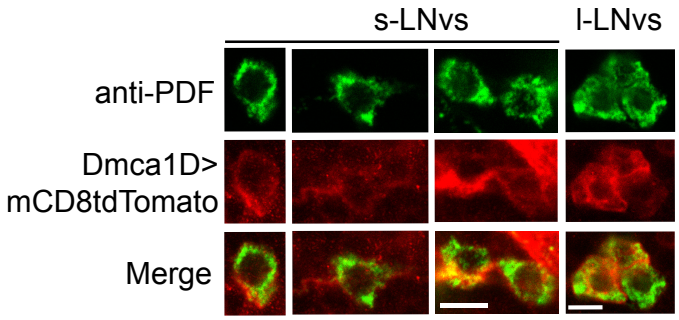

Figure 3.1 Dstac is similar to vertebrate Stac1 and Stac3 and expressed by a subset of neurons and by body wall muscles.

Alignment of the amino acid sequences of the SH3 domains (A) and CRD domains (B) between zebrafish Stac1, human Stac1, zebrafish Stac3, human Stac3 and Dstac. Amino acids that are identical among all three genes are highlighted in red; amino acids that are identical between Dstac and Stac1 or Stac3 are highlighted in blue. (C) The expression pattern of the *Dstac-gfp* trap (above) in the third instar larval CNS (left) and in the adult brain (right). Expression of Dstac by body wall muscles determined by labeling by a riboprobe for *Dstac* (below). The larval CNS expression is from a stack of focal planes of the dorsal side of the third instar larval CNS and adult brain expression from a stack of throughout the entire brain. The muscle images are a single focal plane. Boxes in the adult brain panel denote the region where the s- and l-LN_V neurons are located. Scale bars, 75 μm. (D) *Dstac-gfp trap* adult brains labeled with anti-PDF showed colocalized expression of GFP and PDF in the s-LN_V and l-LN_V neurons. High magnification views of s- and l-LN_Vs (left panels). Lower magnification views of LN_Vs showing that only some *Dstac-gfp* neurons express PDF (right panels). Images are single focal planes. Scale bars, 10 μm. (E) Anti-PDF and anti-Dstac labeling of w^{1118} adult brain showed coexpression of PDF and Dstac in the s-LN_Vs and l-LN_Vs (top 3 sets of panels). Lower magnification images of l-LN_Vs showing that anti-Dstac labels PDF^+ neurons but not other neurons in the vicinity (bottom set of panels). Images are single focal planes. Scale bars, 10 μm. (F) Western blots showed anti-Dstac labeled bands (1–4) in control larval muscles (*UAS-DCR2/+;UAS-Luciferase-RNAi/Mef2-GAL4*) and the intensities of all bands were significantly lower in Dstac-RNAi larval muscles (*UAS-Dstac-RNAi/+;UAS-DCR2/Mef2-GAL4*). The protein bands of control and Dstac-RNAi larval muscles were quantified and analyzed by Mann–Whitney U test. (G) *UAS-mCD8-tdTomato/+; Dmca1D-GAL4/+* adult brain labeled with anti-PDF showed colocalized expression of tdTomato and PDF in the s-LN_Vs and l-LN_Vs. Images are single focal planes. Scale bars, 5 μm.

Figure 3.2

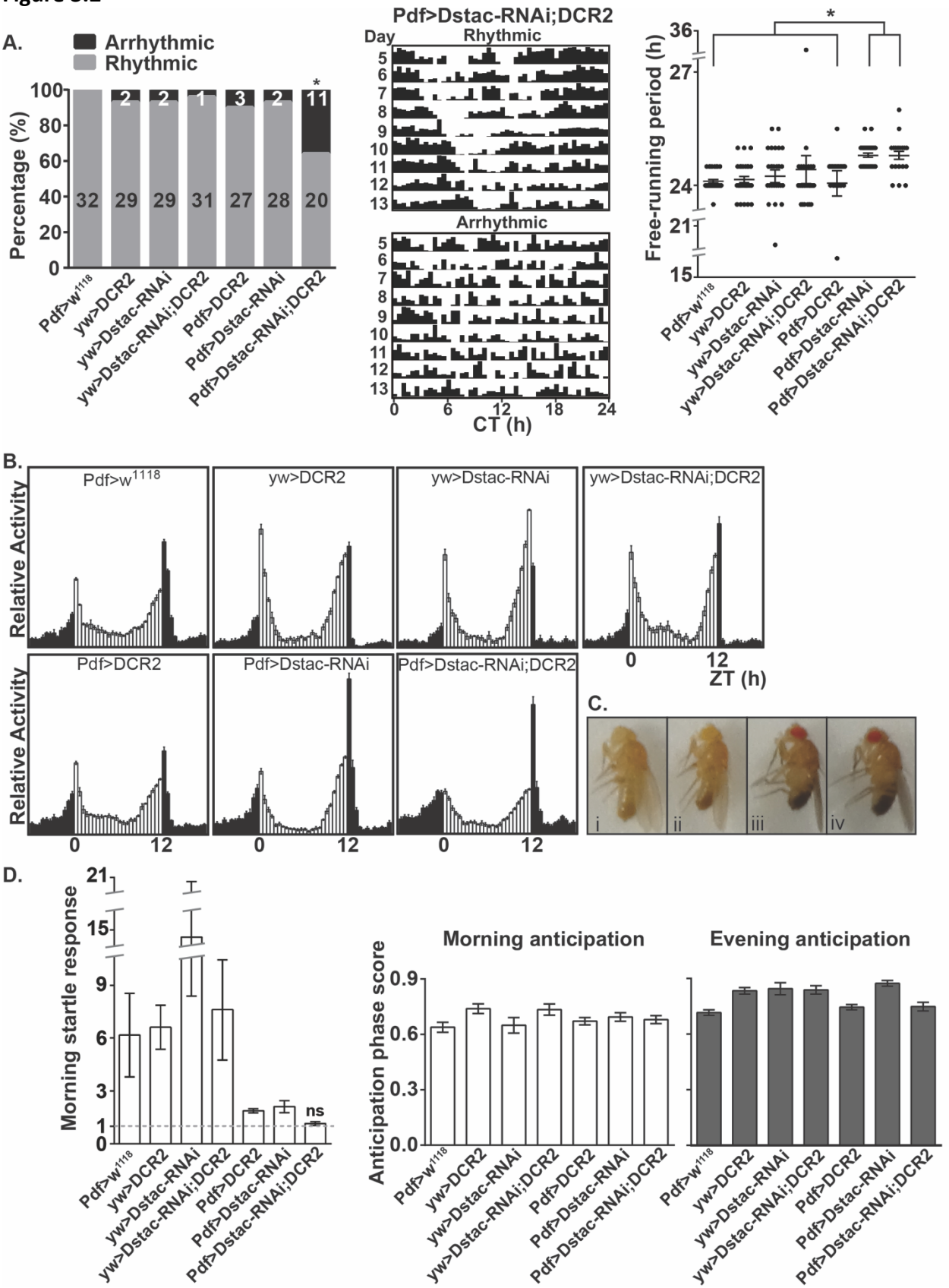
A.
Arrhythmic
Rhythmic
Percentage (%)
100
80
60
40
20
0
32
29
29
31
27
28
20
2
2
1
3
2
11
*
Pdf>w1118
yw>DCR2
yw>Dstac-RNAi
yw>Dstac-RNAi;DCR2
Pdf>DCR2
Pdf>Dstac-RNAi
Pdf>Dstac-RNAi;DCR2
Pdf>Dstac-RNAi;DCR2
Day
Rhythmic
Arrhythmic
5
6
7
8
9
10
11
12
13
0
6
12
18
24
CT (h)
Free-running period (h)
36
27
24
21
15
*
B.
Relative Activity
Pdf>w1118
yw>DCR2
yw>Dstac-RNAi
yw>Dstac-RNAi;DCR2
Pdf>DCR2
Pdf>Dstac-RNAi
Pdf>Dstac-RNAi;DCR2
0
12
ZT (h)
C.
i
ii
iii
iv
D.
Morning startle response
21
15
9
6
3
1
0
ns
Anticipation phase score
Morning anticipation
Evening anticipation
0.9
0.6
0.3
0.0

Figure 3.2 Knocking down Dstac in PDF neurons lead to arrhythmic circadian rhythms in DD and elimination of the morning startle response in LD.

(A) Left, the percentage of rhythmic and arrhythmic flies from day 5 to 13 under DD. * denotes that the Dstac knockdown flies (*Pdf-GAL4/y;UAS-Dstac-RNAi/+;UAS-DCR2/+*) were significantly less rhythmic than all the other control groups (see Table 1). Numbers denote the number of flies that were rhythmic and arrhythmic. Center, actograms from a rhythmic and arrhythmic *Dstac* RNAi fly under DD. Right, the free-running periods of flies displaying significant periodicities under DD and constant temperature from day 5 to 13 in constant darkness. * denotes that both *Dstac* knockdown flies with or without *UAS-DCR2* displayed a slight but significant increase in the free-running periods when compared with the other control groups. Each dot represents an individual fly. (B) The activity histogram of each genotype from day 3 to 6 under LD showed no apparent change in morning and evening anticipation but a decrease morning startle response in *Pdf-GAL4/y;UAS-Dstac-RNAi/+;UAS-DCR2/+* flies. (C) The morphology of *Pdf:GAL4;UAS:DstacRNAi* flies (2–3 days) appeared normal. (i) *yw,PDF-GAL4/y;+;+*. (ii) *yw,PDF-GAL4/y;+;UAS-DCR2/+*. (iii) *yw,PDF-GAL4/y;UAS-Dstac-RNAi/+;+*. (iv) *yw,PDF-GAL4/y;UAS-Dstac-RNAi/+;UAS-DCR2/+*. (D) Left, the value of the normalized morning startle response (see Methods) of *Dstac* knock down flies was not significantly (ns) different from the value of 1 by Wilcoxon Signed Rank test. The values of the normalized morning startle responses of all the other control groups were significantly larger than 1. The morning anticipation (middle) and evening anticipation (right) from day 3 to 6 under LD was not significantly different between the *Dstac* knock down flies and controls (Dunn's multiple comparison test).

3.5 Discussion

The Stac proteins are defined by the unique combination of a SH3 and CRD (Suzuki et al., 1996). The *stac* genes are found widely both in vertebrate and invertebrate lineages. In most vertebrate genomes there is a small family of *stac* genes with *stac3* selectively expressed by skeletal muscles while the other *stacs* are expressed within the nervous system. In *Drosophila*, there appears to be a single *stac* gene. The conclusion that *Dstac* is a *stac* gene is based upon the presence of highly conserved SH3 and CRD of the predicted Dstac protein along with the expression of *Dstac* by both muscles and neurons. The latter is concordant with the expression of vertebrate *stac3* by skeletal muscles and the other vertebrate *stacs* by neurons. One difference between invertebrate *stac* genes and vertebrate *stac* genes is the presence of a BAR domain. BAR domains are associated with membrane curvature (reviewed in Salzer et al., 2017) but the significance of the BAR domain in invertebrate *stacs* including Dstac is unknown. Interestingly, in vertebrates the Bin1 protein from which the BAR domain draws its name contains both BAR and a SH3 domain and like Stac3, associates with $Ca_v1.1$ in skeletal muscle where its BAR domain is associated with the formation of T-tubules in muscle (Lee et al., 2002). Mutations in the BAR domain of bin1 destabilize T-tubules and are associated with centronuclear myopathy in humans (Claeys et al., 2010). Thus the BAR domain may be critical to the function of Dstac in invertebrate muscle.

The expression of Dstac by PDF^+ neurons and the disruption of circadian locomotion when *Dstac* is knocked down in these neurons suggest that Dstac is necessary for normal circadian locomotor rhythms in *Drosophila*. The disruption of such rhythms in *Drosophila* is the first functional phenotype described for a *stac* gene in neurons in any organism.

How does Dstac regulate the function of PDF^+ neurons and circadian locomotion? The fact that Stac3 regulates L-type CaCh in zebrafish skeletal muscles (Linsley et al., 2017) suggests that Dstac might regulate Dmca1D, the *Drosophila* L-type CaCh, in PDF^+ neurons. Indeed PDF^+ neurons appear to express Dmca1D. However, whether Dstac regulates Dmca1D, which in turn regulates circadian locomotion is at present unknown. Testing this hypothesis will require direct examination of a circadian phenotype when Dmca1D is knocked down in the s-LN_Vs and analysis of Dmca1D L-type Ca^{2+} currents in s-LN_Vs in flies with *Dstac* knocked down selectively in these neurons.

If the hypothesis is correct, then an influx of Ca^{2+} into PDF^+ neurons via the Dmca1D channels is critical for proper output presumably involving PDF by these neurons to the circadian network in the brain. l-LN_V neurons fire Na^+ channel dependent action potentials tonically or in bursts (Sheeba et al., 2008; Cao and Nitabach 2008). 2–3 Hz membrane potential oscillations underlie the tonic pattern and slower oscillations of the bursting pattern. Both fast and slower oscillations are dependent on Na^+ and Ca^{2+} influx. Additionally the membrane potential exhibits circadian changes with increasing hyperpolarization as the day progresses and increasing depolarization as the night progresses (Sheeba et al., 2008; Cao and Nitabach 2008). One possibility is that Dstac and Dmca1D might be important for one or both of these changes in excitability in PDF^+ neurons. Alternatively Dstac and Dmca1D might regulate the synaptic and/or paracrine response of PDF^+ neurons to their inputs or the synaptic and/or paracrine output of the PDF^+ neurons. For example, Dstac regulation of Dmca1D might be involved in the potential suppression of basal Ca^{2+} and termination of the circadian Ca^{2+} increase by PDF signaling in s-LN_V neurons (Liang et al., 2017). However there was no effect on

morning anticipation when Dstac was knocked down in the s-LN_V neurons as one might expect from a disruption of signaling by these neurons so how Dstac might affect circadian rhythm may be complex. Further analysis will hopefully flesh out how Dstac and Dmca1D may regulate the function of the PDF^+ neurons and thus circadian rhythms.

3.6 Acknowledgements

We thank Bethany Folk-Middlebrook, Miranda Lum and William Yau for maintaining Drosophila stocks and help with the genetics and characterization of Dstac and Cathy Collins for advise and use of facilities for the genetics.

3.7 Declaration of interest

The authors declare no conflicts of interest.

3.8 Funding

Research was supported by the National Institute of Arthritis and Musculoskeletal and Skin Diseases (NIAMS; RO1 AR063056) to JYK and by the National Science Foundation (IOS 1354046 to OTS. I-UH was supported in part by the Barbour Fellowship (Rackham Graduate School, University of Michigan), JWL by a Rackham Merit Fellowship (University of Michigan) and NIGMS (T32 GM007315), JV by a MCDB Undergraduate Summer Fellowship (University of Michigan) and BF-M by MPREP (NIH 5 R25 GM086262). The content is solely the responsibility of the authors and does not necessarily represent the official views of the National Institutes of Health; Dept. of Molecular, Cellular & Developmental Biology, Univ. of Michigan

[Undergraduate Summer Fellowship]; National Institutes of Health, MPREP [NIH 5 R25

GM086262].

3.9 References

Aken BL, Achuthan P, Akanni W, Amode MR, Bernsdorff F, Bhai J, Billis K, Carvalho-Silva D, Cummins C, Clapham P, et al. 2017. Ensembl 2017. Nucleic Acids Research. 45: D635–42.

Blau J. 2005. The double-time protein kinase regulates the subcellular localization of the Drosophila clock protein period. J Neurosci. 25:5430–37.

Campligio M, Flucher BE. 2017. STAC3 stably interacts through its C1 domain with $Ca_V1.1$ in skeletal muscle triads. Scientific Rep. doi:10.1038/srep41003.

Cao G, Nitabach MN. 2008. Circadian control of membrane excitability in *Drosophila melanogaster* lateral ventral clock neurons. J Neurosci. 28:6493–501.

Claeys KG, Maisonobe T, Bohm J, Laporte J, Hezode M, Romero NB, Brochier G, Bitoun M, Carlier RY, Stojkovic T. 2010. Phenotype of a patient with recessive centronuc- lear myopathy and a novel BIN1 mutation. Neurol. 74:519–21.

Eberl DF, Ren D, Feng G, Lorenz LJ, Van Vactor D, Hall LM. 1998. Genetic and developmental characterization of Dmca1D, a calcium channel alpha1 subunit gene in *Drosophila melanogaster*. Genetics. 148:1159–69.

Harrisingh MC, Wu Y, Lnenicka GA, Nitabach MN. 2007. Intracellular Ca^{2+} regulates free-running circadian clock oscillation *in vivo*. J Neurosci. 27:12489–99.

Helfrich-Forster C. 1997. Development of pigment-disper-sing hormone-immunoreactive neurons in the nervous system of *Drosophila melanogaster*. J Comp Neurol. 380:335–54.

Horstick EJ, Linsley JW, Dowling JJ, Hauser MA, McDonald KK, Ashley-Koch A, Saint-Amant L, Satish A, Cui WW, Zhou W, et al. 2013. Stac3 is a component of the excita- tion-contraction coupling machinery and mutated in Native American myopathy. Nat Commun. 4:1952. doi:10.1038/ncomms2952.

Lee E, Marcucci M, Daniell L, Pypaert M, Weisz OA, Ochoa GC, Farsad K, Wenk MR, De Camilli P. 2002. Amphiphysin 2 (Bin1) and T-tubule biogenesis in muscle. Science. 16:1193–96.

Legha W, Gaillard S, Gascon E, Malapert P, Hocine M, Alonso S, Moqrich A. 2010. *stac1* and *stac2* genes define discrete and distinct subsets of dorsal root ganglia neurons. Gene Expr Patterns. 10:368–75.

Lein ES, Hawrylycz MJ, Ao N, Ayres M, Bensinger A, Bernard A, Boe AF, Boguski MS, Brockway KS, Byrnes EJ, et al. 2007. Genome-wide atlas of gene expression in the adult mouse brain. Nature. 445:168–76.

Liang X, Holy TE, Taghert PH. 2017. A series of suppressive signals within the *Drosophila* circadian neural circuit gen- erates sequential daily outputs. Neuron. 94:1173–89.

Linsley JW, Hsu IU, Groom L, Yarotskyy V, Lavorato M, Horstick EJ, Linsley D, Wang W, Franzini-Armstrong C, Dirksen RT, et al. 2017. Congenital myopathy results from misregulation of a muscle Ca^{2+} channel by mutant Stac3. Proc Natl Acad Sci USA. 114:228–36.

Nelson BR, Wu F, Liu Y, Anderson DM, McAnally J, Lin W, Cannon SC, Bassel-Duby R, Olson EN. 2013. Skeletal muscle-specific T-tubule protein STAC3 mediates voltage-induced Ca^{2+} release and contractility. Proc Natl Acad Sci USA. 110:11881–86.

Nitabach MN, Blau J, Holmes TC. 2002. Electrical silencing of *Drosophila* pacemaker neurons stops the free-running circadian clock. Cell. 109:485–95.

Nitabach MN, Taghert PH. 2008. Organization of the Drosophila circadian control circuit. Curr Biol. 18:R84–93.

Pfeiffenberger C, Lear BC, Keegan KP, Allada R. 2010. Processing circadian data collected from the drosophila activity monitoring (DAM) system. Cold Spring Harb Protoc. 2010(11):pdbprot5519.

Reinholt BM, Ge X, Cong C, Gerrard DE, Jiang H. 2013. Stac3 is a novel regulator of skeletal muscle development in mice. PLoS ONE. 8:e62760.

Renn SCP, Park JH, Rosbash M, Hall JC, Taghert PH. 1999. A *pdf* neuropeptide gene mutation and ablation of PDF neurons each cause severe abnormalities of behavioral

circadian rhythms in *Drosophila*. Cell. 99:791–802.

Rice P, Longden I, Bleasby A. 2000. EMBOSS: The European molecular biology open software suite. Trends in Genetics. 16:276–77.

Rzhepetskyy Y, Lazniewska J, Proft J, Campiglio M, Flucher BE, Weiss N. 2016. A $Ca_V3.2$/Stac1 molecular complex controls T-type channel expression at the plasma mem- brane. Channels. 10:346–54.

Salzer U, Kostan J, Djinovic-Carugo K. 2017. Deciphering the BAR code of membrane modulators. Cell Mol Life Sci. 74:2413–38.

Shafer OT, Taghert PH. 2009. RNA-interference knockdown of Drosophila pigment dispersing factor in neuronal sub- sets: The anatomical basis of a neuropeptide's circadian functions. PLoS ONE. 4(12):e8298.

Sheeba V, Fogle KJ, Holmes TC. 2010. Persistence of morning anticipation behavior and high amplitude morning startle response following functional loss of small ventral lateral neurons in Drosophila. PLoS ONE. 5(7):e11628.

Sheeba V, Gu H, Sharma VK, O'Dowd DK, Holmes TC. 2008. Circadian- and light-dependent regulation of resting membrane potential and spontaneous action potential fir- ing of *Drosophila* circadian pacemaker neurons. J Neurophysiol. 99:976–88.

Sokolove PG, Bushell WN. 1978. The chi square periodo- gram: Its utility for analysis of circadian rhythms. J Theor Biol. 72:131–60.

Stoleru D, Peng Y, Agosto J, Rosbash M. 2004. Coupled oscillators control morning and evening locomotor beha- vior of Drosophila. Nature. 431:862–68.

Suzuki H, Kawai J, Taga C, Yaoi T, Hara A, Hirose K, Hayashizaki Y, Watanabe S. 1996. Stac, a novel neu- ron-specific protein with cystein-rich and SH3 domains. Biochem Biophys Res Commun. 229:902–09.

Venken KJ, Schulze KL, Haelterman NA, Pan H, He Y, Evans-Holm M, Carlson JW, Levis RW, Spradling AC, Hoskins RA, et al. 2011. MiMIC: A highly versatile transposon insertion resource for engineering *Drosophila melanogaster* genes. Nature Methods. 8:737–43.

Wong King Yuen SM, Campiglio M, Tung CC, Flucher BE, Van Petegem F. 2017. Structural insights into binding of STAC proteins to voltage-gated calcium channels. Proc Natl Acad

Sci USA. 114:E9520–8.

Zheng W, Feng G, Ren D, Eberl DF, Hannen F, Dubald M, Hall LM. 1995. Cloning and characterization of a calcium channel α_1 subunit from *Drosophila melanogaster* with similarity to the rat brain type D isoform. J Neurosci. 15:1132–43.

CHAPTER 4. Stac Protein Regulates Release of Neuropeptides

I-Uen Hsu, Jeremy W. Linsley[*], Xiaoli Zhang[*], Jade E. Varineau[#], Drew A. Berkhoudt[#], Lilly E. Reid[#], Miranda C. Lum[#], Allison M. Orzel, Ari Leflein, Haoxing Xu, Catherine A. Collins, Richard I. Hume, Edwin S. Levitan and John Y. Kuwada

[*]These authors contributed equally

[#]These authors contributed equally

[Manuscript SUBMITTED]

4.1 Abstract

Neuropeptides are important for regulating numerous neural functions and behaviors. Release of neuropeptides requires long-lasting, high levels of cytosolic Ca^{2+} that may be due to calcium induced calcium release (CICR) via the ER. However, the molecular regulation of neuropeptide release remains to be clarified. Recently, Stac3 was identified as a key regulator of L-type Ca^{2+} channels (CaCh) and excitation-contraction coupling in vertebrate skeletal muscles. There is a small family of *stac* genes in vertebrates with other members expressed by subsets of neurons in the CNS. The function of neural Stac proteins, however, is poorly understood. *Drosophila* contain a single *stac* gene, *Dstac*, which is expressed by muscles and a subset of neurons including neuropeptide expressing motor neurons. Here genetic manipulations coupled with immunolabeling, Ca^{2+} imaging, electrophysiology and behavioral

analysis revealed that Dstac regulates L-type CaChs (Dmca1D) in *Drosophila* motor neurons and this in turn controls the release of neuropeptides.

4.2 Introduction

Neuropeptides are required for a myriad of brain functions such as regulation of complex social behaviors including emotional behavior (Donaldson and Young, 2008). The activities of many neuropeptides within the brain are now well established but despite the important role neuropeptides play, our understanding of the mechanisms by which neuropeptides are released by neurons and how release is regulated is not as advanced as that of classical neurotransmitters. A greater understanding of neuropeptide release could help untangle the mechanisms of complex behaviors as well as reveal therapeutic targets that could modulate aberrant behaviors.

Release of neuropeptides, which are packaged in dense core vesicles (DCVs) rather than in small synaptic vesicles that contain neurotransmitters, often involves activation of L-type Ca^{2+} channels (CaCh) and Ca^{2+} induced Ca^{2+} release (CICR) (Garcia et al., 2006). Much of what is known about DCV exocytosis is from the study of non-neural cells. For example, in adrenal chromaffin cells the exocytosis of DCVs containing catecholamines and/or peptide hormones involves CICR either via RyR or iP_3R initiated by an influx of Ca^{2+} through voltage-gated CaChs such as L-type CaChs. In neurons the release of neuropeptides is more complex. Neuropeptides can be released from dendrites, cell bodies, axons and presynaptic terminals (Morris and Pow, 1991; Ludwig and Leng, 2006; Sobota et al., 2010) and release can involve a kiss-and-run mechanism (Xia et al., 2009). DCVs are not tightly clustered as are small synaptic vesicles, and

DCVs are generally not associated with presynaptic specializations for release of neurotransmitters such as active zones (van den Pol, 2012). Furthermore, the DCVs within the CNS are not as numerous nor as large as they are in chromaffin cells and neurohypophyseal terminals. In many neurons the release of neuropeptides requires bursts of action potentials (Bondy et al., 1987; Muschol and Salzberg, 2000). Based primarily upon pharmacological experiments it appears that an influx of Ca^{2+} via L-type CaChs is necessary for release of neuropeptides from some neurons (Perney e al., 1986; Cazalis et al., 1987; Rane et al., 1987; Lemos and Nowycky, 1989; Wang et al., 1993; Simmons et al., 1995; Kolarow et al., 2007; Xia et al., 2009) with some cases also involving Ca^{2+} release from internal stores while others not. This suggests the possibility that in neurons neuropeptide release may be initiated by an influx of Ca^{2+} via L-type CaCh.

Drosophila provide an ideal system to study neuropeptide release due to the vast array of molecular and genetic tools available for manipulating them. Numerous neuropeptides are expressed by the *Drosophila* nervous system including proctolin by motor neurons (Anderson et al., 1988; Taylor et al., 2004). Furthermore, larval motor neurons fire bursts of high frequency action potentials (Cattaert and Birman, 2001; Barclay et al., 2002) so motor boutons are likely to have the long-lasting increases in Ca^{2+} transients in motor boutons that are thought to be required for the release of neuropeptides. Motor boutons contain a network of ER (Summerville et al., 2016) and there is a RyR-dependent release of Ca^{2+} from the ER presumably via CICR, which is required for sustained release of neuropeptides at the neuromuscular junction (nmj) of 3rd instar larvae (Shakiryanova et al., 2007). Elegant dynamic examination of DCVs in boutons with fluorescence recovery after photobleaching showed that they are

immobile in the resting state, but they move randomly and release neuropeptides for several minutes following activity-dependent Ca^{2+} increases (Shakiryanova et al., 2005). Furthermore, simultaneous photobleaching and imaging of DCVs suggest that DCVs release neuropeptides via multiple rounds of kiss-and-run events (Wong et al., 2015). Thus, in *Drosophila* neuropeptide release at the neuromuscular junction appears to involve CICR from the ER.

One way to regulate the release of neuropeptides is to control changes in cytoplasmic Ca^{2+} levels. In this regard Stac3 was identified as a regulator of L-type CaChs and excitation-contraction (EC) coupling in zebrafish skeletal muscles (Horstick et al., 2013; Linsley et al., 2017a). Stac3 also regulates EC coupling in murine skeletal muscles (Nelson et al., 2013) and is causal for the congenital Native American myopathy (Horstick et al., 2013). EC coupling is the process that transduces changes in muscle membrane voltage to initiate release of Ca^{2+} from the sarcoplasmic reticulum (SR) and contraction. In vertebrate skeletal muscles EC coupling is mediated by the L-type CaCh, DHPR, which is in the transverse tubule membrane (t-tubules) and is the voltage sensor for EC coupling, and the RyR, which is the Ca^{2+} release channel in the SR (Schneider and Chandler, 1973; Rios and Brum, 1987; Block et al., 1988; Paolini et al., 2004). In zebrafish Stac3 regulates EC coupling by colocalizing with DHPR and RyR, and by regulating DHPR stability and functionality, including the response to voltage of DHPRs but not trafficking of DHPRs (Linsley et al., 2017a, Linsley et al., 2017b).

In mammals *stac3* is a member of a small family of genes along with *stac1* and *stac2*, which are expressed by subsets of neurons (Suzuki et al., 1996; Lein et al., 2007; Legha et al., 2010). The *in vivo* function of the *stac1* and *stac2* genes expressed by neurons is, however, unknown. Recently, a *stac*-like gene, *Dstac*, was identified in *Drosophila* (Hsu et al., 2018).

There is a single *stac* gene in *Drosophila* and it is expressed both by muscles and a subset of neurons including in the lateral ventral neurons (LN_V) that express the neuropeptide, pigment dispersing factor (PDF) in the brain. Previously, genetic manipulation of PDF demonstrated the necessity of PDF for circadian rhythm (Shafer and Taghert, 2009). Interestingly, knocking down *Dstac* selectively in the PDF neurons disrupted circadian rhythm suggesting the hypothesis that Dstac regulates the release of neuropeptides such as PDF. Since Stac3 regulates the L-type CaCh in vertebrate skeletal muscle, Dstac might control neuropeptide release via regulation of the single L-type CaCh in *Drosophila* neurons (Dmca1D; Zheng et al., 1995). We tested this hypothesis by examining the role of Dstac for neuropeptide release by the more accessible presynaptic boutons of motor neurons at the neuromuscular junctions of 3rd instar larvae.

4.3 Methods

4.3.1 *Drosophila melanogaster* strains

All crosses and larvae for experiments were kept at 25 ˚C and supplied with food that uses molasses as sugar source (Food R purchased from LabExpress). The number of flies used in crosses were controlled so the vials were not overcrowded with larvae. All experiments used age and size matched larvae. Both male and female 3rd instar larvae were used. For *in vivo* Ca^{2+} imaging using the microfluidic chip, 2nd instar larvae of both genders were used since 3rd star larvae don't fit in the microfluidic chamber. All experiments were conducted at room temperature (21˚C – 23.5°C). *UAS:Dcr-2* was present in all knockdown experiments using RNAi strains except for the TRiP RNAi lines that don't require Dcr-2.

The following fly stocks were used in this study.

GAL4 stocks: *Proctolin:GAL4* (RRID:BDSC_51972), *daughterless:GAL4* (*da:GAL4*) (From Andreas Wodarz, Wodarz et. al, 1995), *elav:Gal4^{C155};UAS:Dcr-2* (RRID:BDSC_25750), *ShakB:GAL4* (RRID:BDSC_51633), *Mef2:GAL4* (RRID:BDSC_27390).

UAS Stocks: *UAS:Dcr2* (RRID:BDSC_24650 and RRID:BDSC_24651), *UAS:GCaMP6f* (RRID:BDSC_52869), *UAS:mCD8tdtomato* (From Bing Ye), *UAS:mCD8:RFP* (RRID:BDSC_27391), *UAS:mCD8GFP* (RRID:BDSC_32185), *UAS:Dilp2-GFP* (From Edwin Levitan, Wong et al., 2012), *UAS:Dstac-RNAi* (VDRC 103824), *UAS:Dmca1D-RNAi* (RRID:BDSC_33413 and VDRC 51491), *UAS:proctolin-RNAi* (RRID:BDSC_29570), *UAS:Luciferase-RNAi* (RRID:BDSC_31603), *UAS:Dstac^{wt}-GFP* (this study). *Dmca1D-RNAi* VDRC 51491 was used in supplementary Figure 4.4E and BDSC_33413 was used in all other *Dmca1D* KD experiments.

Other stocks: *w^{1118}* (RRID:BDSC_3605), *yw* (RRID:BDSC_1495), *w;Sco/CyO* (RRID:BDSC_2555), *yw;Sco/CyO* (this study), *yw;sp/CyO;p[Δ2-3transposase],sb/Tm6,UbX* (Kenneth Cadigan), *w;Sco/CyO-cre* (RRID:BDSC_1092), *w;L/Cyo;flz9,e^{-}/Tm3,sb,e^{-}* (Kenneth Cadigan), *Dstac-gfp* trap (RRID:BDSC_40742), *Dmca1D^{AR66}/CyO* (From Daniel Eberl, Eberl et al., 1998), *w;Sco/CyO-Dfd-EYFP* (RRID:BDSC_8578), *P{Mae-UAS.6.11}Dstac^{LA00216}* (DGRC 120216), *nos-Cas9* (RRID:BDSC_54591), *Dstac^{ΔSH3}/CyO* (this study), *y[1] w[67c23]; P{y[+t7.7]=CaryP}attP2* (RRID:BDSC_8622).

4.3.2 Generation of *Dstac^{ΔSH3}*

Dstac^{ΔSH3} was generated by CRISPR-mediated homology-directed repair (Gratz et al., 2014). Two gRNA neighboring the targeted genomic DNA sequence encoding for SH3 were cloned into the pCFD3-dU63gRNA vectors (Addgene plasmid # 49410 ;

http://n2t.net/addgene:49410 ; RRID:Addgene_49410). For making the donor plasmid, the DsRed of phD-DsRed-attP vector (Addgene plasmid # 51019 ; http://n2t.net/addgene:51019 ; RRID:Addgene_51019) was swapped with an eGFP by Gibson assembly (Cat# E2611, NEB) to create the phD-eGFP-attp vector and 1-kb homology arms were inserted into the phD-eGFP-attp vector. The two gRNA plasmids and the donor plasmid were injected to the *nos-Cas9* embryos (RRID:BDSC_54591) by a commercial vendor (BestGene). The carriers of the mutation were isolated by crossing the adult flies that grew from the injected embryos with a 2nd chromosome balancer strain, *w;Sco/CyO*. Two founders were isolated by 3xP3-eGFP expression in eyes and confirmed by PCR using primer 1 & 2, primer 3 & 4 and by sequencing using primer 5 and primer 6 (see Supplementary table). Founder 1 and founder 2 were outcrossed with w^{1118} for 5 and 10 generations, respectively; during the outcross, the $Dstac^{\Delta SH3}$ mutations were identified by the 3xP3-eGFP expression in the eyes and confirmed by PCR using primer 1 & 2, primer 3 & 4 and by sequencing using primer 5 and primer 6 (see Supplementary table). The 3xP3-eGFP was removed by crossing with the flies that are transgenic for the Cre recombinase (*w;Sco/Cyo-cre*) for two generations for complete removal of 3xP3-eGFP. $Dstac^{\Delta SH3}$ Founder 1 was used in all *Dstac* mutant experiments.

4.3.3 P-element excision

The P{Mae-UAS.6.11} insertion of $Dstac^{LA00216}$ ([1] w[*]; P{y[+t7.7]=Mae UAS.6.11}CG43729[LA00216]) contains a $yellow^{+}$ gene and was inserted in the 3'UTR of the *Dstac* gene (Bellen et al., 2004). The original $Dstac^{LA00216}$ stock was w^{1118} background and therefore was crossed with *yw* strain to change the genetic background to *yw*. The

yw;Dstac^{LA00216} strain was crossed with *yw;sp/CyO;p[Δ2-3transposase],sb/Tm6,UbX*. The progeny flies with yellow body (loss of the *yellow*$^{+}$ gene) were assayed by PCR using primer 29 & 31 and primer 31 & 33 for detecting excision of p-element. Precise excision of the p-element was confirmed by sequencing using primer 30 and primer 32. See Supplementary table for primer sequences.

4.3.4 Generation of *UAS:Dstac*^{wt}

For making *UAS:Dstac*^{wt} transgenic flies, a *Dstac* cDNA (*CG43729-RE*) that contains a SH3 domain and a CRD domain was amplified from the cDNA of the whole 3rd instar larvae of the *w*^{1118} strain using primer 34 and 35 (see Supplementary table) and the Platinum taq high fidelity DNA polymerase (Cat#11304011, ThermoFischer). The amplified *Dstac* cDNA was cloned and tagged with an eGFP into a modified pJFRC14 vector (Addgene plasmid# 26223 ; http://n2t.net/addgene:26223 ; RRID:Addgene_26223). The plasmid was injected into the strain carrying the *attP2* sites (RRID:BDSC_8622) for integration of the transgene via the *Phic31* integrase. The transgenic flies were isolated and balanced by a commercial vendor (Bestgene).

4.3.5 Molecular Biology

For extracting genomic DNA, 5-6 adult or 3rd instar larval *Drosophila* were crushed thoroughly with a pestle in buffer containing (in mM) 100 Tris-HCl pH 7.5, 100 EDTA, 100 NaCl, 0.3% SDS and 1% Proteinase K (NEB) and incubated at 50 ˚C for 30 minutes followed by addition of potassium acetate and lithium chloride. The mixture was centrifuged and the supernatant

was collected. DNA was precipitated by isopropanol, washed with EtOH and suspended with dH_2O.

For reverse-transcription PCR of CNS and body wall (Figure 4.3B), cDNA of whole 3rd instar larvae, dissected CNS or dissected body wall, was synthesized by SuperScript III reverse transcriptase (Cat#18080044, ThermoFischer) using equal amounts of RNA with oligo-dT primer (Cat#18418012, ThermoFischer). The tissues were thoroughly frozen with dry ice and homogenized with a pestle in TRIzol (Cat#15596018, ThermoFischer) followed by addition of chloroform. RNA was precipitated by isopropanol, washed with EtOH and suspended with DEPC-treated water. The primers used in Figuire 4.3B are RT-PCR primers for CG43729-RC, RE, RH, RN, RO, RP, RQ, RU, RV and GAPDH (primer 8-27, see Supplementary table for primer sequences). The PCR products of each isoform were loaded on an agarose gel. For reverse-transcription PCR of *Dstac*$^{\Delta SH3}$ (Figure 4.2A and Figure 4.3C), same procedures were followed except that the whole 3rd instar larvae were used. For Figure 4.2A, primer 22 & 28 were used for CG43729-RU and primer 24 & 28 for CG43729-RV. For Figure 4.3C, RT-PCR primers for CG43729-RC, -RP, -RU and -RV were used (see Supplementary table). RT-PCR gels were analyzed using ImageJ. The controls and experimental groups were run on the same gel and analyzed at the same time. Single ROIs were drawn over single bands, as well as blank regions directly above or below the bands as background. Background was subtracted from individual PCR bands; the net PCR band intensity was then normalized to GAPDH levels.

For DNA sequencing, gel extraction was performed using the Qiagen gel extraction and purification kit. Sequencing was performed by the LSI sequencing core at the university of Michigan. All DNA constructs and PCR bands of this study were confirmed by sequencing.

4.3.6 Immunostaining

3rd instar larvae were filleted in HL3 solution and fixed in 4% paraformaldehyde in PBS. For immunostaining of *Dmca1DX10 embryos*, stage 12-17 embryos were collected, and the chorion and vitelline membrane removed manually by needles followed by fixation. Immunolabeling followed the procedure described in Hsu et al., 2018. The primary antibodies used were: chicken anti-Dmca1D (1:20 - 1:100) (this study), rabbit anti-Dstac (1:100 - 1:150) (Hsu et al., 2018), chicken anti-GFP (1:1000, Aves Labs Cat# GFP-1010, RRID:AB_2307313), rabbit anti-GFP (1:1000, Torrey Pines Biolabs Cat# TP401 071519, RRID:AB_10013661), anti-prcotolin (1:4000) (Taylor et al., 2004), and rabbit anti-RFP (1:1000, Rockland, Rockland Cat# 600-401-379, RRID:AB_2209751). Secondary antibodies used were (1:1000): Donkey anti-chicken Alexa Fluor 488 (Jackson ImmunoResearch Labs Cat# 703-545-155, RRID:AB_2340375), Goat anti-rabbit Alexa Fluor 647 (Thermo Fisher Scientific, Cat # A-21245, RRID AB_2535813), Goat anti-HRP Cy3 (Jackson ImmunoResearch, Cat # 123-165-021, RRID:AB_2338959), Goat anti-rabbit Alexa Fluor 488 (Thermo Fisher Scientific, Cat # A-11034, RRID: AB_2576217), anti-chicken Alexa Fluor 633 (Sigma-Aldrich, SAB4600127), and Goat anti-HRP Alexa Fluor 594 (Jackson ImmunoResearch Labs Cat# 123-585-021, RRID:AB_2338966).

4.3.7 Antibody production

To generate anti-Dmca1D, the *Dmca1D* cDNA that encodes for the 94 amino acids at the N terminus of the Dmca1D protein (DFERGASGEGGFSPNGNGGPGSGDVSRTARYDSGEGDLGGGNNIMGIDSMGIANIPETMNGTTIGPSGAGGQKGGAAAGAAGQKRQQRRGKPQP) was cloned using primer 40 and 41 (see Supplementary

table) and expressed with a His fusion protein and purified using Ni-NTA agarose (Thermo Fisher Scientific). The purified His-tagged proteins were further purified by NuPAGE 4-12% SDS polyacrylamide gel electrophoresis (SDS-PAGE) using a Bis-Tris Gel (Thermo Fisher Scientific) followed by excision of the appropriate Coomassie-stained band. The gel slices of purified Dmca1D proteins were used to immunize chickens and the IgY was extracted from the yolk by a commercial vendor (ProSci). The Dmca1D antibody was further purified from the IgY with an NHS-activated agarose column (Thermo Fisher Scientific) that was conjugated with the 94-amino acid portion of the Dmca1D protein. The specificity of anti-Dmca1D was confirmed by labeling of the CNS in wt but not in *Dmca1D* null *Drosophila* embryos (Supplementary Figure 4.1D).

4.3.8 Motility assay

Freely moving 3rd instar larvae of both genders were acclimated on a 10 cm 2% agar plate for 1 minute and then recorded for 10 seconds at 7.5 Hz frame rate with a digital camera. For each larva, three trials were run with each run representing one trial. All data were included except for larvae that hit the petri dish wall during the 10-second recoding. The assay was performed at 23.5 ˚C. The larval movement was tracked by the "multitracker" plugin of imageJ that produced the (x,y) location of each larva at each frame. The distance between frames were calculated from the (x,y) location and were summed to get the total distance traveled during the 10 seconds.

For assaying the *Dstac* and *Dmca1D* deficiency and *proctolin KD* larvae, the controls and experimental groups were coded to blind the genotypes. After completing the assay and

analysis, the genotypes were unveiled. Motility assay of *Dmca1D*^{AR66} and control in Supplementary Figure 4.4G was performed using larvae expressing one copy of *nsyb:Dilp2-GFP* and the same genotypes of larvae were used in the Dilp2-GFP release assay. For assaying wt, *Dstac*$^{\Delta SH3}$ and heterozygous siblings in Figure 4.2C, the genotypes of individual larvae were identified by PCR using primer 5, 6, and 7 (See Supplementary table).

For the *Dstac*$^{\Delta SH3}$ rescue experiments in Figure 4.2D, "*Dstac*$^{\Delta SH3}$*/+;da:GAL4/+* " flies were crossed with "*Dstac*$^{\Delta SH3}$*/+, UAS:Dstac*^{wt}*/+* " flies to get progeny that were: heterozygous *Dstac*$^{\Delta SH3}$ (*Dstac*$^{\Delta SH3}$*/+* carrying either *da:GAL4* or *UAS:Dstac*^{wt}), homozygous *Dstac*$^{\Delta SH3}$ (*Dstac*$^{\Delta SH3}$*/Dstac*$^{\Delta SH3}$ carrying either *da:GAL4* or *UAS:Dstac*^{wt}), heterozygous *Dstac*$^{\Delta SH3}$ expressing *Dstac*^{wt} (*Dstac*$^{\Delta SH3}$*/+;da:GAL4>UAS:Dstac*^{wt}), and homozygous *Dstac*$^{\Delta SH3}$ expressing *Dstac*^{wt} (*Dstac*$^{\Delta SH3}$*/ Dstac*$^{\Delta SH3}$*;da:GAL4>UAS:Dstac*^{wt}). For the *Dstac*$^{\Delta SH3}$ rescue experiments in Supplementary Figure 4.4A, "*Dstac*$^{\Delta SH3}$*/+;Mef2:GAL4/+* " flies were crossed with "*Dstac*$^{\Delta SH3}$*/+;UAS:Dstac*^{wt}*/UAS:Dstac*^{wt} " flies to get the progeny that were: heterozygous *Dstac*$^{\Delta SH3}$ (*Dstac*$^{\Delta SH3}$*/+ carrying UAS-Dstac*^{wt}) , homozygous *Dstac*$^{\Delta SH3}$ (*Dstac*$^{\Delta SH3}$*/Dstac*$^{\Delta SH3}$ *carrying UAS-Dstac*^{wt}), and homozygous *Dstac*$^{\Delta SH3}$ selectively expressing *Dstac*^{wt} in body wall muscles (*Dstac*$^{\Delta SH3}$*/ Dstac*$^{\Delta SH3}$*; Mef2:GAL4>UAS:Dstac*^{wt}). Individual larvae were genotyped by PCR after the locomotion assay. Larvae carrying *GAL4* were identified by primer 36 and 37, carrying *UAS:Dstac*^{wt} were identified by primer 38 and 39. The heterozygous and homozygous *Dstac*$^{\Delta SH3}$ larvae were identified by primer 5, 6, and 7. See Supplementary table for primer sequences.

4.3.9 Reproductivity test and larval size measurement

Three males and 3 females of w^{1118} flies one day after eclosion were incrossed. At the same time, $Dstac^{\Delta SH3}$ crosses were set in the same manner as w^{1118} crosses. In order to let the flies acclimate to the breeding environment, the crosses were flipped to a new vial a day after the crosses were set. Two days after the flip of the crosses, the number of embryos from three independent crosses of wt and $Dstac^{\Delta SH3}$ each were counted. For measuring larva size, freely moving 3rd instar larvae were placed on a 2% agar plate. A series of images were taken at 7.5 Hz for 10 seconds. The frames in which larvae were relaxed and not moving were measured for their length and width using imageJ. Lines were drawn longitudinally over a larva for acquiring length or horizontally over a larva for acquiring width. The pixels of the lines were converted to millimeters (mm).

4.3.10 *In vivo* Ca^{2+} imaging

For Ca^{2+} imaging of motor boutons, whole intact larvae selectively expressing GCaMP6f in proctolin+ motor neurons (*Proct:GAL4>UAS:GCaMP6f*) (Chen et al., 2013) were placed into a microfluidics chip (Mishra et al., 2014) and GCaMP fluorescence was observed on a Leica SP8 confocal microscope equipped with a 8,000 Hz resonance scanner and a 63x objective. The *Proct:GAL4* line also expressed *UAS:mCD8tdTomato* to allow visualization of boutons. Female and male 2nd instar larvae were used since 3rd instar larvae were too big to fit into the chip. The larvae were mounted on its side in the chip in order to image the type Is bouton nerve branch on muscle 4. Images were captured every 0.712 sec for 5 min using an imaging volume of 148 x 148 x 10 μm that contained the Is branch. The *mCD8tdTomato* expressed by the *proctolin*:*GAL4* was used to track the boutons during recordings. The combination of an imageJ macro and the

time series analyzer v3 plugin was used to create the region of interest (ROI) and re-center the ROI to the same bouton frame by frame. The position of the ROI was checked and re-adjusted manually. One type Is bouton per branch that stayed in focus throughout the 5-minute live imaging was measured. The 10 frames of GCaMP6f fluorescence before and after the peaks were averaged and used as basal GCaMP6f level (F_{basal}) to calculate the fold change of GCaMP6f fluorescence intensity ($\Delta F/F=F-F_{basal}/F_{basal}$). Prism GraphPad was used to find the peak values and the area under the peaks. Ca^{2+} peaks or area under peaks per bouton were averaged as one experiment sample. Both the experiments and analysis were done blind.

4.3.11 Electrophysiology

Voltage-clamp of RP2 motor neuron cell bodies followed the published protocols (Worrell et al., 2008; Kadas et al., 2017). Briefly, the sheath over the ventral ganglion was removed by focally applying 1% proteinase type XIV in zero Ca^{2+} extracellular saline (Protease type XIV from Streptomyces griseus; Sigma-Aldrich, Cat #P5147; CAS 9036-06-0) using a micropipette with 1 um tip. Once the motor neurons were exposed, the enzyme was washed out with extracellular saline (in mM): 118 NaCl, 2 NaOH, 2 KCl, 4 $MgCl_2$, 1.8 $CaCl_2$, 25 sucrose, 5 trehalose, and 5 HEPES, pH 7.1–7.2 (Jan and Jan 1976). The RP2 motor neurons were identified by anatomy and the expression of *proctolin:GAL4>UAS:mCD8tdTomato*,*UAS:Dilp2-GFP* using an OLYMPUS BX51WI microscope with a 40x dipping lens. The RP2 motor neurons of segments T3 and A1 were voltage-clamped. Thin-walled electrodes (Cat#1B150F-4, World Precision Instruments) were pulled on a P-97 micropipette puller (Shutter Instrument) ~~to~~ and fire polished using an MF-200 micro-forge (World Precision Instruments) to achieve a resistance of

5 MΩ. In order to isolate the *Dmca1D* current, extracellular solution contained Na^+ and K^+ channel blockers (1 uM tetrodotoxin (T5651, Sigma-Aldrich, discontinued), 50 mm Tetraethylammonium (T2265, Sigma-Aldrich) and 1.5 mM 4-aminopyridine (A78403, Sigma-Aldrich)). The internal electrode solution had the KCl replaced with CsCl (in mM: 144 CsCl, 1 $MgCl_2$, 0.5 $CaCl_2$, 5 EGTA, and 10 HEPES, pH 7.1–7.2 (Peng and Wu 2007)). The recordings were acquired using Axopatch 200 (Axon Instruments) and digitized with a Digidata 1320A (Axon Instruments). Extracellular $CaCl_2$ was replaced with 1.8 mM $BaCl_2$ for recording Ba^{2+} currents. To block voltage-gated Ca^{2+} channels, 500 μM Cd^{2+} was added to the extracellular saline. Ca^{2+} currents were induced by voltage steps from -90 mV to +50 mV in 10 mV increments from a holding potential of -70 mV. The linear leakage current was subtracted from all records after acquisition of data. The whole cell capacitance was determined and compensated using the Axopatch 200 capacitance adjustment knob. Current amplitude was normalized to whole cell capacitance and values were reported as current density in the full I-V curve. The analysis was performed using pClamp 10.2 software (Axon Instruments, Molecular Device, California, USA).

For muscle recoding of evoked synaptic potential, 3rd instar larvae were dissected in zero Ca^{2+} HL3 solutions and the nerves severed. Larvae were mounted on an OLYMPUS BX51WI scope with a 10X dipping lens. Muscle 4 of segments A3 and A4 was recorded with thick wall glass electrodes (Cat#1B150F-4, World Precision Instruments) pulled by P-97 micropipette puller (Shutter Instrument). The recording electrode was filled with 3M KCl and had resistances of approximately 60 MΩ. The HL3 solution contained (in mM) 70 NaCl, 5 KCl, 0.65 $CaCl_2$, 20 $MgCl_2$, 10 $NaHCO_3$, 5 trehalose, 115 sucrose, 5 HEPES, pH 7.2. (Stewart et al., 1994). The membrane potential recordings were acquired using Amplifier GeneClamp 500B (Axon

Instruments) and digitized with Digidata 1320A (Axon Instruments). Synaptic potentials from muscles that had a resting membrane potential equal or more negative than -60 mV were collected. A Grass S48 stimulator was used to stimulate the nerve with voltages using a suction electrode. The voltage that triggered the largest and most stable evoked synaptic potential was used to stimulate the nerve at 0.2 Hz for a duration of 1 ms for 10 trials. The 10 trials of evoked synaptic potential of a muscle were averaged as one sample. The analysis was performed using pClamp 10.2 software (Axon Instruments, Molecular Device, California, USA). The graphs in Figure 4.7E were corrected for non-linear summation using the following equation when the amplitude of the evoked synaptic potential was larger than 15% of resting membrane potential: V' = V/[1-f(V/E)]. In the equation, V' is the corrected synaptic potential; V is the measured synaptic potential; f is the membrane capacitance factor; E is the driving force. At the *Drosophila* nmj, E (driving force) is estimated to be approximately 0 mV, and f = 0.55 (McLachlan EM, Martin AR, 1981).

4.3.12 Dilp2-GFP release assay

Previously published procedures for assaying the release of Dilp2-GFP from motor boutons were followed (Shakiryanova et al., 2005). *Proctolin:GAL4>UAS:Dilp2-GFP* was expressed in Dstac KD, $Dstac^{\Delta SH3}$, and *Dmca1D KD* larvae. *nsyb:Dilp2-GFP* was expressed in $Dmca1D^{AR66}$ larvae. Third instar larvae were dissected and analyzed in zero Ca^{2+} HL3 containing (in mM) 0.5 EGTA, 70 NaCl, 5 KCl, 20 $MgCl_2$, 10 $NaHCO_3$, 5 trehalose, 115 sucrose, 5 HEPES, pH 7.2. (Stewart et al., 1994; Shakiryanova et al., 2005). A series of stack images (0.3 um/focal plane) was taken of type Is boutons on muscle 4 between segments A3 to A5. To depolarize

motor boutons, the zero Ca^{2+} HL3 was switched to high KCl HL3 solution containing (in mM) 5 NaCl, 70 KCl, 20 $MgCl_2$, 1.5 $CaCl_2$, 10 $NaHCO_3$, 5 trehalose, 115 sucrose, 5 HEPES, pH 7.2. The sample was depolarized with the high KCl HL3 for 2 minutes. Subsequently, the high KCl HL3 was washed out with zero Ca^{2+} HL3. The same motor branch was relocated and a series of stacked images (0.3 um/focal plane) was obtained. For *Dmca1D*^{AR66} and *Dmca1D KD*, the experiments were performed using a Leica SP5 confocal microscope with a 40x dipping lens. For *Dstac*$^{\Delta SH3}$ and *Dstac KD*, the experiment data were collected using a 40x water immersion on an Olympus BX61W1 and analyzed with Simple PCI software. The controls and experimental groups were coded to blind the genotypes. After completing the assay and analysis, the genotypes were uncovered. The controls and experimental groups were assayed in the same days.

4.3.13 Quantification of immunostaining at motor neuron boutons

Images of type Is boutons on muscle 4 from segments A3 to A5 were acquired at 1024x1024 pixels as z stacks (0.3 um/focal plane) that included total z-axis of motor boutons. The images were acquired with a SP8 confocal microscope with the 100x or 63x oil lens. Confocal settings were kept constant between controls and experimental groups. The volocity software (Perkin Elmer) was used to quantify the immunofluorescence intensity at motor neuron boutons. The anti-HRP labeling of motor bouton membrane was used to set a threshold to draw ROIs over every focal planes of a bouton z-stack. The threshold was carefully set so the ROIs only covered the areas within the boutons. Therefore the average immunofluorescence intensity per total bouton was measured.

4.3.14 Quantification of Dilp2-GFP release

Previously published procedures for quantification of the release of Dilp2-GFP from motor boutons were followed (Shakiryanova et al., 2005). The ROIs were drawn manually over the boutons expressing Dilp2-GFP. For each bouton, Dilp2-GFP levels for all focal plans of a z-stack images were measured. The single focal plane that showed highest Dilp2-GFP level was used for the release analysis. The percentage of Dilp2-GFP release was calculated as: $[(F_{after}-F_{before})/ F_{before}]*100\%$. F_{before} is the Dilp-GFP fluorescence of a single focal plane before high KCl; F_{after} is the Dilp2-GFP fluorescence of a single focal plane after high KCl. For each motor branch, Dilp2-GFP fluorescence from three boutons were averaged and counted as one sample.

4.3.15 Statistical analysis

Statistical analysis was performed using Prism GraphPad software. The normality of data distribution was tested by D'Agostino and Pearson test. If the data fit a normal distribution, parametric tests were used: unpaired t test was used for comparing two groups; ordinary One-Way ANOVA and Tukey's multiple comparisons test were used for comparing multiple groups. If the data were not normally distributed, then nonparametric tests were used: Mann-Whitney test was used for comparing two groups; Kruskal-Wallis test and Dunn's multiple comparisons test were used for comparing multiple groups. For experiment in which the change in results can be predicted by our hypothesis, one-tailed tests were performed; otherwise two-tailed tests were performed. In all figures, ns, *, **, ***, **** represent $P>0.05$, $P<0.05$, $P<0.01$, $P<0.001$, and $P<0.0001$. Error bars are standard errors of the mean.

4.3.16 DATA AND CODE AVAILABILITY

The data that support the findings of this study are available from the Lead Contact upon request.

4.4 Results

4.4.1 Motor Boutons Express Dstac, Dmca1D and Proctolin

The hypothesis that Dstac regulates Dmca1D and the release of neuropeptide by motor boutons at the neuromuscular junction predicts that Dstac, Dmca1D and a neuropeptide are all expressed by motor boutons. We examined the expression of Dstac in the motor boutons by labeling them with anti-Dstac, anti-proctolin and an antibody directed against Dmca1D that we generated (see Methods). Labeling larvae selectively expressing membranous GFP in proctolin+ motor neurons (*Proct:GAL4>UAS:mCD8GFP*) with anti-proctolin confirmed that motor boutons expressed proctolin (Figure 4.1A). Co-labeling larvae with anti-Dstac and anti-Dmca1D showed that both type Ib and Is boutons expressed Dstac and Dmca1D (Figure 4.1B, 4.1C) in addition to proctolin. The specificity of the antibody was demonstrated by labeling *Dmca1D* null embryos (*Dmca1DX10;* Eberl et al., 1998), which are larval lethals, with anti-Dmca1D and finding that there was no detectable labeling in mutant embryos while in control embryos the longitudinal tracts in the CNS were labeled (Supplementary Figure 4.1D). The colocalization of Dstac, Dmca1D and proctolin was confirmed using an independent approach. Examination of 3rd instar larvae from a *Dstac-GFP* gene trap line (Venken et al., 2011; Hsu et al., 2018) that also were transgenic for *ShakB:Gal4 > UAS:mCD8RFP*, which is expressed by a subset of motor neurons in the ventral ganglia (Takizawa et al., 2007), revealed that GFP and RFP were colocalized in the

ventral ganglia (Supplementary Figure 4.1A). This is consistent with Dstac expression by at least some motor neurons in the ventral ganglia. Labeling *ShakB:Gal4 > UAS:mCD8GFP* larvae with anti-proctolin (Taylor et al., 2004) and anti-GFP showed that the neuropeptide, proctolin, is expressed by these motor neurons as well (Supplementary Figure 4.1B). Labeling *Proct:Gal4 > UAS:mCD8GFP* larvae with anti-Dstac (Hsu et al., 2018) further suggested that Dstac is expressed by proctolin+ motor neurons including the RP2 neuron (Supplementary Figure 4.1C). Thus, motor boutons at the neuromuscular junction express Dstac, Dmca1D and the neuropeptide proctolin.

4.4.2 Dstac, Dmca1D, and Proctolin Deficiency in Motor Neurons Decreases Locomotion

The hypothesis that Dstac regulates neuropeptide release by motor boutons predicts that a defect in Dstac should lead to a decrease in the release of proctolin at the neuromuscular junction. This may result in decreased locomotion since proctolin is known to increase contractions when applied to *Drosophila* larval muscles (Omerod et al., 2016). To examine this prediction we assayed a *Dstac* p-element insertion line and generated a CRISPR-Cas9 mediated mutation targeting the SH3 domain of Dstac (see Methods for details). The rationale for targeting the SH3 domain was based upon our earlier finding that the SH3 domain was critical for Stac3 function in vertebrate skeletal muscles. A missense mutation in the SH3 domain of the skeletal muscle gene, *STAC3*, caused Native American myopathy that is characterized by muscle weakness (Horstick et al., 2013) and the corresponding mutation in zebrafish resulted in dysregulation of L-type CaCh in skeletal muscle, disrupted excitation-contraction coupling and decreased locomotion (Linsley et al., 2017a).

We examined 2 founders for the CRISPR-Cas9 mutation (*Dstac*$^{\Delta SH3}$) in which gDNA and cDNA sequencing showed that the SH3 domain of Dstac was deleted resulting in a frame-shift and predicted premature stop codon (Figure 4.2A, Supplementary Text). Offsprings from one founder line were viable with normal morphology (Supplementary Figure 4.2A, 4.2B), and after outcrossing through 5 generations larvae from the outcrossed lines exhibited decreased locomotion (Figure 4.2B). In this line, 3rd instar larvae were normal in size (Supplementary Figure 4.2A, 4.2C) and reproduction (number of embryos produced) by mutant adults was comparable to that of wt (Supplementary Figure 4.2D) suggesting that the mutation does not lead to a generalized lethargic state. The other founder produced a few small larvae, which did not eclose and exhibited decreased locomotion. After outcrossing 10 times this line became viable and eclosed, but larval locomotion was decreased (Figure 4.2C). Thus, it appears that *Dstac*$^{\Delta SH3}$ larvae exhibit decreased locomotion.

Ubiquitous expression of wt Dstac (*da:Gal4 > UAS:Dstac*^{wt} ; Wodarz et al., 1995) in *Dstac*$^{\Delta SH3}$ mutant larvae rescued normal locomotion compared with mutants confirming that the locomotion defect was due to the *Dstac*$^{\Delta SH3}$ mutation (Figure 4.2D). Furthermore, ubiquitous expression of wt *Dstac* in *Dstac*$^{\Delta SH3}$/*Dstac*^{wt} larvae increased locomotion compared with heterozygous controls. These findings in *Dstac*$^{\Delta SH3}$ larvae were corroborated by analysis of a line with a single p-element inserted into the 3' UTR of the *Dstac* locus (Supplementary Figure 4.3A). These larvae also exhibited decreased locomotion and precise excision of the p-element rescued normal locomotion (Supplementary Figure 4.3B). Thus, Dstac is required for normal larval locomotion.

Dstac is alternatively spliced and expressed both by muscles and neurons (Hsu et al., 2018) with some splice variants containing different combinations of the BAR, CRD and SH3 domains (Figure 4.3A). RT-PCR from dissected CNS or body wall, which represents mostly muscle, showed that splice variants were expressed at varying levels in the CNS and body wall of wt larvae (Figure 4.3B). RT-PCR of $Dstac^{\Delta SH3}$ larvae of four of the splice variants; two containing the SH3 domain and two that did not confirmed that the $Dstac^{\Delta SH3}$ mutation actually deleted the SH3 domain from the transcripts. Indeed, transcripts RU and RV that contain the SH3 domain in wt larvae, which were expressed primarily in the CNS, were missing the SH3 domain while transcripts RC and RP without the SH3 domain appeared unaffected in $Dstac^{\Delta SH3}$ mutants (Figure 4.2A, 4.3C). Thus, it appears there is a deficiency in transcripts containing the SH3 domain that is correlated with decreased locomotion in $Dstac^{\Delta SH3}$ larvae.

Since *Dstac* is expressed both by body wall muscles and a subset of neurons (Hsu et al., 2018), the decreased locomotion of the mutants could be due to disruption of muscle and/or neural function. In fact, muscle specific expression of wt Dstac in $Dstac^{\Delta SH3}$ larvae did not rescue the mutant phenotype consistent with the idea that a deficiency of Dstac in neurons could result in decreased locomotion (Supplementary Figure 4.4A). Furthermore, pan-neural knockdown of Dstac (*elav:Gal4 > UAS:* $Dstac^{RNAi}$) using a RNAi line that was previously shown to knockdown Dstac (Hsu et al., 2018) decreased locomotion compared to controls (Supplementary Figure 4.4B). Thus, Dstac is required by neurons for normal locomotion by larvae.

Since larval motor neurons express Dstac, Dmca1D and proctolin we tested whether knocking them down specifically in motor neurons could lead to a locomotion phenotype.

Indeed in larvae with Dstac knocked down selectively in motor neurons (*ShakB:Gal4 > UAS:Dstac^{RNAi}* and *Proct:Gal4 > UAS:Dstac^{RNAi}*), locomotion was decreased compared to controls (Figure 4.4A, Supplementary Figure 4.4C). In these larvae, anti-Dstac labeling showed that Dstac expression was reduced in motor boutons (Supplementary Figure 4.4D) confirming that Dstac was indeed knocked down. Furthermore, in larvae with Dmca1D knocked down in motor neurons (*ShakB:Gal4 > UAS:Dmca1D^{RNAi}* and *Proct:Gal4 > UAS:Dmca1D^{RNAi}*) locomotion was also decreased (Supplementary Figure 4.4E, Figure 4.4B). In these larvae, anti-Dmca1D labeling showed that Dmca1D levels showed a small decrease in boutons (Supplementary Figure 4.4F). The Dmca1D knockdown phenotype was corroborated by a partial-loss-of function mutation of Dmca1D (*Dmca1D^{AR66}*, Eberl et al., 1998) that also exhibited decreased locomotion (Supplementary Figure 4.4G). Finally, knocking down proctolin in motor neurons (*Proct:Gal4 > UAS:Proct^{RNAi}*) also decreased larval locomotion (Figure 4.4C). Thus, deficiency in Dstac, Dmca1D and proctolin in normally proctolin+ motor neurons decreased larval locomotion as hypothesized by the proposed regulation of Dmca1D by Dstac and subsequent release of proctolin at the nmj.

4.4.3 Dstac and Dmca1D Deficiency Decrease Ca^{2+} Transients in Motor Boutons

In zebrafish Stac3 regulates DHPR, the skeletal muscle L-type CaCh (Linsley et al., 2017a). If, by analogy to Stac3, Dstac regulates Dmca1D in motor boutons, then there might be abnormal Ca^{2+} transients in the boutons of *Dstac$^{\Delta SH3}$* larvae. First, we examined whether Ca^{2+} transients in boutons were dependent on Dmca1D by assaying Ca^{2+} transients in *Proct:Gal4 > UAS:GCaMP6f* larvae. Ca^{2+} imaging of motor boutons was performed in completely intact larvae

placed in a microfluidics chamber designed to physically restrained larvae (Mishra et al., 2014). Under these conditions large Ca^{2+} transient increases in free Ca^{2+} within Is boutons of RP2 were observed (Figure 4.5A, 4.5B). These presumably represent endogenous locomotor activity. The peak and area under the curve of Ca^{2+} transients recorded from Dmca1D knockdown larvae (*Proct:Gal4 > UAS: Dmca1D*^{RNAi}) were decreased compared with controls (Figure 4.5C, 4.5D). However, the frequency of transients was comparable between Dmca1D knockdown and control larvae (Figure 4.5E). Thus, it appears that during normal, physiological activation of motor neurons there are Ca^{2+} transients that are dependent on Dmca1D CaChs in the motor boutons.

Ca^{2+} transients were also assayed in the boutons of *Dstac*$^{\Delta SH3}$ and the peak and area under the curve of Ca^{2+} transients were also decreased (Figure 4.5F, 4.5G) but not the frequency (Figure 4.5H). The decrease in Ca^{2+} transients in the boutons of larvae of *Dstac*$^{\Delta SH3}$ mutants is consistent with the hypothesized regulation of Dmca1D by Dstac and subsequent release of neuropeptide.

4.4.4 Dstac Regulates Currents Passed by Dmca1D Channels

In zebrafish Stac3 regulates the voltage response of the L-type CaCh in skeletal muscle (Linsley et al., 2017a). To see if Dstac may also regulate the Dmca1D channels, we performed voltage-clamp analysis of L-type currents in the RP2 motor neurons that express Dstac, Dmca1D and proctolin. Dmca1D channels are the major voltage-dependent Ca^{2+} currents recorded from larval motor neuron cell bodies (Worrell et al., 2008) and are also found in their dendrites and axons (Kadas et al., 2017). RP2 neurons were identified by position and expression of markers

in *Proct:Gal4 > UAS:Dilp2-GFP; UAS:mCD8tdTomato* larvae. L-type currents were isolated by pharmacologically blocking Na^+ and K^+ currents (see Methods). First, we recorded Ca^{2+} and Ba^{2+} currents by stepping to -10 mV from a holding potential of -70 mV. The Ca^{2+} currents peaked shortly after the voltage step and then inactivated while the peak Ba^{2+} currents were larger in amplitude and showed little inactivation (Figure 4.6A). The addition of Cd^{2+} blocked much of the Ba^{2+} current in control larvae confirming earlier results (Worrell et al., 2008). Furthermore, both Ca^{2+} and Ba^{2+} currents were decreased in *Dstac$^{\Delta SH3}$* larvae (Figure 4.6A, 4.6B). A full I-V curve for the Ca^{2+} current showed that peak current occurred at +10 mV in both control (n=8) and mutant (n=11) larvae, and that the currents were significantly decreased in mutants compared to controls at -10 mV, 0 mV, +10 mV and +20 mV (Figure 4.6C, 4.6D, 4.6E). Thus, Dstac regulates the voltage dependent currents of L-type CaChs in motor neurons. This result in conjunction with the decrease in Ca^{2+} transients in motor boutons of *Dstac$^{\Delta SH3}$* larvae suggest that Dstac regulates Dmca1D CaChs in motor boutons.

4.4.5 Dstac and Dmca1D Deficiency Decrease Release of Neuropeptide by Motor Boutons

The final prediction of the hypothesis is that Dstac and Dmca1D regulate the release of neuropeptides by motor boutons. This prediction was examined by assaying type Is boutons of the RP2 motor neuron in larvae expressing the *Drosophila* neuropeptide, Dilp2-GFP, following activation of motor boutons with high K^+ (Wong et al., 2012). In this assay release of Dilp2-GFP causes a decrease in fluorescence within the boutons. Expression of Dilp2-GFP by type Is motor boutons on muscle 4 of Dmca1D KD and control was comparable (Figure 4.7A, left) and the release of Dilp2-GFP was decreased in Dmca1D KD compared with control (Figure 4.7A, middle

and right). Expression of Dilp2-GFP by motor boutons of *Dmca1D*^{AR66} was higher than that by control (Figure 4.7B, left) and the release of Dilp2-GFP was decreased in *Dmca1D*^{AR66} compared with control (Figure 4.7B, middle and right). Thus, deficiencies in Dmca1D resulted in decreased neuropeptide release by motor boutons.

Expression of Dilp2-GFP by motor boutons of Dstac KD and control was comparable (Figure 4.7C, left) and the release of Dilp2-GFP was decreased in Dstac KD compared with control (Figure 4.7C, middle and right). Expression of Dilp2-GFP by motor boutons of *Dstac*$^{\Delta SH3}$ and control was comparable (Figure 4.7D, left) and the release of Dilp2-GFP was decreased in *Dstac*$^{\Delta SH3}$ compared with control (Figure 4.7D, middle and right). Therefore, deficiencies in both *Dmca1D* and *Dstac* resulted in decreased neuropeptide release by motor boutons. Thus, Dmca1D and Dstac regulate the release of neuropeptides by motor boutons.

Finally, whether Dstac also regulates release of the neurotransmitter glutamate found in synaptic vesicles at the nmj was investigated by electrophysiologically recording the synaptic potential following stimulation of the motor nerve. Evoked synaptic potentials in *Dstac*$^{\Delta SH3}$ larvae were comparable to that in wt control (Figure 4.7E). Since application of proctolin, the endogenous neuropeptide released by motor boutons (Anderson et al, 1988), does not affect the membrane potential of body wall muscles (Omerod et al., 2016), this finding suggests that the release of glutamate at the nmj was not affected by *Dstac*$^{\Delta SH3}$. Thus, it appears that Dstac and Dmca1D selectively regulate neuropeptide release, but not glutamate release at the nmj (Figure 4.8).

Figure 4.1

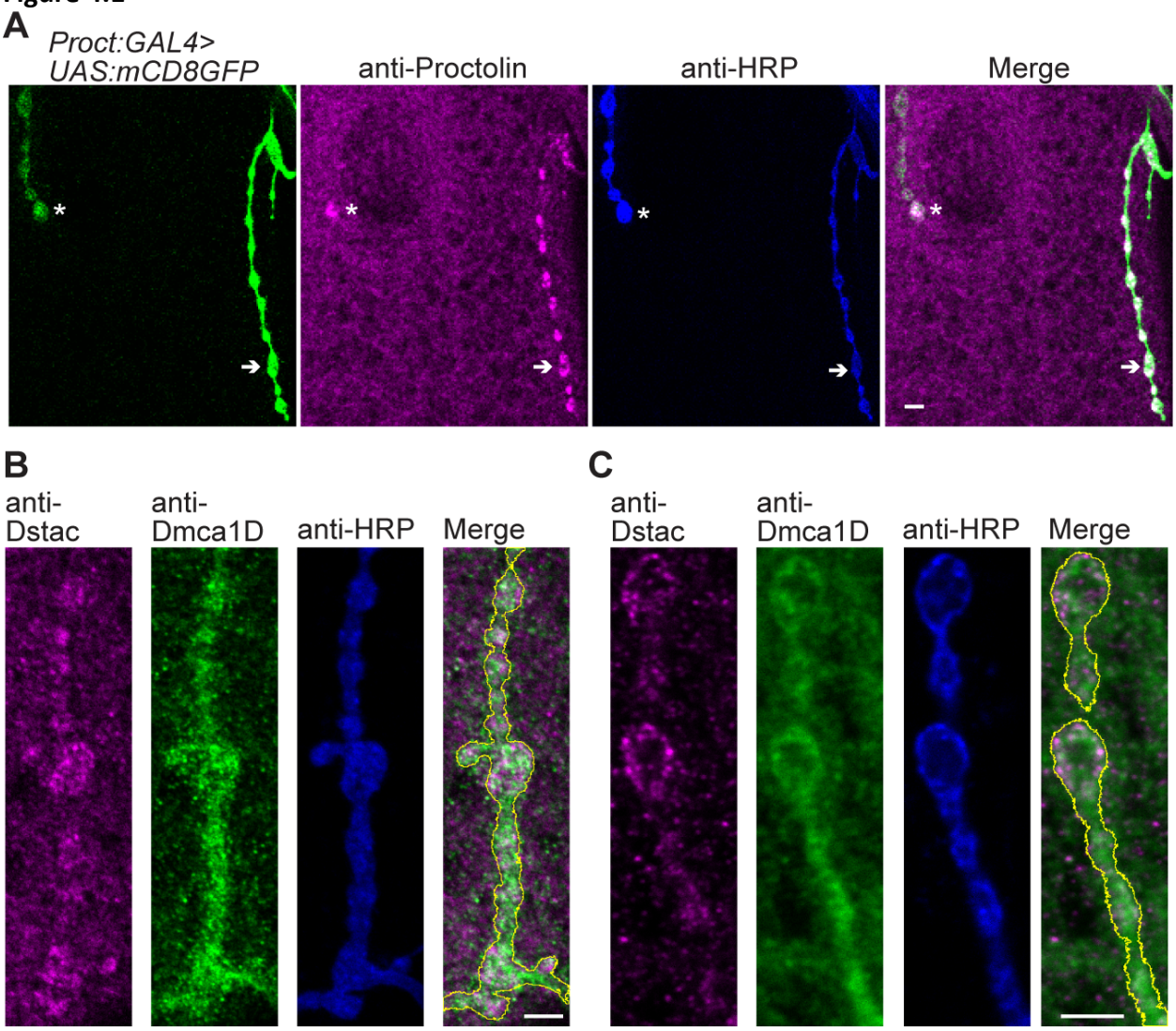

Figure 4.1 Dstac and Dmca1D are expressed by proctolin+ type motor boutons.
(A) Anti-proctolin and anti-HRP labeling of motor nerves in larvae selectively expressing membranous GFP in proctolin+ motor neurons (*Proct:GAL4>UAS:mCD8GFP*) showed expression of mCD8GFP and proctolin at type Ib and type Is branches. The anti-HRP labels an unknown protein that is present on the plasma membrane of motor nerves and boutons. Shown are the type Is branch of the RP2 (arrow) and the type 1b branch of the MN4-Ib motor neuron (asterisk) on muscle 4 (Hoang and Chiba, 2001). Merge is *Proct:GAL4>UAS:mCD8GFP* and anti-Proctolin. The images are a single focal plane. Scale bar, 3 μm. (B), (C) Co-immunolabeling with anti-Dstac and anti-Dmca1D showed co-expression of Dstac and Dmca1D in type Is boutons of RP2 on muscle 4 (B) and type Ib motor boutons of MN4-Ib on muscle 4 (C). Merge is anti-Dstac and anti-Dmca1D. Some of the labeling by both anti-Dstac and anti-Dmca1D beyond the motor nerves may represent muscle labeling since body wall muscles also express Dstac and Dmca1D (Hsu et al., 2018; Ren et al. 1998). The images show a single focal plane. Scale bar, 3 μm. See also Supplementary Figure 4.1.

Supplementary Figure 4.1

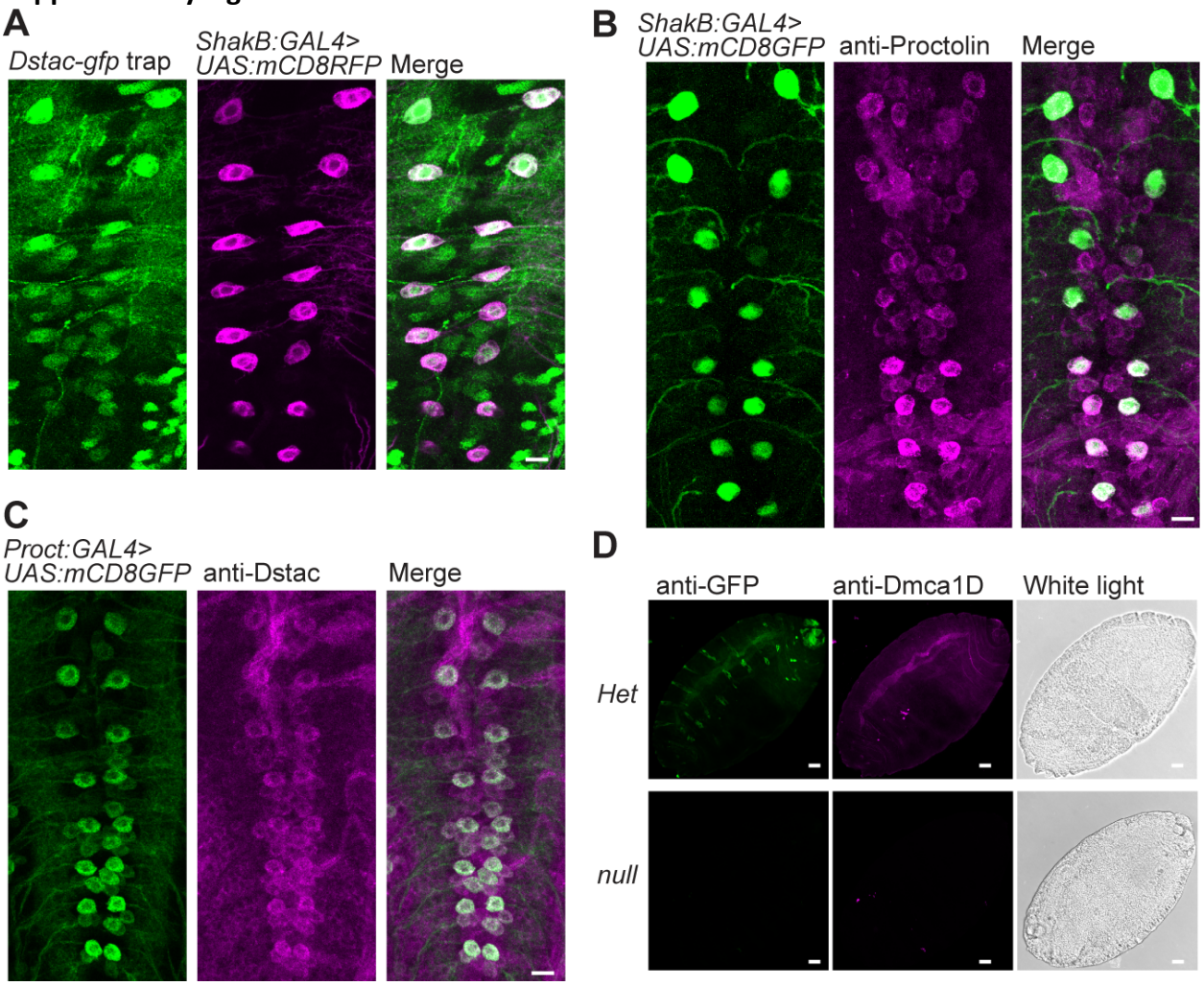

Supplementary Figure 4.1 Dstac is expressed by proctolin+ motor neurons in the ventral ganglia including the RP2 motor neurons in 3rd instar larvae.
(A) Dorsal view of ventral ganglia from larvae transgenic for *Dstac-gfp* trap and *ShakB:Gal4>UAS:mCD8RFP* revealed co-expression of GFP and RFP in the RP2 motor neurons. Shown are a z-stack of confocal images from the dorsal portion of the ventral ganglia. Scale bar, 10 μm. (B) Dorsal view of ventral ganglia from larvae that are *ShakB:Gal4>UAS:mCD8GFP* immunolabeled with anti-proctolin showed that the RP2 motor neurons express proctolin. Scale bar, 10 μm. (C) Dorsal view of ventral ganglia from larvae that are *proct:Gal4>UAS:mCD8GFP* immunolabeled with anti-Dstac showed that RP2 neurons express Dstac. Scale bar, 10 μm. (D) Anti-Dmca1D labels the longitudinal axon tracts in embryos that are heterozygous for the null *Dmca1D* allele, *Dmca1DX10* (*Dmca1DX10/Cyo,Dfd-eYFP*) but not in *Dmca1DX10* homozygous null (*Dmca1DX10/Dmca1DX10*) embryos. The heterozygous *Dmca1DX10* embryos carried the embryonic fluorescent balancer, Cyo,Dfd-eYFP, that was labeled by anti-GFP. Homozygous *Dmca1DX10* embryos were identified by the lack of fluorescent balancer. The images shown are a stack of confocal planes through the entire embryo. Embryos were examined since the *Dmca1D* nulls were larval lethal. Scale bar, 25 μm.

Figure 4.2

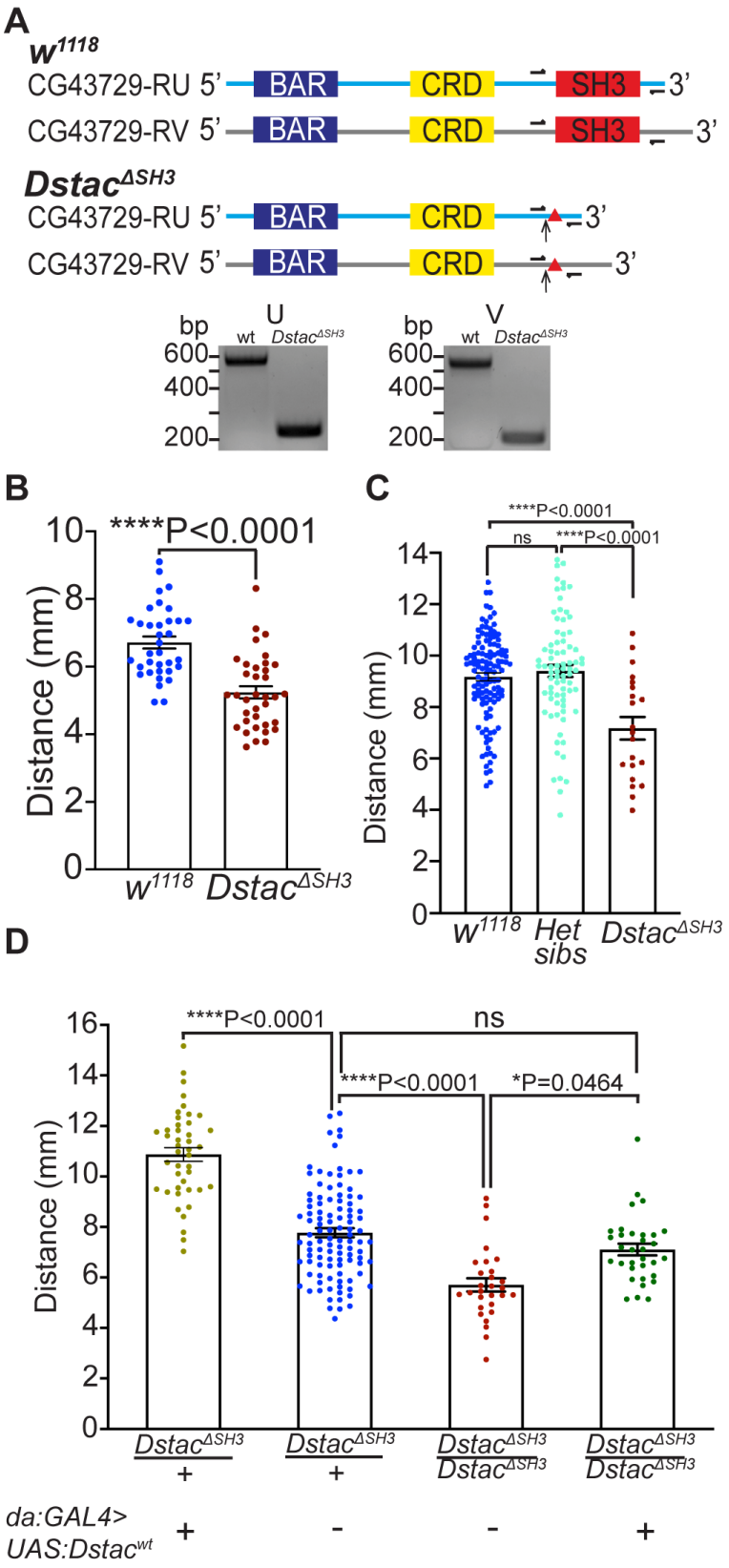
A
w1118
CG43729-RU 5'
BAR
CRD
SH3
3'
CG43729-RV 5'
DstacΔSH3
bp
wt
U
V
600
400
200
B
****P<0.0001
Distance (mm)
w1118
DstacΔSH3
C
ns
Het sibs
D
da:GAL4>
UAS:Dstacwt

Figure 4.2 *Dstac$^{\Delta SH3}$* generated by CRISPR-Cas9 showed reduced locomotion.
(A) Schematic of two Dstac protein variants (CG43729-RU and CG43729-RV) are shown. Arrows denote the location where early stop codons occurred due to the indels (triangles) created by CRISPR-Cas9. Half arrows denote primer sites used to sequence the mutations. All primers used are listed in the STAR Methods. The cDNA PCR fragments of *Dstac$^{\Delta SH3}$* mutants are smaller than wt for both RU and RV variants confirming the deletions of the SH3 domain in the *Dstac* cDNA. The deletions of SH3 were confirmed by sequencing the wt and *Dstac$^{\Delta SH3}$* cDNA bands (Supplementary Text). The translated mutant cDNA sequences showed that an early stop codon was produced in *Dstac$^{\Delta SH3}$* mutants (Supplementary Text). Schematic is not to scale. (B) Offsprings of Founder 1 of *Dstac$^{\Delta SH3}$* after 5 generations of outcrossing showed decreased locomotion compared with wt (wt n=35, *Dstac$^{\Delta SH3}$* n=36, one-tailed, unpaired t test). (C) Offsprings of Founder 2 of *Dstac$^{\Delta SH3}$* after 10 generations of outcrossing (n=21) showed decreased locomotion compared with wt (n=120) and heterozygous siblings (n=78) (one-way ANOVA, Tukey's multiple comparisons test). (D) Expression of *Dstac^{wt}* by heterozygous *Dstac$^{\Delta SH3}$* larvae (n=43) increased locomotion compared with heterozygous controls (n=104) and expression of *Dstac^{wt}* by homozygous *Dstac$^{\Delta SH3}$* (n=33) rescued *Dstac$^{\Delta SH3}$* (n=29) locomotion (Kruskal-Wallis test, Dunn’s multiple comparisons test). The larvae were genotyped by PCR after the locomotion assay.

Figure 4.3

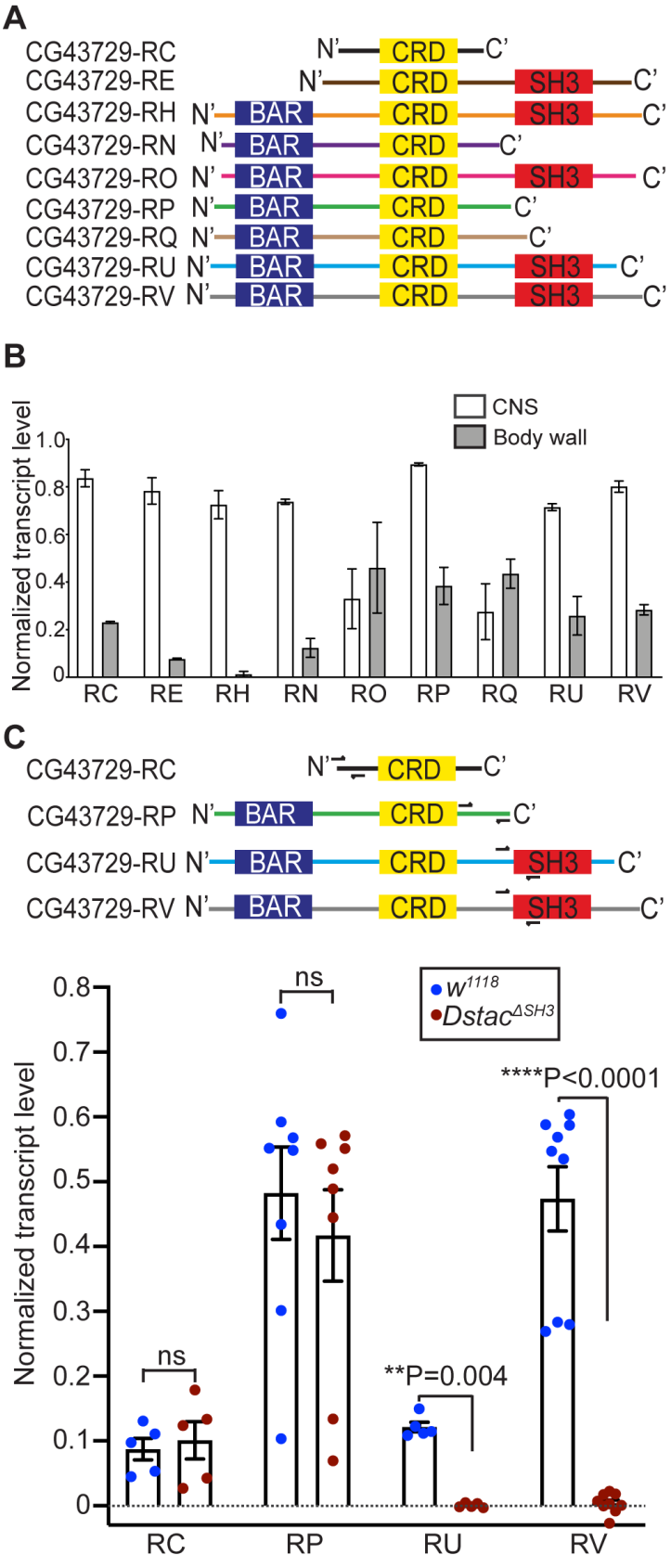
A
CG43729-RC
CG43729-RE
CG43729-RH
CG43729-RN
CG43729-RO
CG43729-RP
CG43729-RQ
CG43729-RU
CG43729-RV
N'
C'
BAR
CRD
SH3
B
CNS
Body wall
Normalized transcript level
1.0
0.8
0.6
0.4
0.2
0
RC
RE
RH
RN
RO
RP
RQ
RU
RV
C
CG43729-RC
CG43729-RP
CG43729-RU
CG43729-RV
w^{1118}
$Dstac^{\Delta SH3}$
ns
ns
**P=0.004
****P<0.0001
Normalized transcript level
0.8
0.7
0.6
0.5
0.4
0.3
0.2
0.1
0
RC
RP
RU
RV

Figure 4.3 Dstac isoforms that contain the SH3 domain are affected in *Dstac$^{\Delta SH3}$*.
(A) Schematic of domain composition of nine Dstac protein variants. Not all variants contain a SH3 domain. (B) Quantification of *Dstac* transcript levels in wt 3rd instar larval CNS and body wall assayed by RT-PCR. Error bars represent SEM. RT-PCR primers for CG43729 (*Dstac*) transcripts and *GAPDH* used for normalization can be found in Supplementary table. (C) Two isoforms without the SH3 domain (CG43729-RC and CG43729-RP) and two isoforms that contain the SH3 domain (CG43729-RU and CG43729-RV), were PCR amplified from wt and *Dstac$^{\Delta SH3}$* cDNA. Half arrows denote the primer sites. The levels of isoforms that don't have SH3 domain (RC and RP) were comparable between wt and *Dstac$^{\Delta SH3}$* (Mann-Whitney test), but the isoforms that normally contained the SH3 domain (RU and RV) were dramatically diminished in *Dstac$^{\Delta SH3}$* (Mann-Whitney test) (RC: wt n=5, *Dstac$^{\Delta SH3}$* n=5; RP: wt n=8, *Dstac$^{\Delta SH3}$* n=8; RU: wt n=5, *Dstac$^{\Delta SH3}$* n=5; RV: wt n=9, *Dstac$^{\Delta SH3}$* n=9; each dot represents one cDNA gel band).

Supplementary Figure 4.2

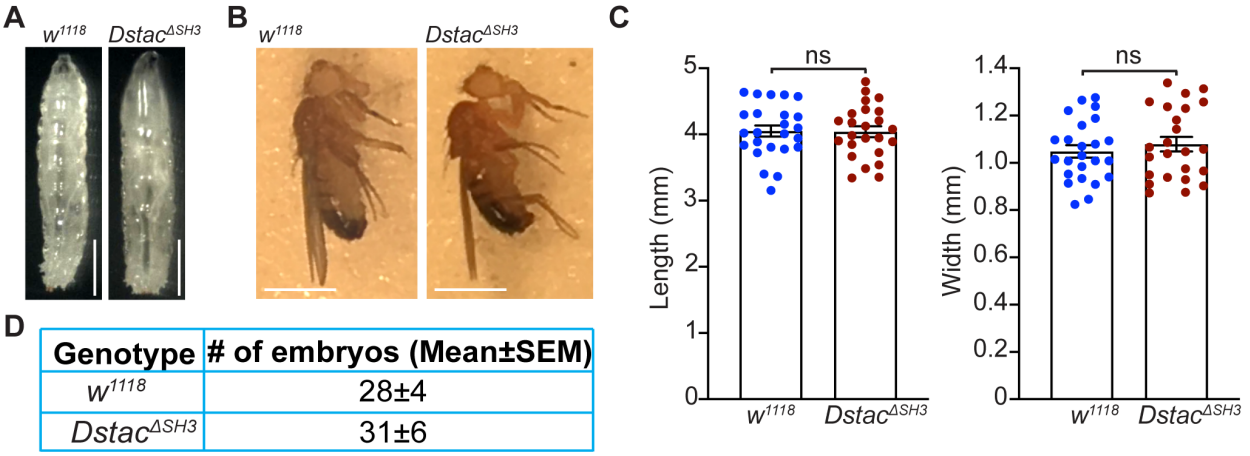

D

Genotype	# of embryos (Mean±SEM)
w^{1118}	28±4
$Dstac^{\Delta SH3}$	31±6

Supplementary Figure 4.2 The general morphology and reproductivity of *Dstac$^{\Delta SH3}$* appear to be normal.

(A) *Dstac$^{\Delta SH3}$* 3rd instar larvae are similar in morphology to wt. Scale bar, 1 mm. (B) *Dstac$^{\Delta SH3}$* can eclose and the adults are similar in morphology to wt. Scale bar, 1 mm. (C) The body width and length of 3rd instar larvae of wt (n=24) and *Dstac$^{\Delta SH3}$* (n=24) larvae are comparable (unpaired t test, p=ns). (D) *Dstac$^{\Delta SH3}$* (n=3) and wt (n=3) adults produced comparable numbers of embryos (Mann-Whitney test, p=ns).

Supplementary Figure 4.3

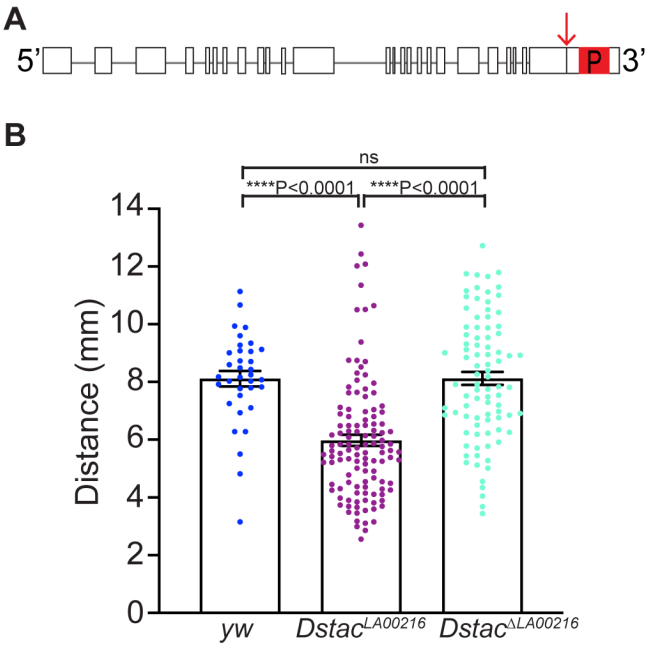

Supplementary Figure 4.3 *Dstac* p-element insertion mutant larvae exhibit decreased locomotion.

(A) Schematic of the *Dstac* genomic locus showing the site of the p-element insertion. Boxes denote exons. The arrow denotes the translation stop site. "P" red box denotes the p-element insertion in the 3'UTR of *Dstac* gene. (B) Larvae of the *Dstac* p-element insertion line, $Dstac^{LA00216}$, (n=119) showed reduced locomotion compared with wt larvae (n=35) (Kruskal-Wallis test, Dunn's multiple comparisons test). Upon precise excision of the p-element by transposase, $Dstac^{\Delta LA00216}$, (n=88), the reduced locomotion of $Dstac^{LA00216}$ was rescued to the level of wt (Kruskal-Wallis test, Dunn's multiple comparisons test).

Figure 4.4

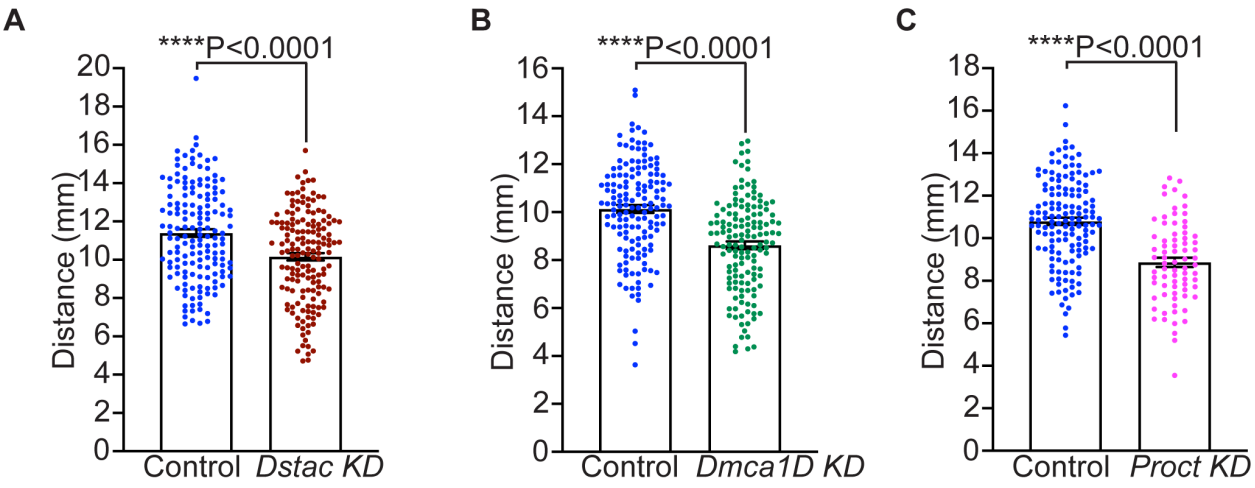

Figure 4.4 Knockdown of Dstac, Dmca1D, and proctolin selectively in proctolin+ motor neurons reduced larval locomotion.
(A) *Dstac*^{RNAi} larvae in which *Dstac* was knocked down in proctolin neurons (*proct:GAL4>UAS:Dstac*^{RNAi}) showed decreased locomotion compared with control *Luciferase*^{RNAi} larvae (*proct:GAL4>UAS:Luciferase*^{RNAi}) (control n=156, *Dstac*^{RNAi} n=156; one-tailed Mann-Whitney test). (B) *Dmca1D*^{RNAi} in which *Dmca1D* was knocked down in proctolin neurons (*proct:GAL4>UAS:Dmca1D*^{RNAi}) showed decreased locomotion compared with control *Luciferase*^{RNAi} larvae (control n=150, *Dmca1D*^{RNAi} n=143; one-tailed, unpaired t test). (C) *proctolin*^{RNAi} larvae in which *proctolin* was knocked down in proctolin neurons (*proct:GAL4>UAS:proctolin*^{RNAi}) showed decreased locomotion compared with control *Luciferase*^{RNAi} larvae (control n=144, *proctolin*^{RNAi} n=75; one-tailed, unpaired t test). See also Supplementary Figure 4.4.

Supplementary Figure 4.4

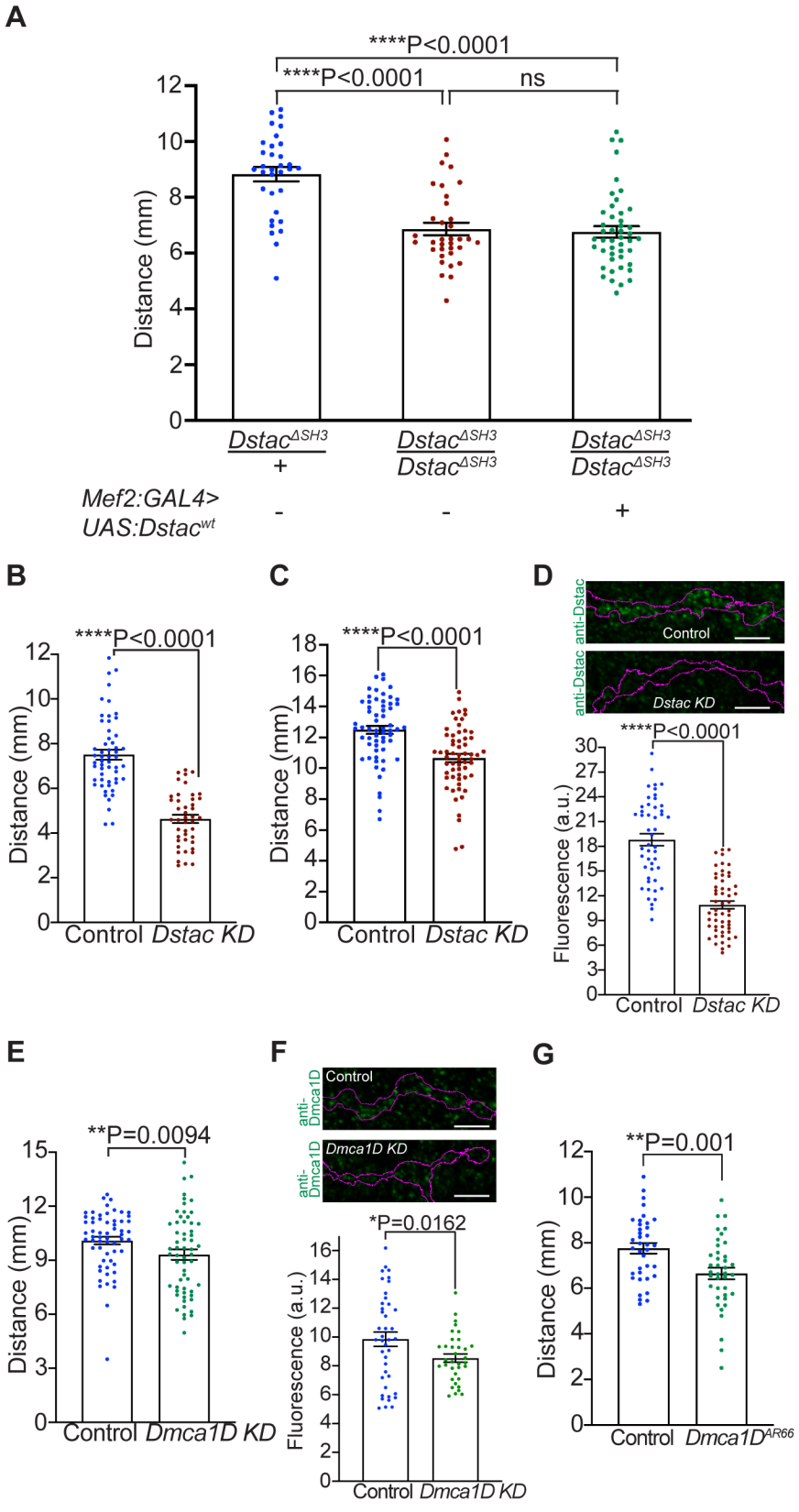

Supplementary Figure 4.4 Dstac and Dmca1D expression by the CNS is required for normal larval locomotion.

(A) Homozygous *Dstac*$^{\Delta SH3}$ expressing *Dstac*^{wt} in body wall muscles (*Mef2:GAL4>UAS:Dstac*^{wt}) (n=46) showed comparable locomotion as homozygous *Dstac*$^{\Delta SH3}$ (n=35) (Kruskal-Wallis test, Dunn's multiple comparisons test), which was lower than *Dstac*$^{\Delta SH3}$ heterozygotes (n=33) (Kruskal-Wallis test, Dunn's multiple comparisons test). (B) Pan-neuronal knockdown of *Dstac* (*elav:Gal4>UAS:Dstac*^{RNAi}) (n=44) reduced larval locomotion compared with wt control larvae (*elav:Gal4>UAS:Luciferase*^{RNAi}) (n=55) (one-tailed, unpaired t test). (C) Knocking down *Dstac* selectively in *ShakB* motor neurons (*ShakB:Gal4>UAS:Dstac*^{RNAi}) (n=60) reduced larval locomotion compared with control (*ShakB:Gal4>UAS:Luciferase*^{RNAi}) (n=60) (one-tailed, unpaired t test). (D) Anti-Dstac labeling of boutons of larvae with Dstac knocked down selectively in proctolin+ motor neurons (*proct:GAL4>UAS:Dstac*^{RNAi}) (n=54 boutons from 6 larvae) confirmed that Dstac was knocked down compared with control boutons (*proct:GAL4>UAS:Luciferase*^{RNAi}) (n=48 boutons from 4 larvae) (one-tailed Mann-Whitney test). Top images are a single focal plane of type Is boutons on muscle 4 of a control and a Dstac KD larva. The motor branches are outlined in magenta. Scale bar, 3 μm. (E) Knocking down *Dmca1D* selectively in *ShakB* motor neurons (*ShakB:Gal4>UAS:Dmca1D*^{RNAi}) (n=59) reduced larval locomotion compared with control (*ShakB:Gal>UAS:Luciferase*^{RNAi}) (n=60) (one-tailed Mann-Whitney test). (F) Anti-Dmca1D labeling of boutons of larvae with Dmca1D knocked down selectively in proctolin+ motor neurons (*proct:GAL4>UAS:Dmca1D*^{RNAi}) (n=35 boutons from 3 larvae) confirmed that Dmca1D was knocked down compared with control boutons (*proct:GAL4>UAS:Luciferase*^{RNAi}) (n=41 boutons from 4 larvae) (one-tailed, unpaired t test). Top images are a single focal plane of type Is boutons on muscle 4 of a control and a Dmca1D KD larvae. Scale bar, 3 μm. (G) Locomotion of *Dmca1D*^{AR66} larvae (n=39) was reduced compared with control (n=37) (one-tailed, unpaired t test).

Figure 4.5

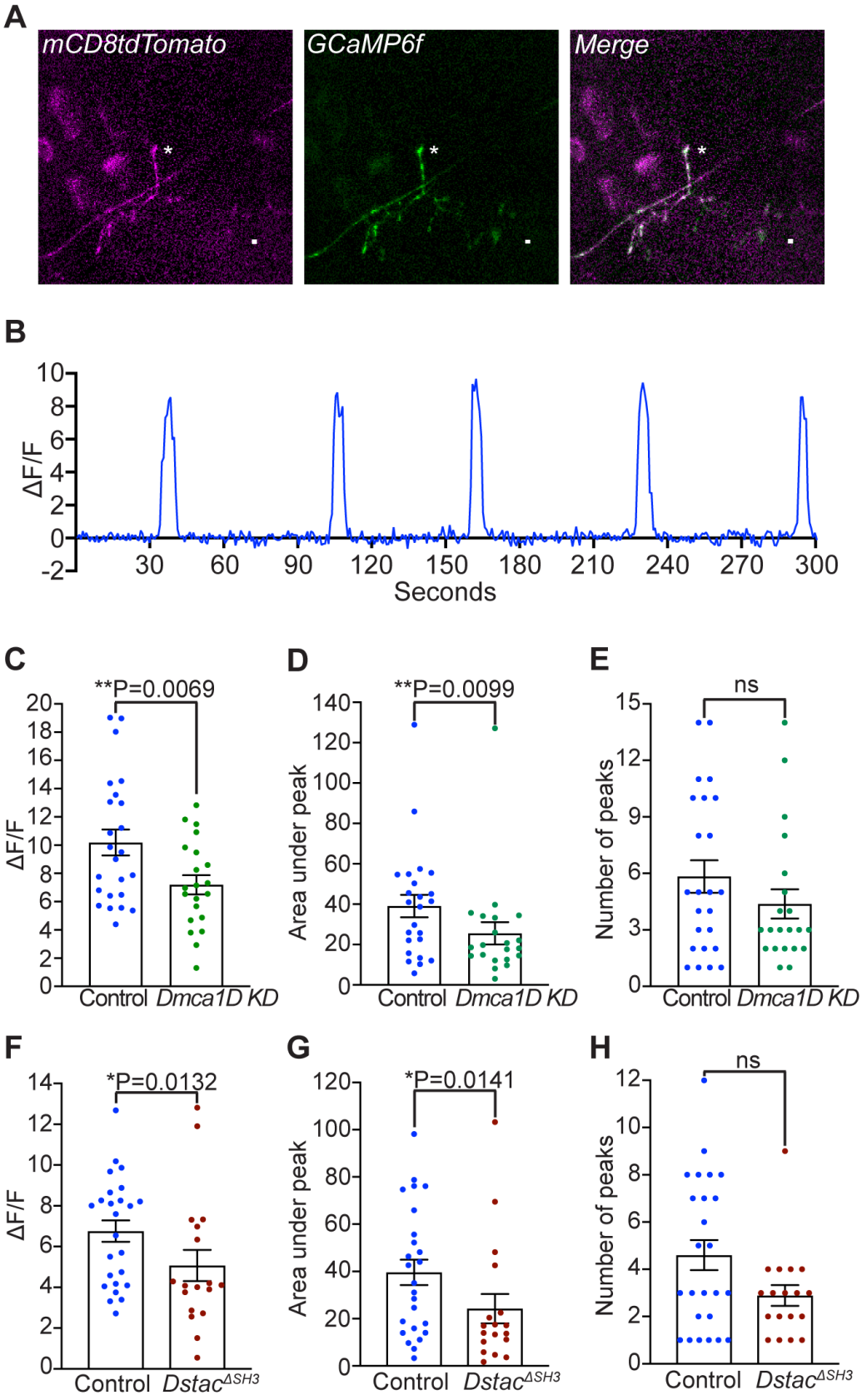
A
mCD8tdTomato
GCaMP6f
Merge
B
ΔF/F
Seconds
C
**P=0.0069
ΔF/F
Control
Dmca1D KD
D
**P=0.0099
Area under peak
Control
Dmca1D KD
E
ns
Number of peaks
Control
Dmca1D KD
F
*P=0.0132
ΔF/F
Control
DstacΔSH3
G
*P=0.0141
Area under peak
Control
DstacΔSH3
H
ns
Number of peaks
Control
DstacΔSH3

Figure 4.5 Deficiencies in Dmca1D and Dstac decrease Ca^{2+} transients in motor boutons.
(A) GCaMP6f expressed selectively in proctolin+ motor boutons of a wt control larva (*Proct:GAL4>UAS:GCaMP6f;UAS:mCD8tdTomato;UAS:Luciferase^{RNAi}*). Asterisk denotes Is motor branch on muscle 4. Scale bar, 3 μm. (B) Example of Ca^{2+} transients from a type Is bouton on muscle 4 in a wt control larva. (C), (D) The peaks and area under the peaks of Ca^{2+} transients in the boutons of *Dmca1D KD* larvae (*Proct:GAL4>UAS:GCaMP6f;UAS:Dmca1D^{RNAi}*) were smaller compared with *wt* control. Peaks (C), one-tailed, unpaired t test. Area under peaks (D), one-tailed Mann-Whitney test. (E) The number of Ca^{2+} transients over 5 min in *Dmca1D KD* and wt control boutons were comparable (Mann-Whitney test). Data in C-E were from 24 boutons in 19 wt control larvae and 21 boutons in 16 *Dmca1D KD* larvae. (F), (G) The peaks and area under the peaks of Ca^{2+} transients in the boutons of *Dstac$^{\Delta SH3}$* larvae (*Proct:GAL4>UAS:GCaMP6f;Dstac$^{\Delta SH3}$*) are smaller compared with *wt* control (one-tailed Mann-Whitney test). (H) The number of Ca^{2+} transients over 5 min in *Dstac$^{\Delta SH3}$* and wt boutons are comparable (Mann-Whitney test). Data in F-H were from 25 boutons in 25 wt control larvae and 18 boutons in 18 *Dstac$^{\Delta SH3}$* larvae. Each data point represents the averaged peaks or area under peaks of Ca^{2+} transients per bouton.

Figure 4.6

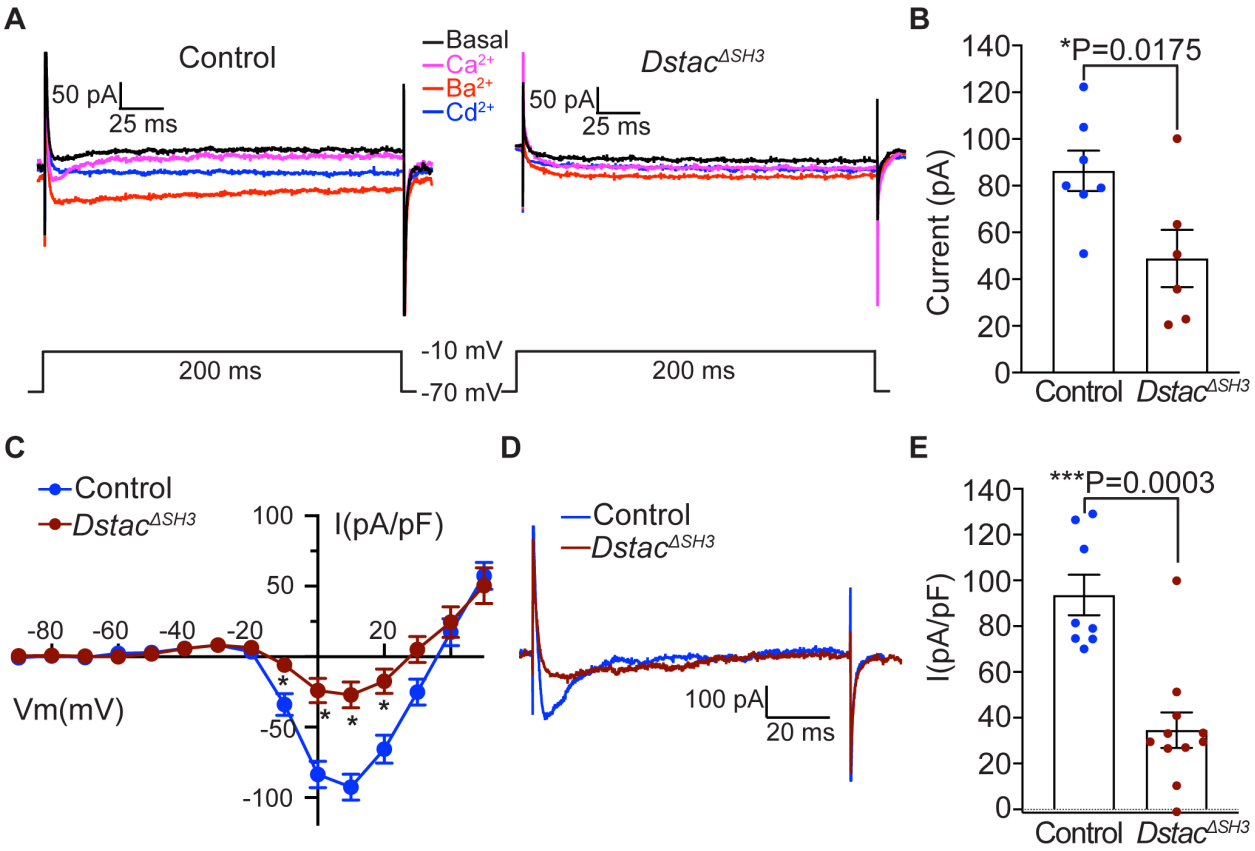

Figure 4.6 Dmca1D currents in RP2 motor neuron cell bodies were largely decreased in *Dstac$^{\Delta SH3}$*.

(A) Voltage-clamp recording in response to a single voltage step of a wt control RP2 (left) and a *Dstac$^{\Delta SH3}$* RP2 (right). The RP2 motor neuron cell bodies were held at -70 mV and stepped to -10 mV for 200 ms in four different solutions. The wt control RP2 cell bodies showed an inward Ca^{2+} current that inactivated and a larger Ba^{2+} current that barely inactivated, whereas *Dstac$^{\Delta SH3}$* RP2 cell bodies showed significantly smaller Ca^{2+} and Ba^{2+} currents. (B) The amplitudes of Ba^{2+} currents from *Dstac$^{\Delta SH3}$* RP2 cell bodies were smaller compared with control (control n=7 cells from 7 larvae, *Dstac$^{\Delta SH3}$* n=6 cells from 6 larvae, one-tailed Mann-Whitney test). The RP2 motor neuron cell bodies were held at -70 mV and stepped to -10 mV for 200 ms. (C) Full I/V curves from control and *Dstac$^{\Delta SH3}$* RP2 cell bodies were created by holding at -70 mV and stepping from -90 mV to +50 mV with 10 mV increments. Ca^{2+} current peaked at +10 mV in both control (n=8) and *Dstac$^{\Delta SH3}$* (n=11) larvae, and the currents were significantly decreased in *Dstac$^{\Delta SH3}$* compared to controls at -10 mV, 0 mV, +10 mV and +20 mV (one-tailed Mann-Whitney test, p value: 0.0034, 0.0004, 0.0003 and 0.0018, respectively). (D) Voltage-clamp Ca^{2+} currents at +10 mV of a control and *Dstac$^{\Delta SH3}$* RP2 cell body. (E) The peak Ca^{2+} current density from the voltage steps of *Dstac$^{\Delta SH3}$* RP2 cell bodies were reduced significantly compared with control. (Control n=8 cells from 8 larvae, *Dstac$^{\Delta SH3}$* n=11 cells from 11 larvae, one-tailed Mann-Whitney test).

Figure 4.7

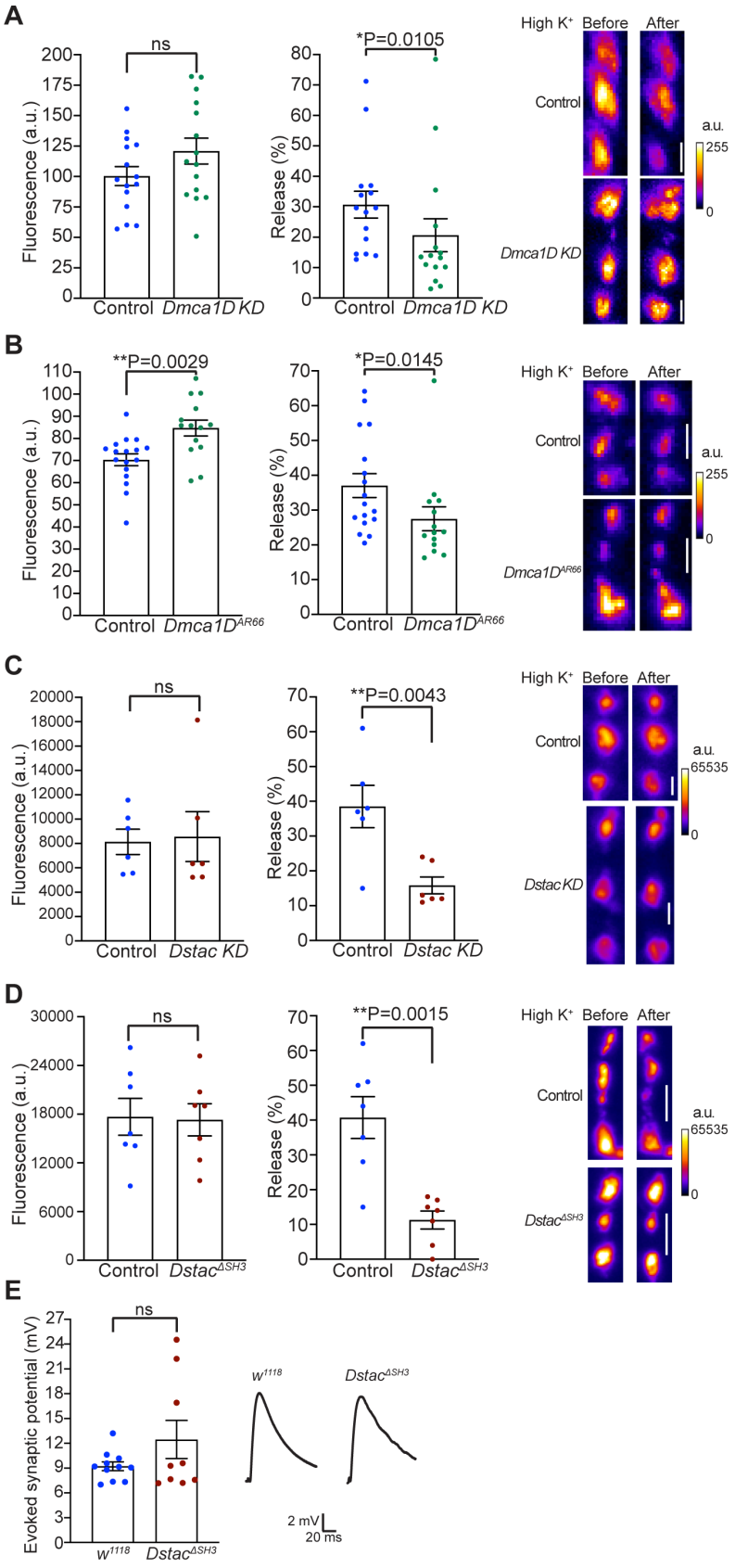
A
ns
*P=0.0105
Fluorescence (a.u.)
Release (%)
Control
Dmca1D KD
High K+ Before After
Control
Dmca1D KD
a.u.
255
0
B
**P=0.0029
*P=0.0145
Fluorescence (a.u.)
Release (%)
Control
Dmca1D^AR66
High K+ Before After
Control
Dmca1D^AR66
a.u.
255
0
C
ns
**P=0.0043
Fluorescence (a.u.)
Release (%)
Control
Dstac KD
High K+ Before After
Control
Dstac KD
a.u.
65535
0
D
ns
**P=0.0015
Fluorescence (a.u.)
Release (%)
Control
Dstac^ΔSH3
High K+ Before After
Control
Dstac^ΔSH3
a.u.
65535
0
E
ns
Evoked synaptic potential (mV)
w1118
Dstac^ΔSH3
w1118
Dstac^ΔSH3
2 mV
20 ms

Figure 4.7 Release of neuropeptides is diminished in *Dstac* and *Dmca1D* deficient motor boutons.

(A) Expression of Dilp2-GFP by type Is motor boutons on muscle 4 of Dmca1D KD (n=15) and control (n=15) was comparable (left; unpaired t test). Release of Dilp2-GFP was decreased in Dmca1D KD compared with control (middle; one-tailed Mann Whitney test). Examples of Dilp2-GFP expression before and after exposure to high potassium of control (upper, right) and Dmca1D KD (lower, right). The boutons are shown in pseudocolor. Scale bar, 2 μm. (B) Expression of Dilp2-GFP by motor boutons of $Dmca1D^{AR66}$ (n=14) was higher than that by control (n=17) (left; unpaired t test). Release of Dilp2-GFP was decreased in $Dmca1D^{AR66}$ compared with control (middle; one-tailed Mann Whitney test). Examples of Dilp2-GFP expression before and after exposure to high KCl of control (upper, right) and $Dmca1D^{AR66}$ (lower, right). Scale bar, 2 μm. (C) Expression of Dilp2-GFP by motor boutons of Dstac KD (n=6) and control (n=6) was comparable (left; Mann-Whitney test). Release of Dilp2-GFP was decreased in Dstac KD compared with control (middle; one-tailed Mann-Whitney test). Examples of Dilp2-GFP expression before and after exposure to high KCl of control (upper, right) and Dstac KD (lower, right). Scale bar, 2 μm. (D) Expression of Dilp2-GFP by motor boutons of $Dstac^{\Delta SH3}$ (n=7) and control (n=7) was comparable (left; Mann-Whitney test). Release of Dilp2-GFP was decreased in $Dstac^{\Delta SH3}$ compared with control (middle; one-tailed Mann-Whitney test). Examples of Dilp2-GFP expression before and after exposure to high KCl of control (upper, right) and $Dstac^{\Delta SH3}$ (lower, right). Scale bar, 2 μm. (E) Nerve evoked synaptic potentials of muscle 4 were comparable between wt (n=11) vs $Dstac^{\Delta SH3}$ (n=9) (unpaired t test).

Figure 4.8

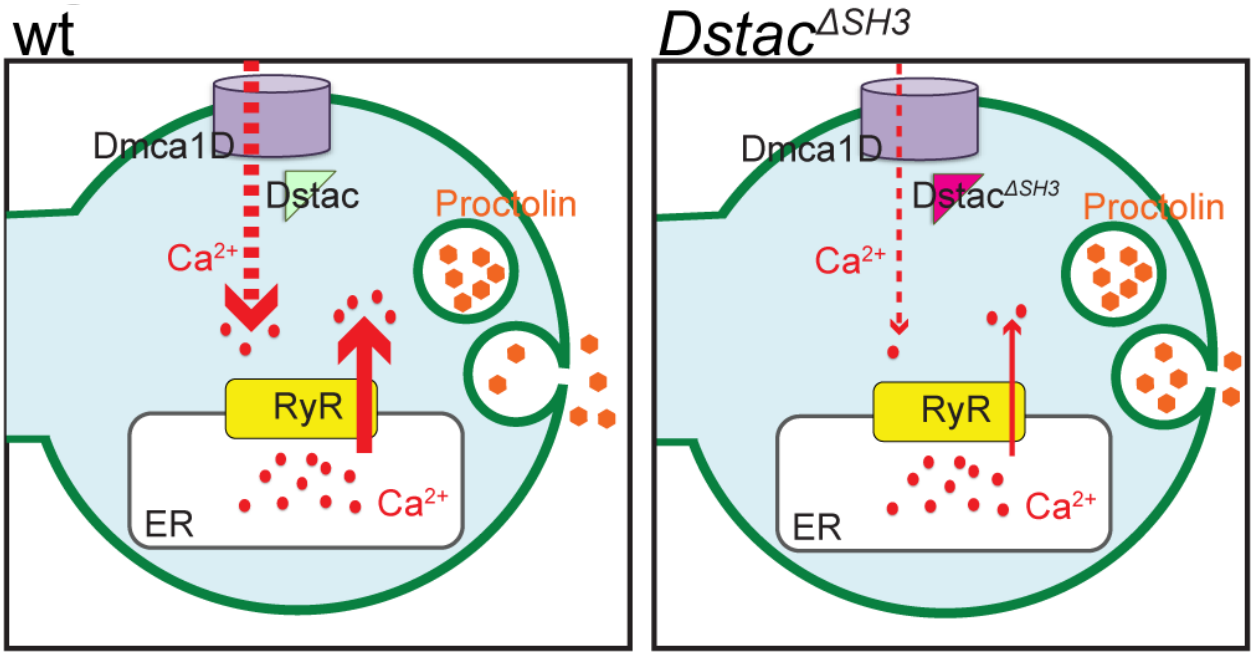

Figure 4.8 Model for the role of Dstac in neuropeptide release from RP2 motor neuron boutons.
In wt (left) Dstac regulates Ca^{2+} influx (circles) through Dmca1D channels (thick dashed arrow) to initiate CICR from the RyR Ca^{2+} release channel in the ER into the cytosol (thick arrow) and subsequent release of proctolin neuropeptide (hexagon) from motor boutons. In *Dstac*$^{\Delta SH3}$ (right) Ca^{2+} influx through Dmca1D channels is decreased (thin dashed arrow) resulting in less CICR (thin arrow), and thus reduced release of proctolin neuropeptide.

Supplementary table. Primers used in this study.

Oligonucleotides	SOURCE	IDENTIFIER
Primer 1 for CRISPR (5’-3’): TGTCGAATGTTGCTCTGTTCC (Forward)	This study	N/A
Primer 2 for CRISPR (5’-3’): GGACAAACCACAACTAGAATGC (Reverse)	This study	N/A
Primer 3 for CRISPR (5’-3’): CTCGACCGCCGGAGTATAAATAG (Forward)	This study	N/A
Primer 4 for CRISPR (5’-3’): GTTGTCCTTGGTCGCATCCTC (Reverse)	This study	N/A
Primer 5 for CRISPR (5’-3’): TTCAATCTCCTAAGTCCCATACACTCCCAT (Forward)	This study	N/A
Primer 6 for CRISPR (5’-3’): GTTCGCGACGATGACGTCT (Reverse)	This study	N/A
Primer 7 for CRISPR (5’-3’): CGTGGCAGCCATTGTGCAAA (Reverse)	This study	N/A
Primer 8 for RT-PCR of CG43729-RC (5’-3’): GAGTGCAGCGCAAGGATCTA (Forward)	This study	N/A
Primer 9 for RT-PCR of CG43729-RC (5’-3’): AACCAGCAGGCTTTAGGCTC (Reverse)	This study	N/A
Primer 10 for RT-PCR of CG43729-RE (5’-3’): CACACGTACACCCCCTCTCT (Forward)	This study	N/A
Primer 11 for RT-PCR of CG43729-RE (5’-3’): GTCGGCTCAACTTTGCTCAC (Reverse)	This study	N/A
Primer 12 for RT-PCR of CG43729-RH (5’-3’): CCAACCACCCCGACAAAATC (Forward)	This study	N/A
Primer 13 for RT-PCR of CG43729-RH (5’-3’): TCGCAGGCCGTTATCTTCTT (Reverse)	This study	N/A
Primer 14 for RT-PCR of CG43729-RN (5’-3’): CGACTAGCAGAAAGTTCTTCGG (Forward)	This study	N/A
Primer 15 for RT-PCR of CG43729-RN (5’-3’): TGTAATCCTTGAGCACGCCG (Reverse)	This study	N/A
Primer 16 for RT-PCR of CG43729-RO (5’-3’): CTCACCAGAATCGTCGGAGC (Forward)	This study	N/A
Primer 17 for RT-PCR of CG43729-RO (5’-3’): TTGGATGCGTTAGTCCAGTG (Reverse)	This study	N/A
Primer 18 for RT-PCR of CG43729-RP (5’-3’): GGAAGAAAAACCGCGATACGG (Forward)	This study	N/A
Primer 19 for RT-PCR of CG43729-RP (5’-3’): AGATGGAGGAGGATGTGGCA (Reverse)	This study	N/A
Primer 20 for RT-PCR of CG43729-RQ (5’-3’): TTGAATGTGCCAAATGCGAAGT (Forward)	This study	N/A
Primer 21 for RT-PCR of CG43729-RQ (5’-3’): GAACCGGAAGAGCCGATCC (Reverse)	This study	N/A

Primer 22 for RT-PCR of CG43729-RU (5’-3’): TAGCTCAGGGACTAACGCATC (Forward)	This study	N/A
Primer 23 for RT-PCR of CG43729-RU (5’-3’): CTTACGGGTGAGAGGCACG (Reverse)	This study	N/A
Primer 24 for RT-PCR of CG43729-RV (5’-3’): TGCCAGAAACACCATCGAGC (Forward)	This study	N/A
Primer 25 for RT-PCR of CG43729-RV (5’-3’): TGGGGATGTCTTACGGGTGA (Reverse)	This study	N/A
Primer 26 for RT-PCR of GAPDH (5’-3’): CACATACTCGGCTCCAGCACT (Forward);	This study	N/A
Primer 27 for RT-PCR of GAPDH (5’-3’): GCAGTCGTAATAGCGAACT (Reverse)	This study	N/A
Primer 28 for RT-PCR (5’-3’): TCACACCTCCTGCAGATACTTG (Reverse)	This study	N/A
Primer 29 for p-element (5’-3’): TGACACTCCAGCAACGGTAAAC (Forward)	This study	N/A
Primer 30 for p-element (5’-3’): TTAGGTGCGGTACGGATAGG (Forward)	This study	N/A
Primer 31 for p-element (5’-3’): CGACGGGACCACCTTATGTTA (Inverted Repeat of p-element)	This study	N/A
Primer 32 for p-element (5’-3’): CTCATAGGCCATAGGGTACACT (Reverse)	This study	N/A
Primer 33 for p-element (5’-3’): ATGAGTGGAGTTCTGTTTGCCT (Reverse)	This study	N/A
Primer 34 for cloning Dstac (5’-3’): ATGCGCGTTATCGTTCTCAAA (Forward)	This study	N/A
Primer 35 for cloning Dstac (5’-3’): TCACACCTCCTGCAGATACTTG (Reverse)	This study	N/A
Primer 36 for GAL4 (5’-3’): GCCGTCACAGATAGATTGGCTTC (Forward)	This study	N/A
Primer 37 for GAL4 (5’-3’): GTCGGATGGCTTGCCCTTCCTG (Reverse)	This study	N/A
Primer 38 for *UAS:Dstac*^{wt}*-eGFP* (5’-3’): CGCAGCTGAACAAGCTAAAC (Forward)	This study	N/A
Primer 39 for *UAS:Dstac*^{wt}*-eGFP* (5’-3’): TCGCAGGCCGTTATCTTCTT (Reverse)	This study	N/A
Primer 40 for Dmca1D antibody (5’-3’): AAAGCTAGCGACTTCGAGCGTGGAGCCTCCGGCG A (Forward)	This study	N/A
Primer 41 for Dmca1D antibody (5’-3’): GAAAAGCTTTCATGGTTGCGGTTTTCCACGACGCT GTTGT (Reverse)	This study	N/A

Supplementary text

Sequencing results of *Dstac* Genomic DNA

wt *(w^{1118})*

Exons encode for SH3
gRNA1 target sequence
gRNA2 target sequence
PAM

CTTGCATTCGATTAACCAAACCAAACCAAACCGTATCCATTGAGCCTGTCCTGGAGCAGGGACTAACGCATCCAAAACCATTAC
AGCACCATCGAGCCCCTCGCATCCGGGCCGCAAGCTATTGTATGCCACCCGTGGAATGCGTGGTGGCAGCGTCGATCTGCCGG
ACGAGATGGAGAAGTCGCAGTCCTCGGCCAGCACCTCGCCGTGCCTCTCACCCGTAAGACATCCCCAGGTAGACCCCACTCCA
CTCCTCCAACTACCACCCCTATTGTTCTTGAGTTAATTTCGTCTGATCCGCTCGTTTGAATGATTGCACATTAGCCTAGCAATGGT
ATTAACCCAAACCCAACACACGCTTCACCTATTTCAAGAAAACCCATCGTCTGTTGCCCACGAATCTGTATGTCATCATCTACAA
CTTCAAGGCGCGACATGCCGATGAACTGGATCTAAAGGCTGGCTACAAGGTGAGCTAATCATACGGGGACGGACTATCTACTC
CAAACACCCACTTTATAAATGAATGGGCGTATGAATAAATAAACAAGGCGCTTTGTTTAATCCGCTAAGCGGTGTACTTAGTTT
GCACAATGGCTGCCACG…TATTAATAGTATTCTAGTTGGCGAAAGGACACTTCTTCTTTCTGTATACAAGAATAATATCAAGTC
CTCTCCGAACCGGCATATTAATGAATATGTCTTAGTGAACAAGAGTAATAAAATTACCTAATTAATTAGCTTCTAGAAGCCGGA
TTAAACTTTTGAAAACTCTCGCTTCTGAAAACTAGGTGACTGTCATTGACAATTCAGATCCGGACTGGTGGAAGGGAAAAGTG
CTGGGACGAGTTGGATACTTCCCATCCAAGTACTGTGTGCGTCTGAATGCCAACGAGAAGCCACTGCAGGTGACCCACAATCT
CCAGGTGTCGGACAGTGAACGCGGCGAGAATCTTACCCTTCTAAGGGACCAGATTGTCATACAGGTGAGACCCACAAGCCCA
AACCATTCTCTCTTCCTCCCCTAACTTTGTTCACATGTCATCCATTTACCAAACAAGACCGGCGACGAGGTAAACGGCATGGTAA
TGATCCGAGCCGCCGAG

***Dstac*$^{\Delta SH3}$**

attP
loxP
gRNA1 target sequence that was cut by Cas9
gRNA2 target sequence that was cut by Cas9
PAM

CTTGCATTCGATTAACCAAACCAAACCAAACCGTATCCATTGAGCCTGTCCTGGAGCAGGGACTAACGCATCCAAAACCATTAC
AGCACCATCGAGCCCCTCGCATCCGGGCCGCAAGCTATTGTATGCCACGTAGTGCCCCAACTGGGGTAACCTTTGAGTTCTCTC
AGTTGGGGGCGTAGATAACTTCGTATAATGTATGCTATACGAAGTTATGCATGGTAATGATCCGAGCCGCCGAGCACGGGCA
GGGCTACTGCCCCATCAAGTATCTGCAGGAGGTGTGACA

Sequencing results of *Dstac cDNA*

wt CG43729-RU

cDNA encodes for SH3
gRNA1 target sequence
gRNA2 target sequence
PAM

AAGCTATTGTATGCCACCCGTGGAATGCGTGGTGGCAGCGTCGATCTGCCGGACGAGATGGAGAAGTCGCAGTCCTCGGCCA
GCACCTCGCCGTGCCTCTCACCCGTAAGACATCCCCAGAAAACCCATCGTCTGTTGCCCACGAATCTGTATGTCATCATCTACAA
CTTCAAGGCGCGACATGCCGATGAACTGGATCTAAAGGCTGGCTACAAGGTGACTGTCATTGACAATTCAGATCCGGACTGGT
GGAAGGGAAAAGTGCTGGGACGAGTTGGATACTTCCCATCCAAGTACTGTGTGCGTCTGAATGCCAACGAGAAGCCACTGCA
GGTGACCCACAATCTCCAGGTGTCGGACAGTGAACGCGGCGAGAATCTTACCCTTCTAAGGGACCAGATTGTCATACAGACCG
GCGACGAGGTAAACGGCATGGTAATGATCCGAGCCGCCGAGCACGGGCAGGGCTACTGCCCCATCAAGTATCTGCAGGA

***Dstac*$^{\Delta SH3}$ CG43729-RU**

attP

loxP

gRNA1 target sequence that was cut by Cas9

gRNA2 target sequence that was cut by Cas9

PAM

Stop codon

AAGCTATTGTATGCCACG**TAG**TGCCCCAACTGGGGTAACCTTTGAGTTCTCTCAGTTGGGGGCGTAGATAACTTCGTATAATGT
ATGCTATACGAAGTTATGCATGGTAATGATCCGAGCCGCCGAGCACGGGCAGGGCTACTGCCCCATCAAGTATCTGCAGGA

wt CG43729-RV

cDNA encodes for SH3

gRNA1 target sequence

gRNA2 target sequence

PAM

AAGCTATTGTATGCCACCCGTGGAATGCGTGGTGGCAGCGTCGATCTGCCGGACGAGATGGAGAAGTCGCAGTCCTCGGCCA
GCACCTCGCCGTGCCTCTCACCCGTAAGACATCCCCAGAAAACCCATCGTCTGTTGCCCACGAATCTGTATGTCATCATCTACAA
CTTCAAGGCGCGACATGCCGATGAACTGGATCTAAAGGCTGGCTACAAGGTGACTGTCATTGACAATTCAGATCCGGACTGGT
GGAAGGGAAAAGTGCTGGGACGAGTTGGATACTTCCCATCCAAGTACTGTGTGCGTCTGAATGCCAACGAGAAGCCACTGCA
GGTGACCCACAATCTCCAGGTGTCGGACAGTGAACGCGGCGAGAATCTTACCCTTCTAAGGGACCAGATTGTCATACAGACCG
GCGACGAGGTAAACGGCATGGTAATGATCCGAGCCGCCGAG

***Dstac*$^{\Delta SH3}$ CG43729-RV**

attP

loxP

gRNA1 target sequence that was cut by Cas9

gRNA2 target sequence that was cut by Cas9

PAM

Stop codon

AAGCTATTGTATGCCACG**TAG**TGCCCCAACTGGGGTAACCTTTGAGTTCTCTCAGTTGGGGGCGTAGATAACTTCGTATAATGT
ATGCTATACGAAGTTATGCATGGTAATGATCCGAGCCGCCGAG

Dstac* proteins according to Sequencing results of *Dstac cDNA

wt CG43729-RU

SH3

KLLYATRGMRGGSVDLPDEMEKSQSSASTSPCLSPVRHPQKTHRLLPTNLYVIIYNFKARHADELDLKAGYKVTVIDNSDPDWWKG
KVLGRVGYFPSKYCVRLNANEKPLQVTHNLQVSDSERGENLTLLRDQIVIQTGDEVNGMVMIRAAEHGQGYCPIKYLQ

***Dstac$^{\Delta SH3}$* CG43729-RU**
*denotes STOP

KLLYAT*CPNWGNL*VLSVGGVDNFV*CMLYEVMHGNDPSRRARAGLLPHQVSAG

wt CG43729-RV
SH3

KLLYATRGMRGGSVDLPDEMEKSQSSASTSPCLSPVRHPQKTHRLLPTNLYVIIYNFKARHADELDLKAGYKVTVIDNSDPDWWKG
KVLGRVGYFPSKYCVRLNANEKPLQVTHNLQVSDSERGENLTLLRDQIVIQTGDEVNGMVMIRAAE

***Dstac$^{\Delta SH3}$* CG43729-RV**
*denotes STOP

KLLYAT*CPNWGNL*VLSVGGVDNFV*CMLYEVMHGNDPSRR

4.5 Discussion

Pharmacological experiments suggest that the release of neuropeptides by neurons involves Ca^{2+} influx via L-type CaChs (Perney e al., 1986; Cazalis et al., 1987; Rane et al., 1987; Lemos and Nowycky, 1989; Wang et al., 1993; Sasaki et al., 2005; Kolarow et al., 2007; Xia et al., 2009) and CICR from internal Ca^{2+} stores (Ludwig et al., 2002). In *Drosophila* the release of neuropeptides at the neuromuscular junction also appears to involve CICR (Shakiryanova et al., 2007), but it was unknown whether Ca^{2+} influx via the L-type CaCh Dmca1D triggers CICR. The results from this study established that Dmca1D is required for the normal release of neuropeptides at the neuromuscular junction and suggested a mechanism by which Dstac regulates Dmca1D and the release of neuropeptides at the *Drosophila* nmj. First, Dstac, Dmca1D and proctolin are all expressed by motor boutons. Second*, Dstac* mutations and *Dmca1D* knockdowns decrease Ca^{2+} transients in motor boutons. Third, *Dstac* mutations decrease currents through Dmca1D channels in motor neurons. Fourth, mutations and knockdowns of *Dstac* and *Dmca1D* decrease the release of neuropeptides by motor boutons. Fifth, mutations and knockdowns of *Dstac*, *Dmca1D* and *Proct* decrease locomotion. Thus, Dstac regulates voltage-dependent influx of Ca^{2+} through Dmca1D channels, which leads to an increase in cytosolic Ca^{2+} perhaps involving CICR, and the release of neuropeptides at the neuromuscular junction. This in turn controls the intensity of muscle contractions and thus locomotion by *Drosophila* larvae.

Our experiments demonstrated that normal levels of Dilp2-GFP release by motor boutons requires Dstac. The endogenous neuropeptide expressed by these boutons is proctolin (Anderson et al., 1988; this study) so the presumption is that proctolin release by the boutons

also requires Dstac. Previous studies showed that proctolin increases muscle contractions in a variety of arthropods (Bishop and O'Shea, 1982; Adams and O'Shea, 1983; Bishop et al., 1987) including *Drosophil*a larvae without affecting the membrane voltage of muscles (Omerod et al., 2016). Thus, a decrease in proctolin predicts a decrease in locomotion by larvae. In fact, we found that larvae in which proctolin was knocked down selectively in motor neurons exhibited decreased locomotion. Furthermore, *Dstac* mutant larvae and larvae with *Dstac* selectively knocked down in motor neurons also showed decreased locomotion. These findings are consistent with the requirement of Dstac for the release of proctolin by motor boutons.

A deficiency in Dstac reduces the release of neuropeptides but not the synaptic potential due to the release of glutamate at the larval neuromuscular junction. Since Dstac regulates Dmca1D, normal synaptic function at the neuromuscular junction when Dstac is deficient suggests that Dmca1D is dispensable for synaptic release of glutamate. This is consistent with previous evidence that *cacophony* (Ca_V2) is the most important CaCh for producing fast EPSPs mediated by the release of glutamate (Lee et al., 2014).

Knockdown of Dmca1D specifically in motor neurons decreased the influx of Ca^{2+} into motor boutons at the neuromuscular junction and both the *Dmca1D* KD and *Dmca1D*^{AR66} mutation decreased the release of neuropeptide. This is consistent with the requirement for the influx of Ca^{2+} through the Dmca1D channels in the boutons for normal neuropeptide release. However, the decrease in Dmca1D in the dendrites, cell bodies and axons leading to the boutons of motor neurons may also contribute to decreased release of neuropeptide. Motor neuron specific knockdown of Dmca1D also leads to a decrease in the synaptic response of motor neurons to the central pattern generator and a decrease in duration and maximal

firing rate of action potential bursts initiated by synaptic input to motor neurons (Kadas et al., 2017). These appear to be due to the decrease in Dmca1D currents in both the dendrites and axons of motor neurons. Therefore, normal activation of Dmca1D channels in boutons in intact larvae is likely to require Dmca1D channels in dendrites and axons of motor neurons. Thus, Dmca1D in dendrites, axons and boutons is likely required for normal Ca^{2+} influx into boutons and the release of neuropeptides.

We previously showed that Dstac and Dmca1D were expressed and that Dstac was required in the LN_V neurons in the brain for normal circadian rhythm of locomotor behavior in *Drosophila* (Hsu et al., 2018). These neurons express the neuropeptide, pigment dispersing factor (PDF) (Helfrich-Forster, 1997; Renn et al., 1999), that is critical for circadian rhythm (Shafer and Taghert, 2009). Thus, it is possible that Dstac may regulate Dmca1D and the release of PDF by these neurons and that the release of PDF by LN_V neurons is essential for normal circadian rhythm. There are approximately 50 neuropeptide and peptide hormone genes in the *Drosophila* genome (Hewes and Taghert, 2001; Nassel and Zandawala, 2019). Whether Dstac regulates the release of other neuropeptides remains to be investigated, but given the wide range of time scales, cellular actions and sites of release of different neuropeptides and peptide hormones one might imagine several different mechanisms for the regulation of their release including those not involving Dstac. In fact, the finding that *Dstac* mutant larvae are normal in size and morphology and eclose properly is consistent with the possibility that Dstac does not regulate the release of peptide hormones such as Dilp2 or eclosion hormone.

Dstac is also expressed by body wall muscles in *Drosophila* (Hsu et al., 2018). Of note in vertebrates, *stac3* is expressed selectively by skeletal muscles and required for EC coupling

(Horstick et al., 2013; Nelson et al., 2013; Linsley et al., 2017a). In vertebrate skeletal muscles EC coupling involves the direct interaction of the L-type CaCh, DHPR, which is the voltage detector for EC coupling in the t-tubules, with the ryanodine receptor, which is the Ca^{2+} release channel in the SR (Nakai et al., 1996; Grabner et al., 1999; Paolini et al., 2004). Stac3 regulates EC coupling in skeletal muscles by regulating the stability and properties of the L-type CaCh in skeletal muscles (Linsley et al., 2017a). The muscle expression of Dstac suggests that Dstac might regulate EC coupling in larval body wall muscles of *Drosophila* just as Stac3 in vertebrate skeletal muscles. In some invertebrate muscles including those of *Drosophila*, EC coupling is thought to involve CICR (Gyorke and Palade, 1992; Maryon et al., 1998; Sullivan et al., 2000; Takekura and Franzini-Armstrong, 2002; Collet, 2009). Thus, Dstac might regulate EC coupling by controlling the stability and voltage dependency of Dmca1D in *Drosophila* muscles.

There are few known regulators of neuropeptide release and DCV exocytosis. Most recently the RAB3/RIM pathway was found to be required for fusion of DCVs at the presynaptic terminals of mammalian hippocampal neurons (Persoon et al., 2019). Earlier the cytosolic calcium-activated protein for secretion (CAPS) was identified to be necessary for normal Ca^{2+} dependent release of norepinephrine (NE) by permeabilized PC12 cells (Walent et al., 1992). Interestingly CAPS appears to be specific for release from DCVs since antibody block with anti-CAPS decrease DCV exocytosis but not synaptic vesicle exocytosis in semi-intact, rat brain synaptosomes (Tandon et al., 1998). *In vivo* mutations in CAPS result in defective locomotion, feeding, egg laying and failure to recover from the dauer stage in nematodes (Brenner, 1974; Avery et al., 1993) and an apparent failure to exocytose DCVs by motor boutons in larval

Drosophila (Renden et al., 2001). In flies unlike in mammalian neurons CAPS appears also to regulate release of glutamate from synaptic vesicles as well DCV exocytosis.

In our experiments, deficiencies of *Dmca1D* and *Dstac* decreased neuropeptide release by motor boutons but did not eliminate release. This could be due to incomplete inhibition of Dmca1D and Dstac by the knockdowns and mutations of these genes. Alternatively, it is possible that other CaChs in boutons might contribute to the increase in cytosolic Ca^{2+} necessary for normal release of neuropeptides. Dmca1A, the CaCh required for release of neurotransmitter by boutons (Kawasaki et al., 2000), might participate in neuropeptide release independently of Dstac. Other CaChs found in motor neurons such as the T-type CaCh, DmαG/CaαIT (Ryglewski et al., 2012; Jeong et al., 2015), and TRPV1 (Wong et al., 2014) could also participate in neuropeptide release. In this regard, Stac1, which is expressed by vertebrate neurons, is sufficient for the surface localization of $Ca_V3.2$, a mammalian T-type CaCh, in cultured cells and coimmunoprecipitates with $Ca_V3.2$ (Rzhepetskyy et al., 2016). Finally, how Dstac regulates Dmca1D channels is unknown. It is possible that regulation of Dmca1D by Dstac may be a direct one since Stac3 directly binds the cytoplasmic loop between repeats II and III of $Ca_V1.1$ and $Ca_V1.2$ (Wong King Yuen et al., 2017). Future analysis of neuropeptide release may elucidate answers to these issues.

4.6 AUTHOR CONTRIBUTIONS

Conceptualization, I.H., J.W.L. and J.Y.K.; Methodology, I.H. and J.Y.K.; Formal Analysis, I.H.; Investigation, I.H., J.W.L., X.Z., D.A.B., J.E.V., L.E.R., M.C.L., A.M.O., R.I.H. and A.L.; Resources, R.I.H., H.X., C.A.C., E.S.L. and J.Y.K.; Writing-Original Draft, I.H. and J.Y.K.; Writing-Review &

Editing, I.H., J.W.L., R.I.H., H.X., C.A.C., E.S.L. and J.Y.K.; Supervision, J.Y.K.; Funding Acquisition, E.S.L. and J.Y.K.

4.7 ACKNOWLEDGEMENTS

We thank Dick Nassel (Stockholm University) for sharing anti-proctolin, Christopher Vecsey (Skidmore College) and Carsten Duch (Johannes Gutenberg University of Mainz) for protocols for desheathing the larval CNS, William Yau, Naveen Jasti and Bethany Folk-Middlebrook (University of Michigan) for technical assistance. This project was funded by NIAMS (R01 AR063056) to J.Y.K., NINDS (RO1 NS069844) to C.A.C. and NINDS (RO1 NS032385) to E.S.L. I.H. was supported by a Rackham International Student Fellowship, Rackham Barbour Scholarship, Rackham Predoctoral Fellowship, Rackham Research Grant and Rackham 1-Term Fellowship from the University of Michigan; J.W.L. by a Rackham Merit Fellowship from the University of Michigan and NIGMS (T32 GM007315); M.C.L., A.M.O., L.E.R. and J.E.V. by Summer Research Fellowships from the University of Michigan.

4.8 DECLARATION OF INTERESTS

The authors declare no competing interests.

4.9 REFERENCES

Adams, M.E. and O'Shea, M. (1983). Peptide co-transmitter at a neuromuscular junction. Science *221*, 286-289.

Anderson, M.S., Halpern, M.E., and Keshishian, H. (1988). Identification of the neuropeptide transmitter proctolin in Drosophila larvae: characterization of muscle fiber-specific neuromuscular endings. J Neurosci *8*, 242-255.

Avery, L., Bargmann, C.I., and Horvitz, H.R. (1993). The *Caenorhabditis elegans* unc-31 gene affects multiple nervous system-controlled functions. Genetics *134*, 455–464.

Barclay, J.W., Atwood, H.L., and Robertson, R.M. (2002). Impairment of central pattern generation in Drosophila cysteine string protein mutants. J. Comp. Physiol. A Neuroethol. Sens. Neural Behav. Physiol. *188*, 71-8.

Bellen, H.J., Levis, R.W., Liao, G., He, Y., Carlson, J.W., Tsang, G., Evans-Holm, M., Hiesinger, P.R., Schulze, K.L., Rubin, G.M., Hoskins, R.A., Spradling, A.C. (2004). The BDGP gene disruption project: single transposon insertions associated with 40% of Drosophila genes. Genetics *167*, 761-781.

Berwin, B., Floor, E., and Martin, T.F. (1998). CAPS (mammalian UNC-31) protein localizes to membranes involved in dense-core vesicle exocytosis. Neuron *21*, 137-45.

Bishop, C.A. and O'Shea, M. (1982). Neuropeptide proctolin (H-Arg-Try-Leu-Pro-Thr-OH): immunocytochemical mapping of neurons in the central nervous system of the cockroach. J. Comp. Neurol. *207*, 223-238.

Bishop, C.A., Wine, J.J., Nagy, F., and O'Shea, M.R. (1987). Physiological consequences of a peptide cotransmitter in a crayfish nerve-muscle preparation. J. Neurosci. *7,* 1769-1779.

Block, B.A., Imagawa, T., Campbell, K.P., and Franzini-Armstrong, C. (1988) Structural evidence for direct interaction between the molecular components of the transverse tubule/sarcoplasmic reticulum junction in skeletal muscle. J. Cell Biol. *107*, 2587-2600.

Bondy, C.A., Gainer, H., and Russell, J.T. (1987). Effects of stimulus frequency and potassium channel blockade on the secretion of vasopressin and oxytocin from the neurohypophysis. Neuroendocrinol. *46*, 258-267.

Brenner S. (1974). The genetics of *Caenorhabditis elegan*s. Genetics *77,* 71-94.

Cattaert, D. and Birman, S. (2001) Blockade of the central pattern generator of locomotor rhythm by noncompetitive NMDA receptor antagonists in *Drosophila* larvae. J. Neurobiol. *48*, 58-73.

Cazalis, M., Dayanithi, G., and Nordman, J.J. (1987) Hormone release from isolated nerve endings of the rat neurohypophysis. J. Physiol. *390*, 55-70.

Chen, T.-W., Wardill, T.J., Sun, Y., Pulver, S.R., Renninger, S.L., Baohan, A., Schreiter, E.R., Kerr, R.A., Orger, M.B., Jayaraman, V.*, et al.* (2013). Ultrasensitive fluorescent proteins for imaging neuronal activity. Nature *499*, 295-300.

Collet, C. (2009). Excitation-contraction coupling in skeletal muscle fibers from adult domestic honeybee. Pflugers Arch. *458*, 601-12.

Donaldson, Z.R. and Young, L.J. (2008). Oxytocin, Vasopressin, and the neurogenetics of sociality. Science *322*, 900-904.García, A.G., García-De-Diego, A.M., Gandía, L., Borges, R., and García-Sancho, J. (2006). Calcium signaling and exocytosis in adrenal chromaffin cells. Physiol. Rev. *86*, 1093-1131.

Eberl, D.F., Ren, D., Feng, G., Lorenz, L.J., Van Vactor, D., Hall, L.M. (1998). Genetic and developmental characterization of Dmca1D, a calcium channel alpha1 subunit gene in Drosophila melanogaster. Genetics *148*, 1159-1169.

García, A.G., García-De-Diego, A.M., Gandía, L., Borges, R., and García-Sancho, J. (2006). Calcium signaling and exocytosis in adrenal chromaffin cells. Physiol. Rev. *86*, 1093-1131.

Grabner, M., Dirksen, R.T., Suda, N., and Beam, K.G. (1999) The II-III loop of the skeletal muscle dihydropyridine receptor is responsible for the bi-directional coupling with the ryanodine receptor. J. Biol. Chem. *274*, 21913–21919.

Gratz, S. J., Ukken, F. P., Rubinstein, C. D., Thiede, G., Donohue, L. K., Cummings, A. M. and O'Connor-Giles, K. M. (2014). Highly specific and efficient CRISPR/Cas9-catalyzed homology-directed repair in Drosophila. Genetics *196*, 961-971.

Györke S. and Palade P. (1992). Calcium-induced calcium release in crayfish skeletal muscle. J .Physiol. *457*, 195-210.

Helfrich-Forster, C. (1997). Development of pigment-dispersing hormone-immunoreactive neurons in the nervous system of *Drosophila melanogaster*. J. Comp. Neurol. *380*, 335–54.

Hewes, R.S. and Taghert P.H. (2001). Neuropeptides and neuropeptide receptors in the *Drosophila melanogaste*r genome. Genome Res. *11*, 1126-42.

Hoang, B. and Chiba, A. (2001). Single-cell analysis of *Drosophila* larval neuromuscular synapses. Dev. Biol. *229*, 55-70.

Horstick, E.J., Linsley, J.W., Dowling, J.J., Hauser, M.A.,, McDonald, K.K., Ashley-Koch, A., Saint-Amant, L., Satish, A., Cui, W.C., Zhou, W., Sprague, S.M., Franzini-Armstrong, C., Hirata, H., and Kuwada, J.Y. (2013). Stac3 is a component of the excitation-contraction coupling machinery and mutated in Native American myopathy. Nature Communications *4*, 1952-1952.

Hsu, I-U., Linsley, J.W., Varineau, J., Shafer, O.T. and Kuwada, J.Y. (2018). *Dstac* is required for normal circadian activity rhythms in *Drosophila*. Chronobiology International, 1-11.
Jan LY and Jan YN. (1976) Properties of the larval neuromuscular junction in Drosophila melanogaster. J. Physiol. *262*, 189–214.

Jeong, K., Lee, S., Seo, H., Oh, Y. Jang, D., Choe, J., Kim, D., Lee, J.H., and Jones, W.D. (2015). Ca-α1T, a fly T-type Ca^{2+} channel, negatively modulates sleep. Scientific Reports, 5:17893.

Kadas, D., Klein, A., Krick, N., Worrell, J.W., Ryglewski,S., and Duch, C. (2017). Dendritic and axonal L-type calcium channels cooperate to enhance motoneuron firing output during *Drosophila* larval locomotion. J. Neurosci. *37*, 10971–10982.

Kawasaki, F., Felling, R., and Ordway R.W. (2000). A temperature-sensitive paralytic mutant defines a primary synaptic calcium channel in *Drosophila*. J. Neurosci. *20*, 4885-4889.

Kolarow, R., Brigadski, T. and Lessmann, V. (2007). Postsynaptic secretion of BDNF and NT-3 from hippocampal neurons depends on calcium calmodulin kinase II signaling and proceeds via delayed fusion pore opening. J. Neurosci. *27*, 10350-10364.

Lee, J., Ueda, A., and Wu, C-F. (2014) Distinct roles of *Drosophila cacophony* and *Dmca1D* Ca^{2+} channels in synaptic homeostasis: Genetic interactions with *slowpoke* Ca^{2+}-activated BK channels in presynaptic excitability and postsynaptic response. Dev. Neurobiol. *74*, 1-15

Legha, W., Gaillard, S., Gascon, E., Malapert, P., Hocine, M., Alonso, S., and Moqrich, A. (2010). *stac1* and *stac2* genes define discrete and distinct subsets of dorsal root ganglia neurons. Gene Expr. Patterns *10*, 368–75.

Lein, E.S., Hawrylycz, M.J., Ao, N., Ayres, M., Bensinger, A., Bernard, A., Boe, A.F., Boguski, M.S., Brockway, K.S., Byrnes, E.J., et al. (2007). Genome-wide atlas of gene expression in the adult mouse brain. Nature, *445*, 168–76.

Lemos, J.R. and Nowycky, M.C. (1989). Two types of calcium channels coexist in peptide-releasing vertebrate nerve terminals. Neuron *2*, 1419-1426.

Linsley, J.W., Hsu, I-U., Groom, L., Yarotskyy, V., Lavorato, M., Horstick, E.J., Linsley, D., Wang, W., Franzini-Armstrong, C., Dirksen, R.T., and Kuwada, J.Y. (2017a) Congenital myopathy results from misregulation of a muscle Ca2+ channel by mutant Stac3. Proc. Natl. Acad. Sci. USA *114*, 228-236.

Linsley, J.W., Hsu, I-U., Wang, W., and Kuwada, J.Y. (2017b). Transport of the alpha subunit of the voltage gated L-type calcium channel through the sarcoplasmic reticulum occurs prior to localization to triads and requires the beta subunit but not Stac3 in skeletal muscles. Traffic *18*, 622-632.

Ludwig, M. and Leng, G. (2006). Dendritic peptide release and peptide-dependent behaviours. Nat. Rev. Neurosci. *7*, 126-136.

Maryon, E.B., Saari, B., and Anderson, P. (1998). Muscle-specific functions of ryanodine receptor channels in *Caenorhabditis elegans*. J. Cell Sci. *111*, 2885-95.

McLachlan, E.M. and Martin, A.R. (1981). Non-linear summation of end-plate potentials in the frog and mouse. J. Physiol. *311*, 307–24

Mishra, B., Ghannad-Rezaie, M., Li, J., Wang, X., Ye, B., Chronis, N., Collins, C.A. (2014). Using microfluidics devices for live imaging and study of injury responses in *Drosophila* larvae. J. Vis. Exp. *84*, e50998.

Morris, J.F. and Pow, D.V. (1991). Widespread release of peptides in the central nervous system: quantitation of tannic acid-captured exocytoses. Anat. Rec. *231*, 437-45.

Muschol, M. and Salzberg, B.M. (2000). Dependence of transient and residual calcium dynamics on action p-potential patterning during neuropeptide secretion. J. Neurosci. *20*, 6773-6780.

Nakai, J., Dirksen, R.T., Nguyen, H.T., Pessah, I.N., Beam, K.G., and Allen, P.D. (1996) Enhanced dihydropyridine receptor channel activity in the presence of ryanodine receptor. Nature *380*, 72–75.

Nässel, D.R. and Zandawala, M. (2019). Recent advances in neuropeptide signaling in Drosophila, from genes to physiology and behavior. Prog. Neurobiol. *179*, 101607.

Nelson, B.R., Wu, .F, Liu, Y., Anderson, D.M., McAnally, J., Lin, W., Cannon, S.C., Bassel-Duby, R., Olson, E.N. (2013). Skeletal muscle-specific T-tubule protein STAC3 mediates voltage induced Ca^{2+} release and contractility. Proc. Natl. Acad. Sci. USA *110*, 11881-11886.

Omerod, K.G., LePine, O.K., Bhutta, M.S. Jung, J., Tattersall, G.J., and Mercier, A.J. (2016). Characterizing the physiological and behavioral roles of proctolin in Drosophila melanogaster. J Neurophysiol. *115*, 568-580.

Paolini, C., Fessenden, J.D., Pessah, I.N., and Franzini-Armstrong C. (2004). Evidence for conformational coupling between two calcium channels. PNAS *101*, 12748-12752.

Peng, I.F. and Wu, C.F. (2007) Drosophila cacophony channels: a major mediator of neuronal Ca2+ currents and a trigger for K+ channel homeostatic regulation. J Neurosci 27: 1072–1081, 2007.

Perney, T.M., Hirning, H.D., Leeman, S.E., and Miller, R.J. (1986). Multiple calcium channels mediate neurotransmitter release from peripheral neurons. Proc. Natl. Acad. Sci. *83*, 6656-6659.

Persoon, C.M., Hoogstraaten, R.I., Nassal, J.P., van Weering, J.R.T., Kaeser, P.S., Toonen, R.F., and Verhage, M. (2019). The RAB3-RIM pathway Is essential for the release of neuromodulators. Neuron *104*, 1065-1080.

Pfeiffer, B.D., Ngo, T.T., Hibbard, K.L., Murphy, C., Jenett, A., Truman, J.W., and Rubin, G.M. (2010). Refinement of tools for targeted gene expression in Drosophila. Genetics. *186*, 735-755.

Rane, S.G., Holz IV, G.G., and Dunlap, K. (1987). Dihydropyridine inhibition of neuronal calcium current and substance P release. Pflugers Arch. *409*, 361-366.

Ren, D., Xu, H., Eberl, D.F., Chopra, M., and Hall, L.M. (1998). A mutation affecting dihydropyridine-sensitive current levels and activation kinetics in Drosophila muscle and mammalian heart calcium channels. J. Neurosci. *18*, 2335-2341.

Renden, R., Berwin, B., Davis, W., Ann, K., Chin, C.T., Kreber, R., Ganetzky, B., Martin, T.F., and Broadie, K. (2001). Drosophila CAPS is an essential gene that regulates dense-core vesicle release and synaptic vesicle fusion. Neuron *31*, 421-37.

Renn, S.C.P., Park, J.H., Rosbash, M., Hall, J.C., and Taghert, P.H. (1999). A pdf neuropeptide gene mutation and ablation of PDF neurons each cause severe abnormalities of behavioral circadian rhythms in *Drosophila*. Cell *99*, 791–802.

Rios, E. and Brum, G. (1987). Involvement of dihydropyridine receptors in excitation-contraction coupling in skeletal muscle. Nature *325*, 717-720.

Ryglewski, S., Lance, K. Levine, R.B., and Duch, C. (2012). Ca_V2 channels mediate low and high voltage activated calcium currents in *Drosophila* motoneurons. J. Physiol. *590.4*, 809-825.

Rzhepetskyy, Y., Lazniewska, J., Proft, J., Campiglio, M., Flucher, B.E., and Weiss, N. (2016). A $Ca_V3.2$/Stac1 molecular complex controls T-type channels at the plasma membrane. Channels *10*, 346-354.

Port, F., Chen, H.M., Lee, T., and Bullock, S.L. (2014). Optimized CRISPR/Cas tools for efficient germline and somatic genome engineering in *Drosophila*. Proc Natl Acad Sci U S A *111*, E2967-2976

Sasaki, N., Dayanithi, G., and Shibuya, I. (2005). Ca^{2+} clearance mechanisms in neurohypohysial terminals of the rat. Cell Calcium *37*, 45-56.

Schneider, M.F. and Chandler, W.K. (1973). Voltage dependent charge movement of skeletal muscle: a possible step in excitation-contraction coupling. Nature *242*, 244-246.

Shafer, O.T., and Taghert, P.H. (2009). RNA-interference knockdown of Drosophila pigment dispersing factor in neuronal subsets: the anatomical basis of a neuropeptide's circadian functions. PLoS ONE *4*, e8298.

Shakiryanova, D., Tully, A., Hewes, R.S., Dietcher, D.L., and Levitan, E.S. (2005) Activity-dependent liberation of synaptic neuropeptide vesicles. Nature Neurosci. *8*, 173-178.

Shakiryanova, D., Klose, M.K., Zhou, Y., Gu, T., Deitcher, D.L., Atwood, H.L., Hewes, R.S., and Levitan, E.S. (2007). Presynaptic ryanodine receptor-activated calmodulin kinase II increases vesicle mobility and potentiates neuropeptide release. J Neurosc *27*, 7799-7806.

Simmons, M. L., Terman, G. W., Gibbs, S. M. and Chavkin, C. (1995). L-type calcium channels mediate dynorphin neuropeptide release from dendrites but not axons of hippocampal granule cells. Neuron *14*, 1265-1272.

Sobota, J.A., Mohler, W.A., Cowan, A.E., Eipper, B.A., and Mains, R.E. (2010). Dynamics of peptidergic secretory granule transport are regulated by neuronal stimulation. BMC Neurosci. *11*, 32.

Stewart, B.A., Atwood, H.L., Renger, J.J., Wang, J. and Wu, C.F. (1994) Improved stability of Drosophila larval neuromuscular preparations in haemolymph-like physiological solutions. J. Comp. Physiol. A *175*, 179–191.

Sullivan, K.M., Scott, K., Zuker, C.S., and Rubin, G.M. (2000). The ryanodine receptor is essential for larval development in *Drosophila melanogaster*. Proc. Natl. Acad. Sci. USA *23*, 5942-5947.

Summerville, J.B., Faust, J.F., Fan, E., Pendin, D., Daga, A., Formella, J., Stern, M., and McNew, J.A. (2016). The effects of ER morphology on synaptic structure and function in Drosophila melanogaster. J. Cell Sci. *129*, 1635-1648.

Suzuki, H., Kawai, J., Taga, C., Yaoi, T., Hara, A., Hirose, K., Hayashizaki, Y., and Watanabe, S. (1996). Stac, a novel neuron-specific protein with cysteine-rich and SH3 domains. Biochem. Biophys. Res. Comm. *229*, 902-909.

Takekura, H. and Franzini-Armstrong, C. (2002). The structure of Ca(2+) release units in arthropod body muscle indicates an indirect mechanism for excitation-contraction coupling. Biophys J. *83*, 2742-53.

Takizawa, E., Komatsu, A., and Tsujimura, H. (2007). Identification of common excitatory motoneurons in *Drosophila melanogaster* larvae. Zool. Sci. *24*, 504-513

Tandon, A., Bannykh, S., Kowalchyk, J.A., Banerjee, A., Martin T.F., and Balch, W.E. (1998). Differential regulation of exocytosis by calcium and CAPS in semi-intact synaptosomes. Neuron *21*, 147-54.

Taylor, C.A.M., Winther, A.M.E., Siviter, R.J., Shirras, A.D., Isaac, R.E., and Nassel, D.R. (2004) Identification of proctolin preprohormone gene (proct) of Drosophila melanogaster: expression and predicted prohormone processing. J. Neurobiol. *58*, 379-391.

Tse, F.W. and Tse, A. (1999) Regulation of exocytosis via release of Ca^{2+} from intracellular stores. Bioassays *21*, 861-865.

van den Pol, A.N. (2012) Neuropeptide transmission in brain circuits., Neuron *76*, 98-115

Venken, K.J., Schulze, K.L., Haelterman, N.A., Pan, H., He, Y., Evans-Holm, M., Carlson, J.W., Levis, R.W., Spradling, A.C., Hoskins, R.A., and Bellen, H.J. (2011). MiMIC: a highly versatile transposon insertion resource for engineering Drosophila melanogaster genes. Nature Methods *8*, 737-743.

Walent, J.H., Porter, B.W., and Martin, T.F. (1992). A novel 145 kd brain cytosolic protein reconstitutes Ca(2+)-regulated secretion in permeable neuroendocrine cells. Cell *70,* 765-75.

Wang, X., Treistman, S.N., Wilson, A., Nordmann, J.J., and Lemos, J.R. (1993) Ca^{2+} channels and peptide release from neurosecretory terminals. J. Neurophysiol. *70*, 64-68.

Wasle, B. and Edwardson, J.M. (2002). The regulation of exocytosis in the pancreatic acinar cell. Cell Signal *14*, 191-197.

Wodarz, A., Hinz, U., Engelbert, M., and Knust, E. (1995) Expression of Crumbs confers apical character on plasma membrane domains of ectodermal epithelia of Drosophila. Cell *82*, 67-76.

Wong, C., Chen, K., Lin, Y.Q., Chao, Y., Duraine, L., Lu, Z., Yoon, W.H., Sullivan, J.M., Broadhead, G.T., Sumner, C.J., Lloyd, T.E., Macleod, G.T., Bellen, H.J., and Venkatachalam, K. (2014). A TRPV channel in Drosophila motor neurons regulates presynaptic resting Ca^{2+} levels, synapse growth, and synaptic transmission. Neuron *84*, 764-777.

Wong, M.Y., Zhou, C., Shakiryanova, D., Lloyd, T.E., Deitcher, D.L., and Levitan, E.S. (2012). Neuropeptide delivery to synapses by long-range vesicle circulation and sporadic capture. Cell *148*, 1029-1038.

Wong, M.Y., Cavolo, S.L., and Levitan, E.S. (2015) Synaptic neuropeptide release by dynamin dependent partial release from circulating vesicles. Mol. Bio. Cell *26*, 2466-74.

Wong King Yuen, S.M., Campiglio, M., Tung, C.C., Flucher, B.E., and Van Petegem, F. (2017). Structural insights into binding of STAC proteins to voltage-gated calcium channels. Proceedings of the National Academy of Sciences *114*, E9520-E9528.

Worrell, J.W. and Levine, R.B. (2008). Characterization of voltage-dependent Ca2+ currents in identified *Drosophila* motoneurons in situ. J. Neurophysiol. *100*, 868-878.

Xia, X., Lessmann, V., and Martin, T.F. (2009). Imaging of evoked dense-core-vesicle exocytosis in hippocampal neurons reveals long latencies and kiss-and-run fusion events., J. Cell. Sci. *122*, 75-82.

Zheng, W., Feng, G., Ren, D., Hannan, F.L., Eberl, D.F., et al. (1995). Cloning and characterization of a calcium channel a1 subunit from *Drosophila melanogaster* with similarity to the rat brain type D isoform. J. Neurosci., *15*, 1132–1143.

CHAPTER 5. Conclusions and Future Directions

This dissertation research uncovered the role of a novel gene, *Dstac*, in the *Drosophila* CNS and muscles. The demonstration that Dstac regulates the release of neuropeptides by neurons via regulation of Dmca1D, the *Drosophila* L-type Ca_v channel advanced our understanding of the mechanism by which neurons release neuropeptide. Since Stac proteins are found in both invertebrates and vertebrates as are neuropeptides, the regulation of neuropeptide release by Stac proteins may be one applicable to many different organisms. Furthermore, since neuropeptides are involved in complex brain circuits underlying psychological states and behaviors and are associated with brain diseases such as epilepsy (van den Pol, 2012), the identification of Stac proteins as regulators of neuropeptide release might lead to a better understanding of neuropeptide associated brain disorders. In this chapter, I will summarize the results from my studies and describe possible future directions.

5.1 Summary

5.1.1 Dstac regulates EC coupling of *Drosophila* body-wall muscles.

In Chapter 2, I showed that Dstac regulates EC coupling of *Drosophila* larval body-wall muscles as Stac3 does in vertebrate skeletal muscles. My Ca^{2+} imaging experiments performed

in live, intact *Drosophila* larvae showed that during normal locomotion, there are Ca^{2+} transients in body-wall muscles dependent on Dstac and Dmca1D. In zebrafish Stac3 regulates the expression levels of $Ca_v1.1$ in the T tubule portion of the triadic junctions of T tubules and SR by regulating the stability of $Ca_v1.1$ (Linsley et al., 2017a; Linsley et al., 2017b). Similarly, my experiments showed that *Dstac* regulates the expression levels of *Drosophila* L-type Ca_v channel, Dmca1D, at T tubules. By analogy to Stac3, Dstac might regulate the expression level of Dmca1D by regulating the stability of Dmca1D. Live imaging of Dmca1D fused with a photoconvertible protein in wt and *Dstac* mutant muscles in future experiments will test whether the decrease in Dmca1D in *Dstac* mutants is due to a decrease in Dmca1D stability. Since invertebrate muscles may involve CICR during EC coupling (Collet, 2009; Györke and Palade, 1992; Takekura and Franzini-Armstrong, 2002), the results in larval muscles suggest the possibility that Dstac regulates Ca^{2+} influx through Dmca1D channels which induces CICR during EC coupling of *Drosophila* body-wall muscles.

5.1.2 Dstac is required for normal circadian rhythm.

Studies described in Chapter 3 provided the first evidence for the function of Stac proteins in neurons. Dstac was found to be expressed by subsets of neurons, including the s-LN_v and l-LN_v neurons of the adult *Drosophila* brain. These neurons were thought to release the neuropeptide, PDF, to regulate circadian rhythms in adult flies (Shafer and Taghert, 2009). Interestingly, the s-LN_v and l-LN_v neurons expressed the L-type Ca_v channel, Dmca1D, in addition to Dstac and PDF. In fact knocking down Dstac specifically in these neurons resulted in

defective circadian rhythm. These finding suggested the hypothesis that Dstac might regulate Dmca1D in the s-LN_v and l-LN_v neurons to regulate release of PDF and thereby circadian activity. However, PDF neurons are small and deep in the *Drosophila* brain making them difficult to access. Therefore, we decided to move to the more easily accessible system of *Drosophila* larval NMJ to examine a potential role for Dstac and Dmca1D for the release of neuropeptides.

5.1.3 Dstac regulates release of neuropeptides.

Experiments in Chapter 4 demonstrated that *Dstac* regulated Ca^{2+} influx through the Dmca1D channels and the subsequent release of neuropeptides by the motor boutons at the larval neuromuscular junction. Using antibodies against Dstac and Dmca1D that I generated, I showed that Dstac and Dmca1D are present in motor boutons that release the proctolin neuropeptide which was found to enhance muscle contractions (Ormerod et al., 2016). The latter predicted that deficiencies in Dstac, Dmca1D and proctolin in the motor boutons should all decrease locomotion. Indeed, this was borne out showing that Dstac, Dmca1D and proctolin are all necessary for normal locomotion. Since a long lasting increase in Ca^{2+} in boutons was required for the release of neuropeptides, I then examined activity dependent Ca^{2+} transients in motor boutons by Ca^{2+} imaging of live, intact larvae. This showed that both Dstac and Dmca1D were required for normal Ca^{2+} transients in the motor boutons. To examine whether Dstac might regulate Dmca1D channels, voltage-clamp analysis of motor neurons was performed. These experiments showed that Dstac regulates the voltage response of Dmca1D channels in motor neurons. Finally, the role of Dstac and Dmca1D for the release of neuropeptides was

assayed directly by live imaging of motor boutons expressing a GFP fusion and *Drosophila* Dilp2 neuropeptide. These experiments demonstrated that both Dstac and Dmca1D regulated neuropeptide release. Thus the experimental results shown in Chapter 4 established that Dstac regulates the voltage dependent influx of Ca^{2+} through Dmca1D channels, which in turn initiates the release of neuropeptides.

5.2 Future directions and experiments

5.2.1 Does Dstac regulate Ca^{2+} influx via Dmca1D in *Drosophila* body-wall muscles?

Voltage-clamp of *Drosophila* motor neurons demonstrated that Dstac regulates Ca^{2+} influx via the L-type Ca_v channel, Dmca1D. However, it's unknown whether Dstac also regulates Ca^{2+} influx via Dmca1D in *Drosophila* body-wall muscles. Both the L- and T-type Ca^{2+} currents are present in *Drosophila* larval body-wall muscles (Gielow et al., 1995). Blocking T-type Ca^{2+} currents with amiloride or genetically, or voltage-clamping the muscles above -30 mV can isolate the L-type Ca^{2+} currents since at these voltages T-type channels are inactivated. This would allow one to test whether Dstac regulates Dmca1D in larval muscles. Furthermore, it may be possible to block Dmca1D either pharmacologically or genetically to assay whether T-type Ca^{2+} channels are regulated by Dstac. Since *Dmca1D* nulls are larval lethals (Eberl et al., 1998), experiments using *Dmca1D* nulls may be doable in embryos. In addition to these experiments, it may be possible to assay T currents since they are activated at low voltages compared with Dmca1D currents which are activated at high voltages.

5.2.2 Does Ca^{2+} influx via Dmca1D regulate CICR in *Drosophila* body-wall muscles?

Genetically or pharmacologically inhibiting RyR or SERCA diminished *Drosophila* body-wall muscle contraction, demonstrating that Ca^{2+} release from SR is crucial for muscle contraction (Sanyal et al., 2005; Sullivan et al., 2000). My Ca^{2+} imaging of body-wall muscles of larvae in which *Dmca1D* was knocked down showed that normal Ca^{2+} transients mediating muscle contractions require Dmca1D. This suggests that the Ca^{2+} currents passed by Dmca1D are required for inducing Ca^{2+} release from SR to activate muscle contraction.

Concurrent recording of cytosolic Ca^{2+} transients and *Dmca1D* Ca^{2+} currents by imaging and electrophysiology would allow direct measurements of intracellular Ca^{2+} increase in response to *Dmca1D* Ca^{2+} influx. Using this method, if the Dmca1D dependent Ca^{2+} transients involve CICR in *Drosophila* body-wall muscles, inhibiting SR Ca^{2+} store should lead to a decrease in cytosolic Ca^{2+} transients while not affecting Dmca1D Ca^{2+} current amplitude recorded by electrophysiology. The results of these experiments might test whether Ca^{2+} via Dmca1D can by itself lead to muscle contraction and parse out the relative importance of CICR for muscle contraction.

5.2.3 Does CICR at motor neuron boutons locally initiate release of neuropeptides?

Previous experiments using pharmacological manipulations suggest that DCV mobilization requires CICR to potentiate neuropeptide release by *Drosophila* motor boutons (Shakiryanova et al., 2007). In this dissertation I found that the L-type Dmca1D channels in motor boutons were necessary for normal neuropeptide release. Thus I hypothesize that Ca^{2+}

influx via Dmca1D channels initiates CICR. In order to directly test the requirement of CICR for DCV exocytosis, we need to examine release of Ca^{2+} from the ER during neuropeptide release. In principle this could be done by concurrent measurements of ER luminal Ca^{2+} using fluorescence Ca^{2+} indicators tethered in the ER lumen (de Juan-Sanz et al., 2017; Solovyova et al., 2002; Suzuki et al., 2014) and DCV exocytosis using reporters for DCV exocytosis such as pHluorin tagged neuropeptide Y (NPY- pHluorin) (Zhu et al., 2007). One could do the experiment in boutons of live, intact larvae to see whether under normal conditions DCV exocytosis requires CICR. Furthermore, one could do the experiment with release of Ca^{2+} from the ER inhibited by RyR blockers such as dantrolene or high concentrations of ryanodine in order to see if CICR is required for neuropeptide release. Oppositely, one could activate ER Ca^{2+} release by RyR agonists such as caffeine or low concentrations of ryanodine and test if this triggers neuropeptide release. Alternatively, the heat inducible *SERCA* mutant fly strain would be useful in temporal control of ER Ca^{2+} store inhibition.

5.2.4 Does Dstac regulate neuropeptide release by other neurons?

There are 50 neuropeptides in the *Drosophila* genome (Nassel and Zandawala, 2019). I found that Dstac regulates the release of proctolin by motor boutons and since *Dstac* is expressed by other neurons in the CNS it is possible Dstac in these neurons may also be responsible for the release of other neuropeptides. One neuropeptide that probably is not regulated by Dstac is tachykinin which is required for aggression in male *Drosophila* (Asahina et al., 2014) since Dstac appears not to be expressed by the tachykinin+ neurons in the brain

(unpublished). Labeling the *Drosophila* brain of *Dstac-gfp* trap flies with anti-tachykinin found no co-labeling. However, another neuropeptide, sNPF, is an intriguing possible target for Dstac (unpublished). The DP cell is a prominent neuron in the ventral ganglia of *Drosophila* that express sNPF (Hu et al., 2017). The release of sNPF by the DP neurons mediates responses of larvae to painful mechanical stimuli. Interestingly the DP neurons appear to express *Dstac* suggesting that Dstac may regulate the release of sNPF by DP neurons as well as proctolin by motor neurons. This can be tested using methods similar to ones employed to demonstrate Dstac regulation of proctolin release.

5.2.5 Are the Stac proteins present in all peptidergic neurons?

As mentioned above, currently around 50 neuropeptides in *Drosophila melanogaster* and over a hundred neuropeptides in mammals haven been identified (Nassel and Zandawala, 2019). Recent single-cell transcriptomic sequencing of mouse neocortical neurons showed that every mouse neocortical neuron expresses at least one or multiple neuropeptides and neuropeptide receptors and thus form highly complex modulatory circuits (Smith et al., 2019). As mentioned above, it appears that not all peptidergic neurons are Dstac positive. This suggests that Dstac might regulate neuropeptide release by a certain type of neuropeptide neuron. Since my experiments showed that Dstac regulates Ca^{2+} influx via Dmca1D and therefore Ca^{2+} transients within motor boutons to regulate neuropeptide release, it's likely that Dstac is expressed in the Dmca1D positive neuropeptide neurons that require certain levels and durations of cytosolic Ca^{2+} increase for DCV exocytosis. However, it's again unclear whether all

neuropeptide neurons express the L-type Ca_v channel, Dmca1D, and whether all Dmca1D positive neurons express Dstac. Single-cell transcriptomic data (Smith et al., 2019; Tasic et al., 2016; Tasic et al., 2018) would help provide primary insights on associating the expression of the *stac* genes and L-type Ca_v channels with certain types of neuropeptide neurons.

5.3 References

Asahina, K., Watanabe, K., Duistermars, B.J., Hoopfer, E., González, C.R., Eyjólfsdóttir, E.A., Perona, P., and Anderson, D.J. (2014). Tachykinin-expressing neurons control male-specific aggressive arousal in Drosophila. Cell 156, 221-235.

Collet, C. (2009). Excitation-contraction coupling in skeletal muscle fibers from adult domestic honeybee. Pflugers Arch 458, 601-612.

de Juan-Sanz, J., Holt, G.T., Schreiter, E.R., de Juan, F., Kim, D.S., and Ryan, T.A. (2017). Axonal Endoplasmic Reticulum Ca(2+) Content Controls Release Probability in CNS Nerve Terminals. Neuron 93, 867-881.e866.

Eberl, D.F., Ren, D., Feng, G., Lorenz, L.J., Van Vactor, D., and Hall, L.M. (1998). Genetic and developmental characterization of Dmca1D, a calcium channel α1 subunit gene in Drosophila melanogaster. Genetics 148, 1159-1169.

Gielow, M., Gu, G., and Singh, S. (1995). Resolution and pharmacological analysis of the voltage-dependent calcium channels of Drosophila larval muscles. The Journal of Neuroscience 15, 6085-6093.

Györke, S., and Palade, P. (1992). Calcium-induced calcium release in crayfish skeletal muscle. J Physiol 457, 195-210.

Hu, C., Petersen, M., Hoyer, N., Spitzweck, B., Tenedini, F., Wang, D., Gruschka, A., Burchardt, L.S., Szpotowicz, E., Schweizer, M.*, et al.* (2017). Sensory integration and neuromodulatory feedback facilitate Drosophila mechanonociceptive behavior. Nature neuroscience 20, 1085-1095.

Linsley, J.W., Hsu, I.U., Groom, L., Yarotskyy, V., Lavorato, M., Horstick, E.J., Linsley, D., Wang, W., Franzini-Armstrong, C., Dirksen, R.T., and Kuwada, J.Y. (2017a). Congenital myopathy results

from misregulation of a muscle Ca2+ channel by mutant Stac3. Proc Natl Acad Sci U S A 114, E228-E236.

Linsley, J.W., Hsu, I.U., Wang, W., and Kuwada, J.Y. (2017b). Transport of the alpha subunit of the voltage gated L-type calcium channel through the sarcoplasmic reticulum occurs prior to localization to triads and requires the beta subunit but not Stac3 in skeletal muscles. Traffic (Copenhagen, Denmark) 18, 622-632.

Nassel, D.R., and Zandawala, M. (2019). Recent advances in neuropeptide signaling in Drosophila, from genes to physiology and behavior. Prog Neurobiol 179, 101607.

Ormerod, K.G., LePine, O.K., Bhutta, M.S., Jung, J., Tattersall, G.J., and Mercier, A.J. (2016). Characterizing the physiological and behavioral roles of proctolin in Drosophila melanogaster. Journal of Neurophysiology 115, 568-580.

Sanyal, S., Consoulas, C., Kuromi, H., Basole, A., Mukai, L., Kidokoro, Y., Krishnan, K.S., and Ramaswami, M. (2005). Analysis of Conditional Paralytic Mutants in Drosophila Sarco-Endoplasmic Reticulum Calcium ATPase Reveals Novel Mechanisms for Regulating Membrane Excitability. Genetics 169, 737-750.

Shafer, O.T., and Taghert, P.H. (2009). RNA-interference knockdown of Drosophila pigment dispersing factor in neuronal subsets: the anatomical basis of a neuropeptide's circadian functions. PLoS One 4, e8298.

Shakiryanova, D., Klose, M.K., Zhou, Y., Gu, T., Deitcher, D.L., Atwood, H.L., Hewes, R.S., and Levitan, E.S. (2007). Presynaptic ryanodine receptor-activated calmodulin kinase II increases vesicle mobility and potentiates neuropeptide release. Journal of Neuroscience 27, 7799-7806.

Smith, S.J., Sümbül, U., Graybuck, L.T., Collman, F., Seshamani, S., Gala, R., Gliko, O., Elabbady, L., Miller, J.A., Bakken, T.E.*, et al.* (2019). Single-cell transcriptomic evidence for dense intracortical neuropeptide networks. eLife 8, e47889.

Solovyova, N., Veselovsky, N., Toescu, E.C., and Verkhratsky, A. (2002). Ca(2+) dynamics in the lumen of the endoplasmic reticulum in sensory neurons: direct visualization of Ca(2+)-induced Ca(2+) release triggered by physiological Ca(2+) entry. The EMBO journal 21, 622-630.

Sullivan, K.M., Scott, K., Zuker, C.S., and Rubin, G.M. (2000). The ryanodine receptor is essential for larval development in Drosophila melanogaster. Proceedings of the National Academy of Sciences of the United States of America 97, 5942-5947.

Suzuki, J., Kanemaru, K., Ishii, K., Ohkura, M., Okubo, Y., and Iino, M. (2014). Imaging intraorganellar Ca2+ at subcellular resolution using CEPIA. Nature Communications 5, 4153.

Takekura, H., and Franzini-Armstrong, C. (2002). The structure of Ca(2+) release units in arthropod body muscle indicates an indirect mechanism for excitation-contraction coupling. Biophys J 83, 2742-2753.

Tasic, B., Menon, V., Nguyen, T.N., Kim, T.K., Jarsky, T., Yao, Z., Levi, B., Gray, L.T., Sorensen, S.A., Dolbeare, T.*, et al.* (2016). Adult mouse cortical cell taxonomy revealed by single cell transcriptomics. Nature Neuroscience 19, 335-346.

Tasic, B., Yao, Z., Graybuck, L.T., Smith, K.A., Nguyen, T.N., Bertagnolli, D., Goldy, J., Garren, E., Economo, M.N., Viswanathan, S.*, et al.* (2018). Shared and distinct transcriptomic cell types across neocortical areas. Nature 563, 72-78.

van den Pol, A. (2012). Neuropeptide Transmission in Brain Circuits. Neuron 76, 98-115.

Zhu, D., Zhou, W., Liang, T., Yang, F., Zhang, R.-Y., Wu, Z.-X., and Xu, T. (2007). Synaptotagmin I and IX function redundantly in controlling fusion pore of large dense core vesicles. Biochemical and Biophysical Research Communications 361, 922-927.

APPENDICES

APPENDIX 1

Appendix 1 describes my experiments contributing to the 1st collaboration work with Dr. Jeremy Linsley in the Kuwada lab that was published in 2017 as "Linsley, J.W., Hsu, I.U., Groom, L., Yarotskyy, V., Lavorato, M., Horstick, E.J., Linsley, D., Wang, W., Franzini-Armstrong, C., Dirksen, R.T., and Kuwada, J.Y. (2017). Congenital myopathy results from misregulation of a muscle Ca^{2+} channel by mutant Stac3. Proc Natl Acad Sci U S A 114, E228-E236. https://doi.org/10.1073/pnas.1619238114". The work of this paper characterized the mechanisms by which Stac3 regulates $Ca_v1.1$ during EC coupling of vertebrate skeletal muscles.

APPENDIX 1.1 Quantitative immunofluorescence imaging showed that Stac3 is required for normal $Ca_v1.1$ expression at the T tubules of skeletal muscles.

In order to examine the levels of RyR and $Ca_v1.1$ at the triadic junctions of wt and *stac3-/-* zebrafish skeletal muscles, I performed quantitative immunolabeling of dissociated wt and *stac3-/-* zebrafish skeletal muscles with antibodies against RyR and $Ca_v1.1$. I found that the levels of RyR at junctional SR of wt and *stac3-/-* zebrafish skeletal muscles are comparable (Appendix Figure 1.1A-B). However, the level of $Ca_v1.1$ at T tubules of *stac3-/-* zebrafish skeletal muscles was decreased compared with that of wt (Appendix Figure 1.1C-D). The decrease in $Ca_v1.1$ expression at the plasma membrane of T tubules of *stac3-/-* skeletal muscles was confirmed by immunolabeling with an antibody recognizing an extracellular epitope of $Ca_v1.1$ (Appendix Figure 1.1E-F). These results suggest that Stac3 is necessary for normal $Ca_v1.1$

expression level at the plasma membrane within the triads, but not required for normal RyR expression level at the junctional SR.

APPENDIX 1.2 Embryos expressing *stac3NAM* exhibit decreased swimming.

Experiments performed by Jeremy and others of this work showed that *stac3NAM*-expressing myofibers are able to release a low level of Ca^{2+} in response to voltage-clamp depolarization and electrical stimulation. This predicts that muscle *actin:stac3NAM-EGFP; stac3−/−* transgenic embryos should exhibit more mobility than *stac3−/−* embryos. I performed motility assays of wt, wt rescued (muscle *actin:stac3WT-EGFP; stac3−/−)*, *stac3NAM* rescued (muscle *actin:stac3NAM-EGFP; stac3−/−*) and *stac3-/-* zebrafish embryos at 56 hpf (hours post fertilization), 72 hpf, and 96 hpf. At all stages tested, *muscle actin:stac3NAM* transgenic embryos were significantly more motile than *stac3−/−* embryos but less motile than *stac3−/−* embryos expressing muscle *actin:stac3WT* (Appendix Figure 1.2A-B). This suggests that the stable and consistent expression of *stac3NAM* within transgenic fish used in this study is likely sufficient for the low-level swimming observed in these fish despite low-level Ca^{2+} transients observed in *stac3NAM* muscle fibers. These results showed that transgenic expression of *stac3NAM* in stac3-/- skeletal muscles partially rescued the motility of *stac3-/-* zebrafish embryos.

Appendix Figure 1.1

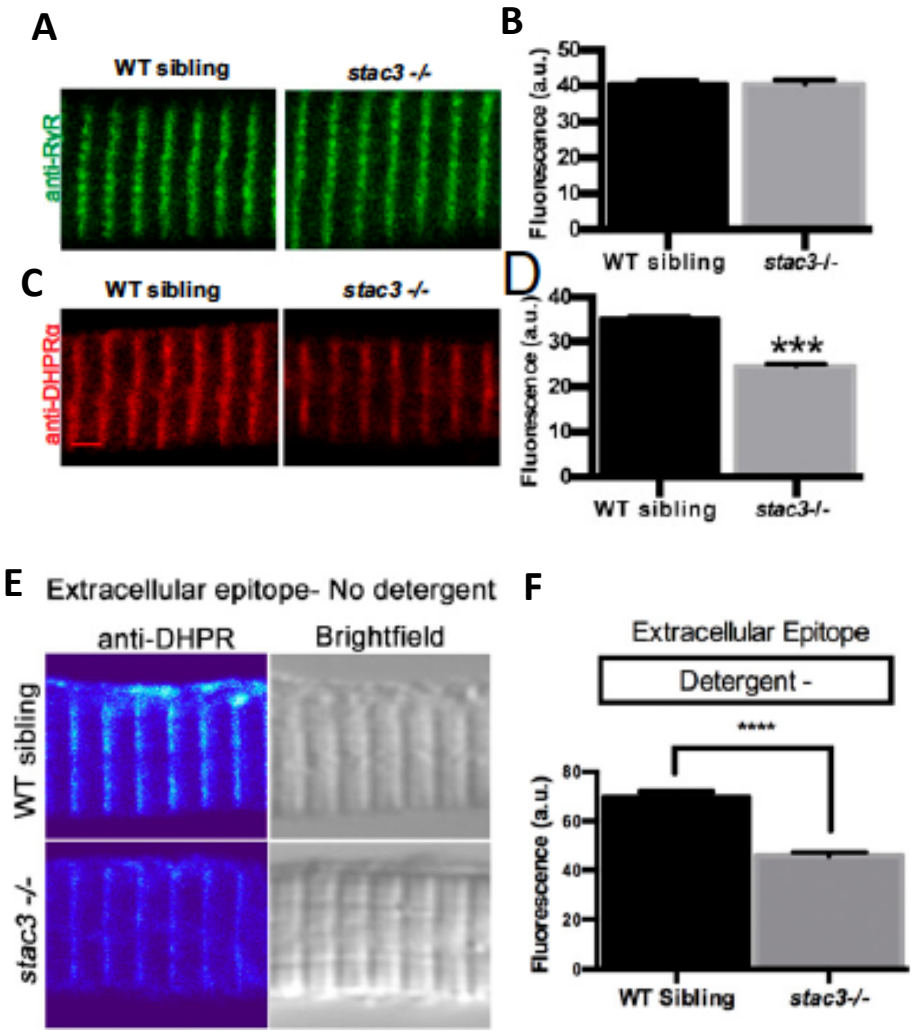

Appendix Figure 1.1 DHPRα1 but not RyR1 is reduced in T-tubule striations of stac3 mutants. (A) Immunofluorescence labeling of WT sibling and *stac3−/−* disassociated myotubes with anti-pan RyR (34c). (B) Mean immunofluorescence intensity of anti-RyR in *stac3−/−* compared with WT siblings showing no difference in triadic RyR (t test, P = 0.89, n = 85 WT sibling, n = 50 *stac3−/−*). a.u., arbitrary units. (C) Immunofluorescence labeling of WT sibling and *stac3−/−* disassociated myotubes with mAb1 1A against a cytoplasmic region of DHPRα1S (15). (D) Mean mAb1 1A labeling in WT siblings and *stac3−/−* showing a decrease in triadic DHPRα1S (t test, ***P < 0.0001, n = 216WT sibling, n = 264 *stac3−/−*). (E) Immunofluorescence (Left) and bright-field images (Right) of WT sibling and *stac3−/−* disassociated myotubes labeled without detergent with anti-DHPRα1S that recognizes an extracellular epitope. (F) Histogram showing that there is a decrease in T-tubule triadic DHPRα1S in *stac3−/−* dissociated myotubes (n = 160 WT sibling, n = 125 *stac3−/−*, t test, ****P < 0.0001).

Appendix Figure 1.2

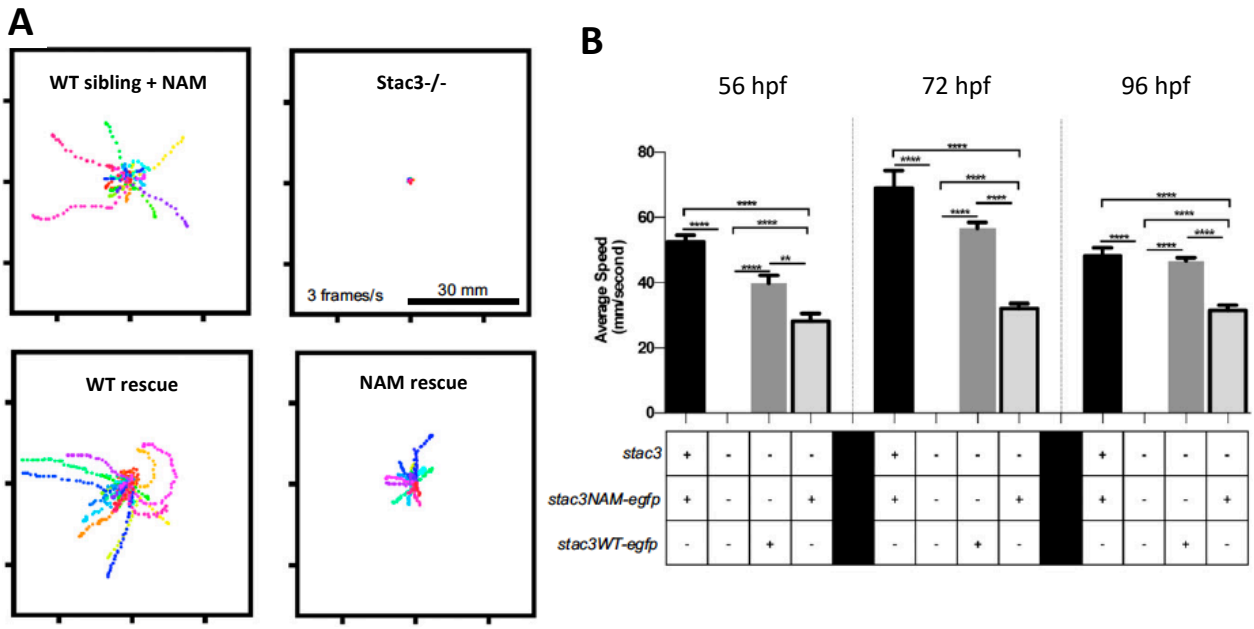

Appendix Figure 1.2 Stac3NAM transgenic zebrafish have reduced motility.
(A) Overlaid traces of touch-evoked swimming by transgenic 72-hpf WT siblings expressing *stac3NAM-EGFP* (WT sibling + NAM), *stac3−/−*, *transgenic stac3−/−;stac3WT-EGFP* (WT rescue), *transgenic stac3−/−;stac3NAM-EGFP* (NAM rescue), and *stac3−/−* showing that whereas *stac3−/−* embryos do not swim, NAM rescue embryos do. (B) Histograms of the speed of swimming by WT sibling + NAM (n = 55, 11, and 32 at 56, 72, and 96 hpf, respectively), *stac3−/−* (n = 15, 15, and 15), WT rescue (n = 8, 20, and 91), and NAM rescue (n = 18, 55, and 58) show that NAM rescue zebrafish exhibit partial rescue of swimming compared with WT rescue (ANOVA Tukey multiple comparisons, ****P < 0.0001, **P < 0.001).

APPENDIX 2

Appendix 2 describes my experiments contributing to the 2nd collaboration work with Dr. Jeremy Linsley in the Kuwada lab that was published in 2017 as "Linsley JW, Hsu I-U, Wang W, Kuwada JY. Transport of the alpha subunit of the voltage gated L-type calcium channel through the sarcoplasmic reticulum occurs prior to localization to triads and requires the beta subunit but not Stac3 in skeletal muscles. Traffic.2017;18:622–632. https://doi.org/10.1111/tra.12502". The work of this paper complements the results from Linsley et al., PNAS 2017 showing that Stac3 regulates the levels of $Ca_v1.1$ at T tubule plasma membrane through regulating the stability rather than trafficking of $Ca_v1.1$.

APPENDIX 2.1 SR/ER export machinery and Golgi outposts localize nearby triads.

Because the SR is not continuous with the T tubules, DHPRs must translocate from SR membrane to the T tubule membranes. Previous studies described trafficking of membrane proteins through the longitudinal SR/ER membrane in skeletal muscle to ER exit sites (ERES) distributed throughout the mammalian myofiber (Kaisto and Metsikkö, 2003). Immunolabeling with anti-Sec23b, a marker for ERES, and anti-DHPRα revealed that ERES localized to the triadic regions in zebrafish skeletal muscles as well thus providing a potential site for translocation to the T tubules at triads (Appendix Figure 2.1A). Furthermore, the Golgi marker, anti-GM130, labeled what appears to be Golgi outposts in the triadic regions that flank triads in zebrafish muscles (Appendix Figure 2.1B) as found in some mammalian muscles (Percival and Froehner,

2007; Percival et al., 2007; Ralston et al., 1999). Thus, a pathway localized to the triadic regions of SR and T tubules that includes SR to local Golgi to T tubule could potentially provide a trafficking pathway for DHPRs.

APPENDIX 2.2 DHPR transport along the longitudinal SR is differentially affected by EC coupling mutations.

Because both the β subunit of DHPRβ (DHPRβ) and Stac3 are required for normal expression of DHPRα at the triad, we investigated the roles of the two proteins for transport of DHPRα through the SR. Both *stac3−/−* mutants and *relaxed* (*DHPRβ* null) mutants have decreased triadic expression of DHPR when assayed by anti-DHPRα immunolabeling (25% and 60% reductions, respectively) (Linsley et al., 2017; Schredelseker et al., 2005). Nevertheless, the proportion of anti-DHPRα signal at longitudinal SR membrane is increased in *relaxed* mutants compared to WT sibling, but not different in *stac3−/−* mutants compared to WT siblings (Appendix Figure 2.2). This suggests the distribution of DHPR is differentially affected by each mutation.

APPENDIX 2.3 Benchmark experiments of eGFP-DHPR alpha subunit fluorescence recovery after photobleaching (FRAP).

In order to assay DHPRα dynamically in the longitudinal SR membrane, whole animal live cell imaging flourescence recovery after photobleaching (FRAP) experiments were performed on myofibers expressing EGFP-DHPRα. To benchmark our FRAP analysis, additional FRAP was performed on skeletal muscle fibers expressing EGFP (heat shock induced from

transgenic *hsp70:EGFP* zebrafish), and the diffusion rate of cytoplasmic EGFP was found to be comparable to published reports (62.8 μm/second) (Swaminathan et al., 1997). EGFP-DHPRα trafficking within live zebrafish skeletal muscle proceeds at a slow diffusion rate compared to EGFP diffusion alone (Appendix Figure 2.3).

During FRAP experiments, the fluorescence recovery of EGFP-DHPRα showed migration of EGFP-DHPRα along the longitudinal SR within the region that was photobleached, before accumulating at triadic areas in WT embryos. An alternative interpretation of fluorescence recovery might be that it represents local translation of new EGFP-DHPRα from translational machinery in the SR. However, trafficking in the SR membrane persisted in the presence of cyclohexamide, which blocks translation of new protein in zebrafish (Appendix Figure 2.4).

Appendix Figure 2.1

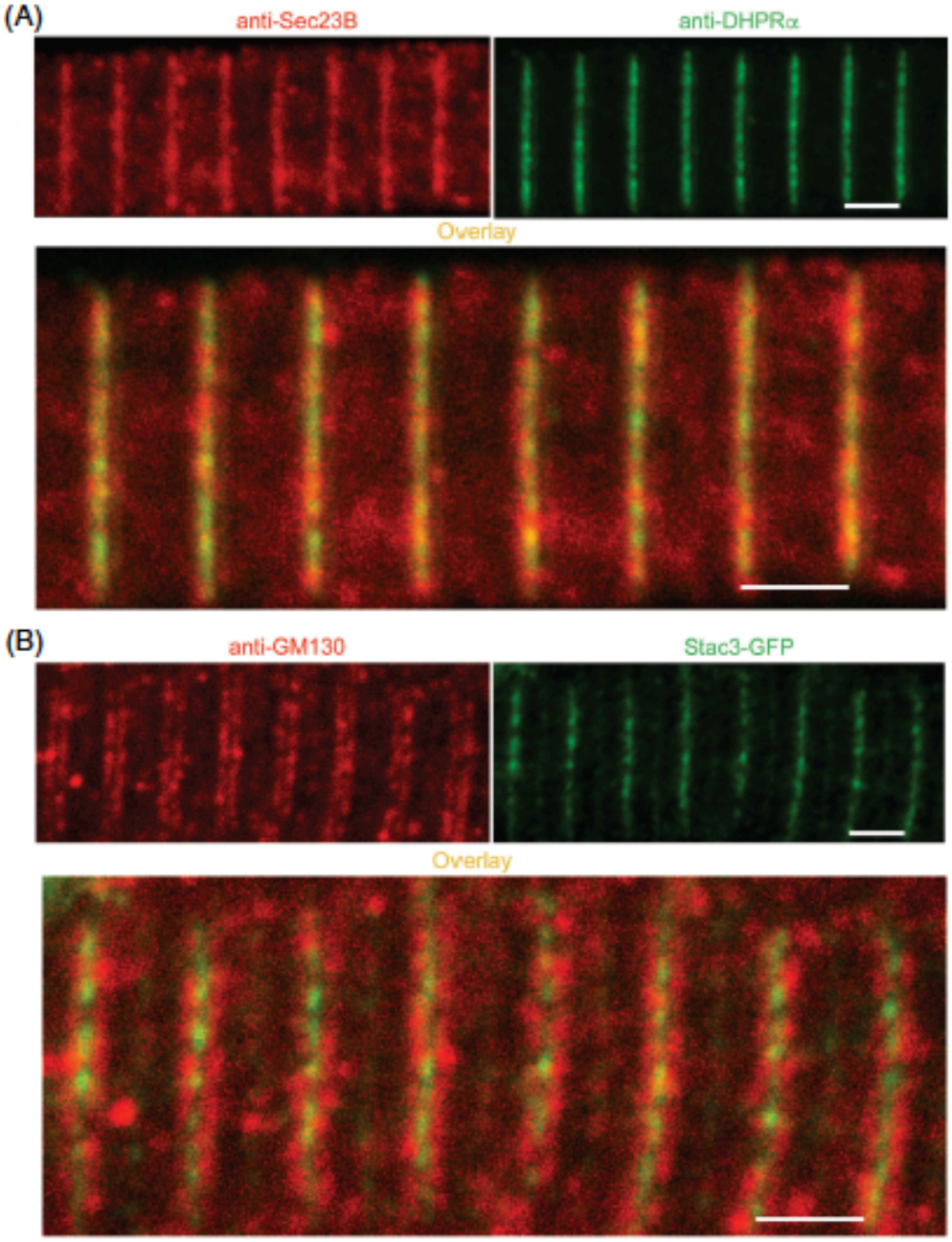

Appendix Figure 2.1 ER exit sites and Golgi outposts localize to triads.
(A) WT muscle fiber colabeled with anti-DHPRα (left) and anti-sec23B (middle) which labels ERES, showing co-localization at T tubules. (B) Whole-mount immunolabeling of transgenic *muscle actin:stac3-EGFP* muscle fiber showing anti-GM130 labeling flanks T tubules (scale bars, 2 µm).

Appendix Figure 2.2

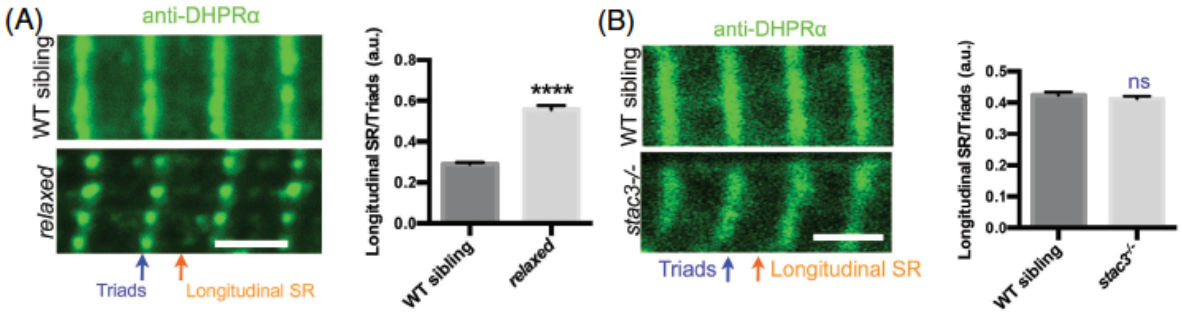

Appendix Figure 2.2 EC coupling component mutations differentially affect longitudinal SR trafficking.

(A) WT sibling and *relaxed* mutant muscle fibers labeled with anti-DHPRα (left) and quantification of the ratio of the signal at the longitudinal SR (orange arrow) to the triad (blue arrow) (right) showing increased DHPRα at the longitudinal SR in *relaxed* mutants (n = 68) compared to WT siblings (n = 86; T test P < .0001). (B) WT sibling and *stac3−/−* mutant muscle fibers labeled with anti-DHPRα (left) and quantification of the ratio of the signal at the longitudinal SR (orange arrow) to the triad (blue arrow) (right) showing DHPRα levels in longitudinal SR are the same in *stac3−/−* mutants (n = 127) as in WT siblings (n = 126; t test ns P = .39).

Appendix Figure 2.3

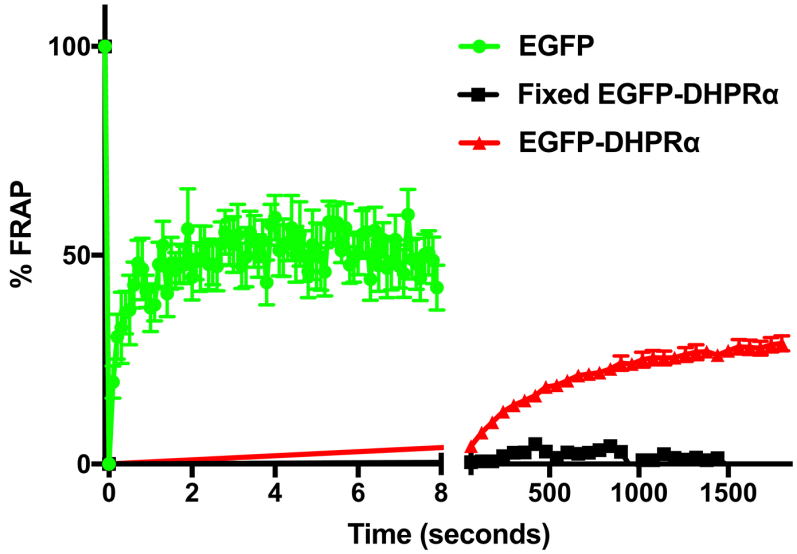

Appendix Figure 2.3 Benchmarking of EGFP-DHPRα fluorescence recovery after photobleaching.
Mean quantification of time course of FRAP of EGFP and EGFP-DHPRα expressed in WT. EGFP alone (thick green line and circles), EGFP-DHPRα (thick red line and triangles), and Fixed EGFP-EGFP-DHPRα (thick black line and squares) are shown. Vertical thick green line depicts bleaching.

Appendix Figure 2.4

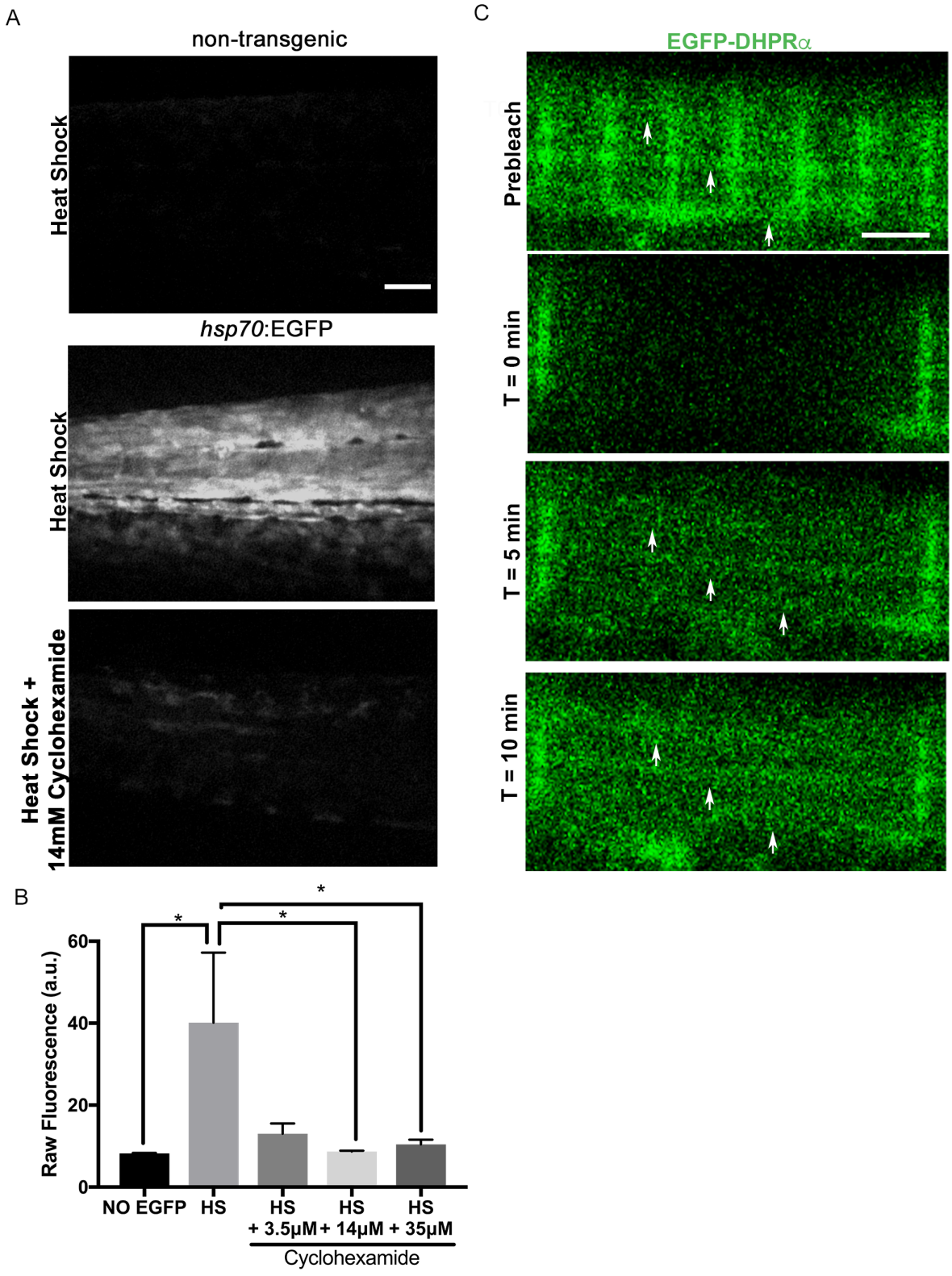

Appendix Figure 2.4 Longitudinal SR trafficking persists in the presence of cyclohexamide treatment which blocks translation. (A) Micrographs of tails of zebrafish embryos after heat shock without EGFP expression (top), with induced *hsp70*:EGFP, and with induced *hsp70*:EGFP in the presence of 14μM cyclohexamide. (Scale bar, 30μm)**.** (B) Histogram of quantification of mean EGFP fluorescence after heat shock showing increased fluorescence after heat shock in transgenic *hsp70*:EGFP embryos (n=15) versus non transgenic (n=15, ANOVA Tukey's, $p<0.05$). EGFP fluorescence after heat shock was reduced in *hsp70*:EGFP embryos incubated in 14μM (n=15, ANOVA Sidak's $p<0.05$) or 35μM cyclohexamide (n=16, ns, $p < 0.05$), but not 3.5μM (n=15, ns, $p=0.05$) compared to heat shocked *hsp70*:EGFP embryos. (C) Time course for FRAP of EGFP-DHPRα expressed in WT incubated in 14μM Cyclohexamide. Shown are EGFP-DHPRα before (prebleach), after photobleaching (T=0, 5, 10 min). White arrows indicate EGFP-DHPRα recovery in longitudinal striations. (Scale bar, 1μm).

Appendix References

Kaisto, T., and Metsikkö, K. (2003). Distribution of the endoplasmic reticulum and its relationship with the sarcoplasmic reticulum in skeletal myofibers. Exp Cell Res 289, 47-57.

Linsley, J.W., Hsu, I.U., Groom, L., Yarotskyy, V., Lavorato, M., Horstick, E.J., Linsley, D., Wang, W., Franzini-Armstrong, C., Dirksen, R.T., and Kuwada, J.Y. (2017). Congenital myopathy results from misregulation of a muscle Ca2+ channel by mutant Stac3. Proc Natl Acad Sci U S A 114, E228-E236.

Percival, J.M., and Froehner, S.C. (2007). Golgi complex organization in skeletal muscle: a role for Golgi-mediated glycosylation in muscular dystrophies? Traffic (Copenhagen, Denmark) 8, 184-194.

Percival, J.M., Gregorevic, P., Odom, G.L., Banks, G.B., Chamberlain, J.S., and Froehner, S.C. (2007). rAAV6-microdystrophin rescues aberrant Golgi complex organization in mdx skeletal muscles. Traffic (Copenhagen, Denmark) 8, 1424-1439.

Ralston, E., Lu, Z., and Ploug, T. (1999). The organization of the Golgi complex and microtubules in skeletal muscle is fiber type-dependent. The Journal of neuroscience : the official journal of the Society for Neuroscience 19, 10694-10705.

Schredelseker, J., Di Biase, V., Obermair, G.J., Felder, E.T., Flucher, B.E., Franzini-Armstrong, C., and Grabner, M. (2005). The β 1a subunit is essential for the assembly of dihydropyridine-receptor arrays in skeletal muscle. Proceedings of the National Academy of Sciences of the United States of America 102, 17219-17224.

Swaminathan, R., Hoang, C.P., and Verkman, A.S. (1997). Photobleaching recovery and anisotropy decay of green fluorescent protein GFP-S65T in solution and cells: cytoplasmic viscosity probed by green fluorescent protein translational and rotational diffusion. Biophys J 72, 1900-1907.